SANDIA REPORT

Continuum Representations of Cellular Solids

M. K. Neilsen

Continuum Representations of Cellular Solids*

M. K. Neilsen
Engineering Mechanics and Material Modeling
Sandia National Laboratories
Albuquerque, New Mexico 87185

Abstract

Cellular materials consist of interconnected struts or plates which form cells. The struts or plates are constructed from a variety of metals, polymers, ceramics and wood products. Cellular materials are often used in impact limiters for shipping containers to protect the contents from accidental impact events. These materials exhibit a variety of complex behavior when subjected to crushing loads. This research focuses on the development of continuum representations of cellular solids that can be used in the finite element analysis of shipping container accidents. A significant portion of this work is the development of a new methodology to relate localized deformations to appropriate constitutive descriptions. This methodology provides the insight needed to select constitutive descriptions for cellular solids that capture the localized deformations that are observed experimentally. Constitutive relations are developed for two different cellular materials, aluminum honeycomb and polyurethane foam. These constitutive relations are based on plasticity and continuum damage theories. Plasticity is used to describe the permanent deformation exhibited by both aluminum honeycomb and polyurethane foam. Continuum damage is needed to capture the change in elastic parameters due to cracking of the polyurethane cell wall materials. The new constitutive description of polyurethane foam is implemented in both static and dynamic finite element codes, and analytical and numerical predictions are compared with available experimental data.

Acknowledgements

Contents

Figures

Tables

1. INTRODUCTION

Cellular materials consist of interconnected plates or struts which form cells. The struts or plates are constructed from a variety of metals, polymers, ceramics and wood products. Materials with a two-dimensional array of cells are referred to as honeycombs and materials with a three-dimensional array of cells are referred to as foams (Figure 1.1). Foams with interconnected plates often form closed-cells and are referred to as closed-cell foams. Foams with interconnected struts are referred to as open-cell foams and are generally much more flexible than closed-cell foams. Foams that permanently deform when subjected to large strains are rigid foams and foams that remain elastic for large strains are flexible foams. The two materials that were closely investigated in this study include a rigid, aluminum honeycomb and a rigid, closed-cell, polyurethane foam.
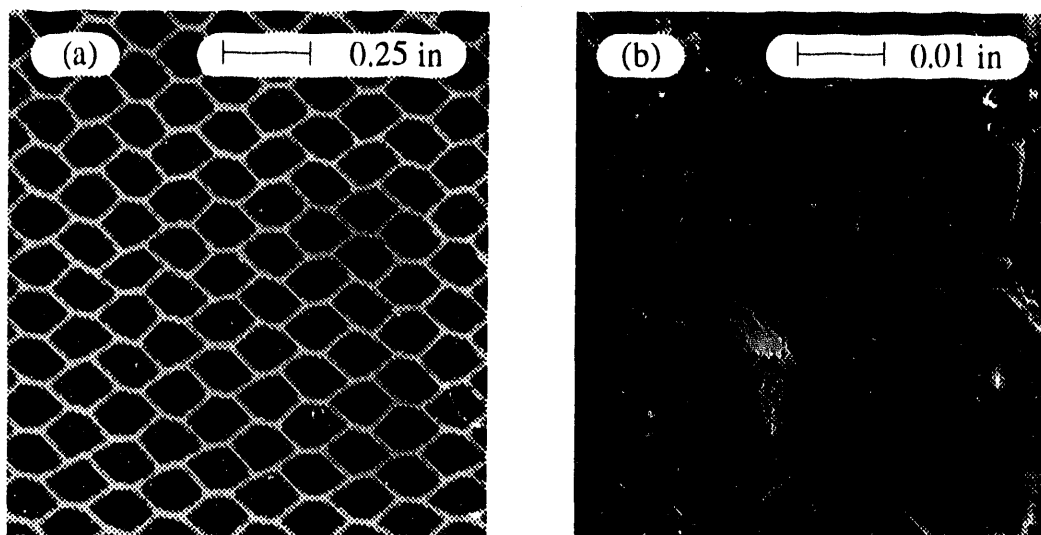
Figure 1.1. Cellular Solids: (a) aluminum honeycomb, (b) polyurethane foam.

Cellular materials have been studied by mathematicians and philosophers for over 300 years (Gibson and Ashby, 1988). Early mathematicians were intrigued by the geometry and packing of individual cells. Cellular solids have a variety of cell shapes and packing arrangements. For example, aluminum honeycomb has regular hexagonal cells and a uniform packing. On the other hand, polyurethane foam has a number of different cell shapes and packing arrangements. For the past few decades, researchers have experimentally measured and analytically investigated the mechanical behavior of cellular solids. The experimental work has included subjecting cellular solids to various load paths and measuring the induced deformation of the sample. The analytical work has concentrated on developing equations that relate the elastic response and initial yield

strength of the cellular material to the cell geometry and the properties of the cell wall material. These investigations indicate that cellular solids have mechanical properties which are not typical of solid materials.

Cellular solids are used in a wide variety of applications that take advantage of the unique properties of these materials. For example, cellular solids are used as fillers and rigidizers in airplane wings and protective packaging for shipping containers (Doyle, 1971). During a shipping container accident, cellular solids are expected to absorb a significant amount of energy by undergoing large inelastic volume reductions. Unfortunately, these materials exhibit a variety of complex behavior when subjected to crushing loads. Continuum representations that are developed to capture the behavior of cellular solids during shipping container accidents must capture these complex behavior.

The purpose of this research was to develop a continuum representation of cellular materials that not only captures the elastic response of these materials but also the plastic deformation, damage and localized deformation that is generated when these materials are subjected to crushing loads. The constitutive relations developed for these materials use a combination of plasticity and continuum damage theories. Plasticity is a well developed theory which was originally used to describe the permanent deformations of metals loaded beyond their elastic limit. Recently, plasticity has also been used to describe the permanent deformations exhibited by concrete, rocks, soils and foams. Continuum damage theories, on the other hand, are just currently being developed (Krajcinovic, 1989). In this paper, a rather general continuum damage theory with a structure similar to existing plasticity theories is presented. Use of a similar structure simplifies the development of coupled plasticity-continuum damage theories which share common yield (damage) surfaces. In this study, a coupled theory is developed for rigid polyurethane foam.

When cellular solids are loaded into the inelastic regime, they often exhibit deformations that are localized into small regions at some point in the loading process. In the past, localization has been associated with loss of positive definiteness of the acoustic tensor (Hill, 1962; Rice, 1976). Here we show that localization should be associated with loss of positive definiteness of the symmetric part of the acoustic tensor. The acoustic tensor depends on both an orientation vector for the localization and on the fourth-order tangent stiffness tensor for the material. A connection between constitutive theories and localization is provided by a spectral analysis of the symmetric part of the tangent stiffness tensor. The eigensystem for the symmetric part of the tangent stiffness tensor is obtained for several different plasticity and continuum damage models. This eigensystem provides information about both diffuse and discontinuous bifurcations. Material properties, boundary conditions, and body geometry are all shown to affect the diffuse and localized deformation modes that are generated. Numerous experimental observations of necking and localization in metal specimens subject to various boundary conditions are explained with a bifurcation analysis of a von Mises plasticity model. Bifurcation analyses are then performed on potential constitutive theories for cellular solids. A comparison

of results from the bifurcation analyses with experimental observations of localized deformations is essential for the identification of appropriate constitutive theories for cellular materials.

Constitutive relations for aluminum honeycombs and rigid polyurethane foams are developed and analyzed. A coupled plasticity and continuum damage model for rigid polyurethane foam is then implemented in both static and dynamic finite element codes. A number of static tests on rigid polyurethane foam are analyzed and the results from the finite element analyses are compared with experimental observations. Finally, a typical impact problem is analyzed using various constitutive models for a polyurethane foam impact limiter to demonstrate the effects of using various constitutive descriptions for the foam.

2. CELLULAR MATERIALS

Literature on the mechanical behavior of cellular material is reviewed in this chapter. The first section includes a discussion on the general behavior of cellular material. In the second section, currently available experimental data for aluminum honeycomb and rigid, polyurethane foam is reviewed. In the final section, existing constitutive theories for these materials are reviewed and the need for improved constitutive theories is discussed.

2.1   General Behavior

Cellular materials generally have a much lower density, thermal conductivity, stiffness, and strength than solid materials (Gibson and Ashby, 1988). A typical stress-strain curve generated from a uniaxial compression test on a cellular solid is shown in Figure 2.1. Initially the cellular solid is linear elastic. When load is applied the cell walls bend but remain linear elastic. As the load is increased, the cell walls begin to elastically buckle, form plastic hinges, or crack. The behavior depends on the cell wall material, temperature, and loading rate. Generally, one layer of cells will completely collapse before a second layer collapses. This generates a narrow region of localized deformation. In this plateau region, a small increase in the applied load will cause additional layers of cells to collapse and the region of localized deformation will continue to grow. It is exactly this behavior that makes cellular materials attractive for use in impact limiters. Once a
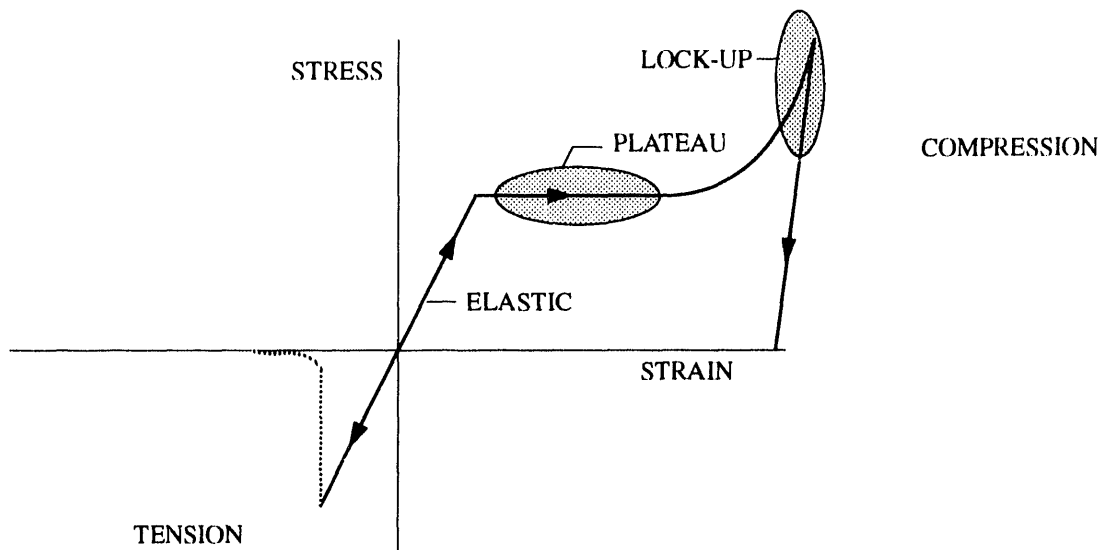
Figure 2.1.   Stress-Strain Curve for Cellular Solid Subjected to Uniaxial Loads.

15

certain load level is reached, the material experiences large volume reductions and absorbs a significant amount of energy with only a small increase in transmitted load. Finally, once all of the cell rows have collapsed, the cell walls are compressed against each other and the load needed to compress the sample further will rapidly increase. This is referred to as densification or lock-up of the cellular solid. The unloading behavior will depend on the character of the cellular material. Flexible cellular materials will elastically unload and return to their undeformed shape. Rigid cellular materials, on the other hand, are permanently deformed and often damaged when they are compressed into the plateau regime. This study focuses on rigid cellular solids which exhibit inelastic deformations.

When cellular solids are subjected to tensile loads, the cell walls will again bend and the material will initially be elastic. As the load is increased, the material will either plastically deform or fracture. The behavior will again depend on the cell wall material, temperature and load-rate. If the material fractures, the applied load will rapidly decrease. If the material plastically deforms, the load will increase as the cell wall sections are rotated and axially stretched. Often a single row of cells will stretch or fracture and the material will also exhibit localization in tension.

2.2 Experimental Data

Two cellular materials that are often used in packaging, aluminum honeycomb and rigid polyurethane foam, have been experimentally evaluated by a number of researchers (Shaw and Sata, 1966; Patel and Finnie, 1969; Zaslawsky, 1973; Klintworth and Stronge, 1988; Gibson and Ashby, 1988; Donald and Maji, 1992). Results from these experimental investigations are briefly summarized in this section.

2.2.1 Aluminum Honeycomb

Aluminum honeycomb consists of interconnected aluminum plates. The plates are connected such that they form hexagonal cells that resemble a bee's honeycomb. This material is not isotropic. In fact, the strength of the material in a direction parallel to the generator axis is approximately 30 times greater than its in-plane strength.

A typical yield surface for an aluminum honeycomb subjected to in-plane loads (Gibson and Ashby, 1988) is shown in Figure 2.2. When this material is subjected to a uniaxial in-plane compressive load the cell walls bend, plastic hinges form near the connection between various cell walls, and cell walls eventually deform and collapse. Generally, a localized region of cells will collapse and begin to densify before cells in other regions collapse. Figure 2.3 shows the localized deformations generated by uniaxial compression in the ribbon direction and uniaxial compression in the transverse direction. The localized deformation zones in these materials are generally oriented along geometrically similar lines. However, the localized deformation is significantly different when the load orientation is changed. Thus, the constitutive description for aluminum honeycomb should

16
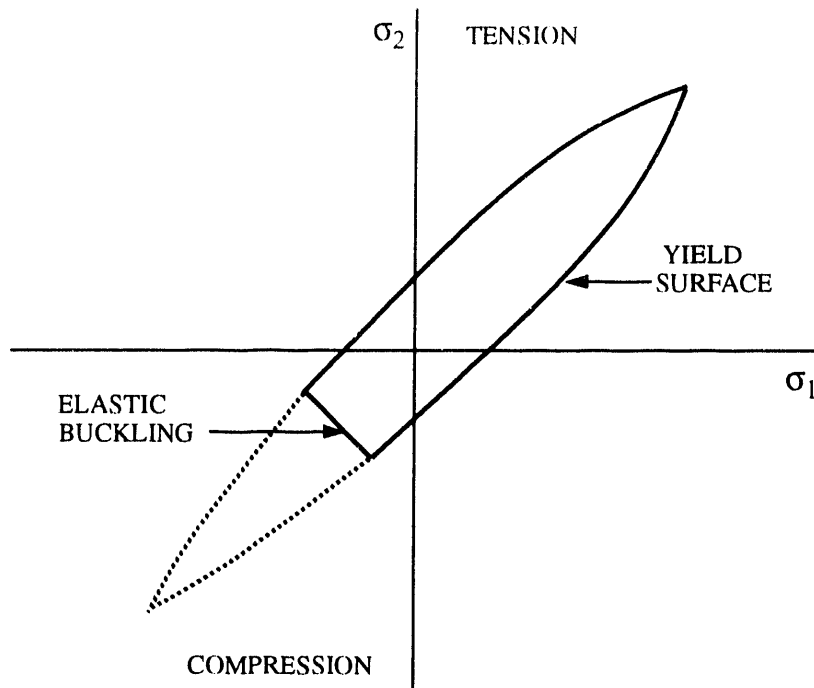
Figure 2.2. Failure Surface for Regular Hexagonal Honeycomb Subjected to In-plane Loads (Gibson and Ashby, 1988).

predict geometry and load dependent localized deformation.

For uniaxial compression, the load-displacement curve consists of an initial linear elastic regime followed by a plateau regime where the cells collapse as plastic hinges form in the cell walls. Finally, a regime of densification is reached where all of the cells have collapsed and begin to densify which causes the load carried by the structure to rapidly increase. The behavior of this material under uniaxial tension is similar to its behavior under uniaxial compression. Plastic hinges form near the connection between various cell walls and cell walls bend and stretch. Again, a localized region of cells will stretch and be elongated before cells in other regions are plastically deformed. Eventually the entire matrix is elongated and the response is equal to the response of the solid cell wall material. The cross section of the sample has, of course, been significantly reduced.

When this material is subjected to uniform biaxial tension, the cell walls are stretched and not bent. Note that the yield surface (Figure 2.2) for aluminum honeycomb is elongated along the biaxial load path. This occurs because the biaxial load needed to stretch the cells walls is significantly higher than the uniaxial load needed to bend the cell walls. Since the permanent deformation exhibited by this material is associated with the formation of plastic hinges in the cell walls, a plasticity model is used to capture the inelastic behavior.

17

Y - Ribbon Direction

X- Transverse Direction
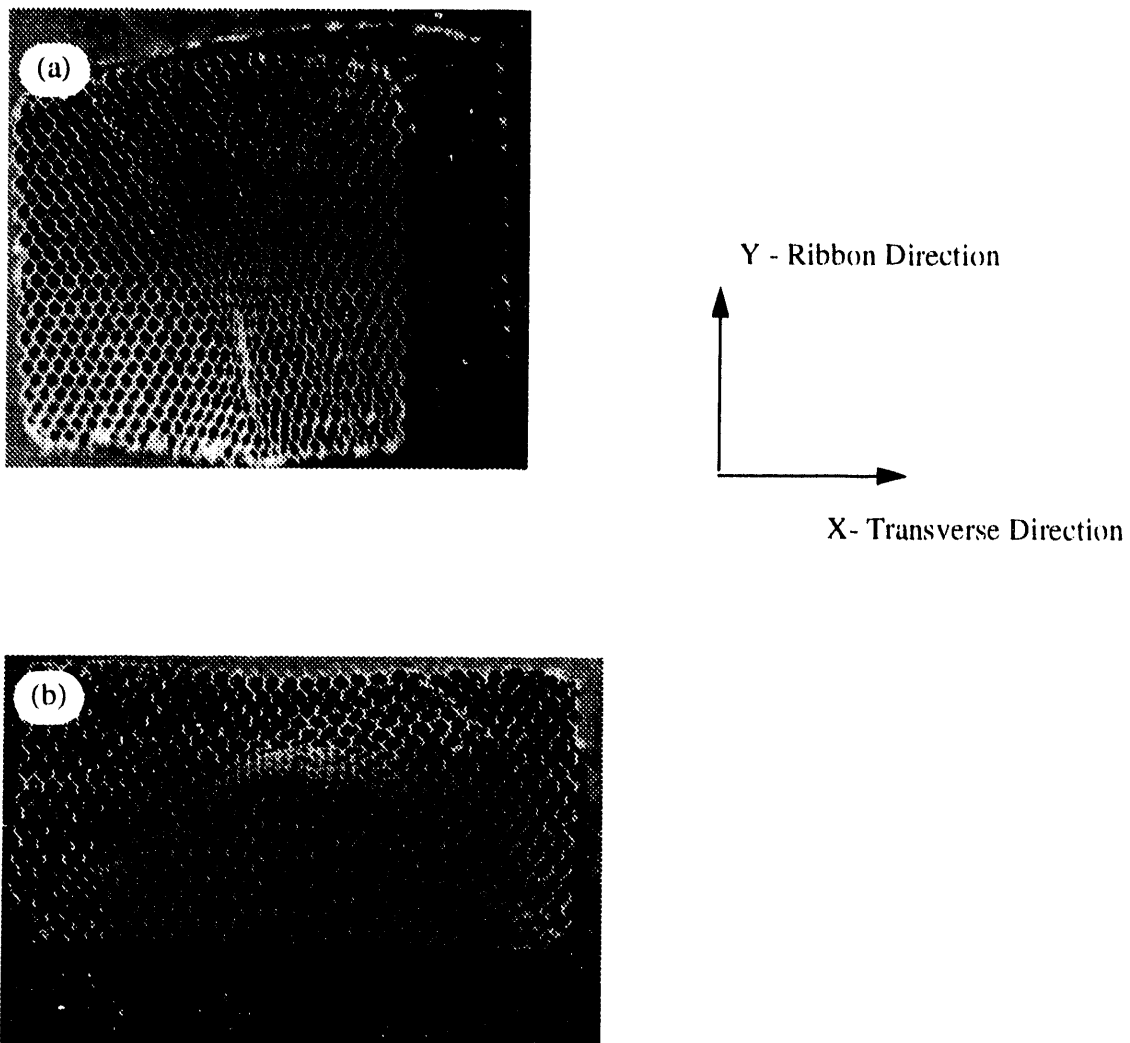
Figure 2.3. Localized In-plane Deformation of Aluminum Honeycomb Subjected to Uniaxial Compression: (a) in the Transverse Direction, (b) in the Ribbon Direction (Donald and Maji, 1992)

FOAM RISE
DIRECTION

σ_2 TENSION

FRACTURE
SURFACE

σ_1

YIELD
SURFACE

COMPRESSION
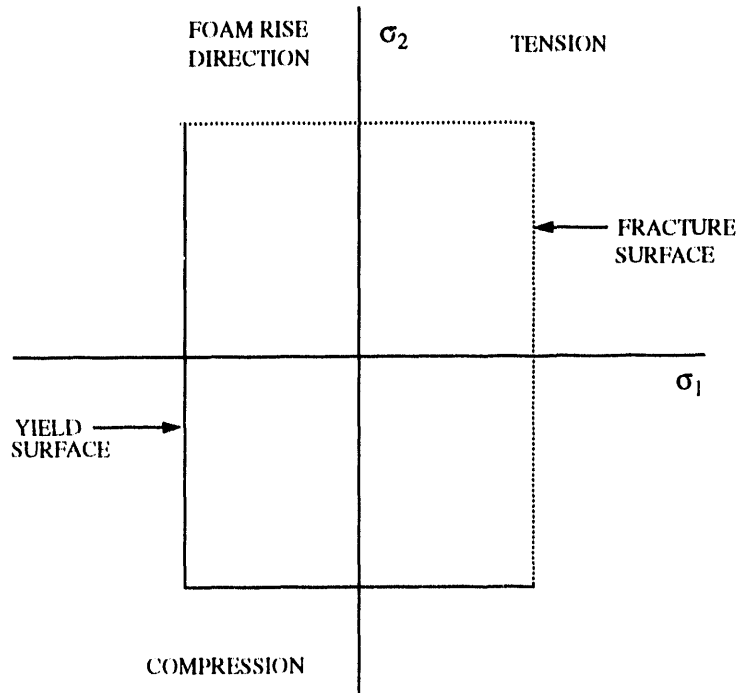
Figure 2.4. Failure Surface for a Rigid, Closed-Cell, Polyurethane Foam (Patel and Finnie, 1969; Gibson and Ashby, 1988).

2.2.2 Polyurethane Foam

Rigid, closed-cell polyurethane foam consists of interconnected plates of polyurethane. The geometry of this material is three-dimensional and the plates are much more randomly distributed than the plates in aluminum honeycomb. This material is manufactured by having a gas expand inside liquid polymer which solidifies in a foamed state. Shaw and Sata (1966), Patel and Finnie (1970), Zaslawsky (1973), and Donald and Maji (1992) have experimentally measured the behavior of polyurethane foam samples subjected to various load paths. Patel and Finnie's (1969) work indicates that the initial failure surface for this material subjected to a plane stress state has the rectangular shape shown in Figure 2.4. The experimental work of Shaw and Sata (1966), Zaslawsky (1973), and Donald and Maji (1992) indicates that the initial yield surface for rigid polyurethane foam can be described using a principal stress criterion.

A load-displacement curve for 20 lb/ft^3 polyurethane foam subjected to cyclic uniaxial compression is shown in Figure 2.5. The initial elastic regime is followed by a plateau regime in which the load required to crush the material remains nearly constant. In this regime, some cell walls are compressed until they buckle while other cell walls are stretched until they crack. When additional load is applied, the cell walls are compressed against other cell walls and the stiffness of the foam approaches a value equal to the stiffness of solid polymer. The slopes of the unloading curves indicate that the material stiffness decreases when the material is compressed into the plateau regime but that the

19
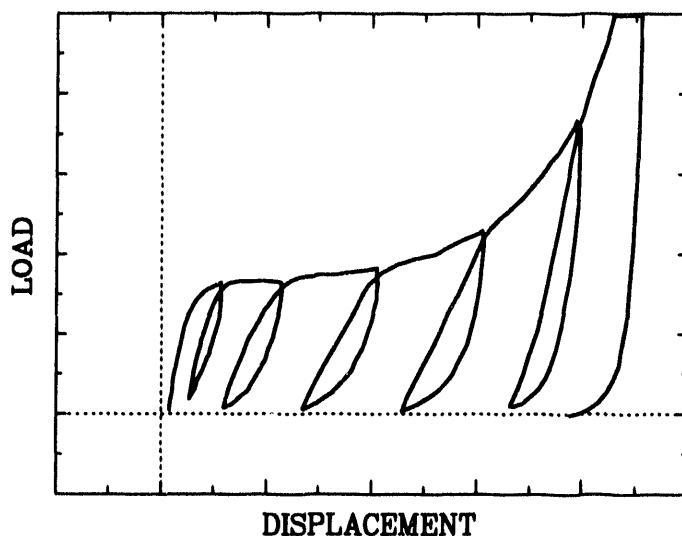
Figure 2.5. Load-Displacement Curve for 20 lb/ft^3 Polyurethane Foam Subjected to Cyclic Uniaxial Compression (Donald and Maji, 1992).

material stiffness actually increases when the material is compressed further into the densification regime. The decrease and subsequent increase in foam stiffness is caused by two distinct deformation mechanisms. The decrease in stiffness occurs due to the cracking and reduced stiffness of the cell walls. The increase in stiffness is due to the interaction between neighboring cell walls as they are compressed together.

2.3 Existing Continuum Representations

Most packages are currently designed using a one-dimensional uniaxial crush model for the cellular solid. This is done due to the lack of adequate experimental data or an accurate constitutive theory for these materials. In a typical design, the uniaxial load-displacement curve is used directly to compute the amount of energy absorbed by the foam for a given uniaxial impact event. This method is accurate for describing the response of impact limiting materials subject to uniaxial loads; however, this simple uniaxial approach cannot be applied to situations involving multiaxial loading. A general continuum representation is needed if multiaxial loading is involved. The uniaxial crush model is adequate for only the simplest of package geometries and loadings.

A variety of researchers (Gibson and Ashby, 1988; Warren and Kraynik, 1987) have studied the linear elastic behavior of various cellular solids. In this work, equations are developed that relate the elastic constants to parameters that define the geometry of the cell (i.e., the thickness of the cell wall and length of a typical cell wall section). Equations that define the critical load beyond which the behavior is no longer linear elastic are also developed by these researchers. These equations are then used to describe the

linear elastic behavior of a group of cells by assuming that all cells have the same initial geometry and deform in the same manner. This work was recently extended (Warren, Kraynik and Stone, 1989) to capture the nonlinear elastic behavior of two-dimensional open cell foams. Results from these micromechanical investigations indicate that the dominant cell deformation mechanism in flexible foams changes from bending for small deformations to stretching for large deformations.

The micromechanical studies of Warren and Kraynik (1987) and others provide a description of the cellular material behavior that is based on an understanding of the behavior at the cell level. These studies provide valuable information about cell deformation mechanisms and the effects of cell geometry or material variations on the global response of the foam. This is important because it allows for the development of an engineered cellular material that meets specific global behavior requirements. Current micromechanical studies accurately capture the linear and nonlinear elastic behavior of cellular materials that have a regular cell geometry. However, a significant extension of the current micromechanical studies would be needed to investigate the effects of irregular cells, to predict inelastic behavior, or to capture localized deformation. Extension of micromechanical studies to inelastic behavior and localization will probably require a complement of analytical and numerical investigations of families of cells.

In this research, a macromechanical approach is used to investigate the behavior of cellular solids. With this approach an extensive experimental investigation is needed to evaluate the deformation and localization exhibited by a large number of cells subjected to various load paths. Results from the experimental investigations are then used to develop a mathematical description of the behavior. This approach allows the development of a model that captures both the elastic and inelastic behavior of the material. An accurate description of each individual cell is not needed; thus, this approach works well for materials that have irregular cells like polyurethane foam. Unfortunately, if the equations are independent of cell geometry then the effect of variations at the cell level cannot be related to variations in global behavior. With this approach localized deformations must be measured during experiments if a model that captures localized deformation is to be developed. Also a thorough understanding of the relationship between localized deformations and constitutive descriptions is needed to develop appropriate constitutive theories for materials exhibiting localization. A significant portion of this work is a development of such an understanding.

Most commercial finite element codes do not have constitutive theories for cellular solids and analysts using these codes are forced to use an inappropriate constitutive description for cellular materials when they are faced with a problem in which these materials are used. A few researchers are currently working on the development of constitutive theories for cellular materials (Neilsen, Morgan and Krieg, 1987; Klintworth and Stronge, 1988; Warren, Kraynik and Stone, 1989; Triantafillou and Gibson, 1990) and this report represents some of that work. Recently, Klintworth and Stronge (1988) investigated the response of aluminum honeycombs subjected to in-plane loads and developed mathemat-

ical expressions for the elastic response and the initial yield functions for this material. Their yield functions describe a family of intersecting yield surfaces in stress space. The yield functions for aluminum honeycomb developed by Klintworth and Stronge (1988) are used in the plasticity theory for aluminum honeycomb presented here. A plasticity model for rigid polyurethane foam, developed by Neilsen, Morgan and Krieg (1987), is used as the basis for the coupled plasticity continuum damage model for polyurethane foam developed in this study.

3. CONTINUUM CONSTITUTIVE THEORIES

This chapter includes a review of elasticity, plasticity and continuum damage theories which may be useful for describing the behavior of cellular solids. The continuum damage theory was developed by Schreyer (1990a) using a structure similar to that of conventional plasticity theory. The use of this structure ensured the development of thermodynamically acceptable constitutive theories and also aided in the identification of continuum damage theories which are analogous to existing plasticity theories. This was helpful in the development of coupled (plasticity with continuum damage) theories which have common yield (damage) surfaces.

3.1 Elasticity

Elasticity theories were developed to described the deformation of materials not loaded beyond their elastic limit. For a class of linear elastic materials, there exists a positive definite strain energy per unit volume, U, (Malvern, 1969), given by

$$U = \tfrac{1}{2}\boldsymbol{\epsilon} : \mathbf{E} : \boldsymbol{\epsilon} \tag{3.1}$$

where $\boldsymbol{\epsilon}$ is the total strain tensor and $\mathbf{E}$ is the fourth-order elastic stiffness tensor. All of the fourth-order tensors used in this report possess the minor symmetries, i.e., $E_{ijkl} = E_{jikl} = E_{ijlk}$. The existence of a strain energy function implies that the elastic stiffness tensor also possesses the major symmetry, i.e., $E_{ijkl} = E_{klij}$.

For small deformations, the constitutive relation is as follows:

$$\boldsymbol{\sigma} = \frac{\partial U}{\partial \boldsymbol{\epsilon}} = \mathbf{E} : \boldsymbol{\epsilon} \tag{3.2}$$

If the material is isotropic, then $\mathbf{E}$ is given by

$$\mathbf{E} = 3K\mathbf{P}^{sp} + 2G\mathbf{P}^{d} \tag{3.3}$$

where K is the bulk modulus and G is the shear modulus. The bulk and shear moduli are related to Young's modulus, E, and Poisson's ratio, v, as follows

$$K = \frac{E}{3(1 - 2v)} \qquad G = \frac{E}{2(1 + v)} \tag{3.4}$$

The fourth-order spherical projection operator, $\mathbf{P}^{sp}$, and the deviatoric projection operator, $\mathbf{P}^{d}$, are given by

$$\mathbf{P}^{sp} = \frac{1}{3}\mathbf{i} \odot \mathbf{i} \qquad \mathbf{P}^{d} = \mathbf{I} - \mathbf{P}^{sp} \tag{3.5}$$

Here $\mathbf{I}$ is the symmetric fourth-order identity tensor and $\mathbf{i}$ is the second-order identity.

3.2 Plasticity

Plasticity theories were originally developed to mathematically describe permanent deformations in metals which are associated with dislocation motion and slip at the microstructural level. An important assumption made by these theories is that the linear elastic properties of the material are not affected by the generation of plastic deformation. This assumption is valid for most metals subjected to only a moderate amount of plastic deformation; however, recent experiments indicate that the stiffness of metals may be affected when large amounts of plastic deformation are generated.

To develop a general framework for plasticity theories, consider the following expression for the strain energy function, U,

$$U = U(\epsilon, \epsilon^p) = \tfrac{1}{2}(\epsilon - \epsilon^p) : \mathbf{E} : (\epsilon - \epsilon^p) \tag{3.6}$$

where ϵ and ϵ^p are the total and plastic strain tensors, respectively. Coleman and Gurtin (1967) have shown that the Clausius-Duhem dissipation inequality can be written as

$$\boldsymbol{\sigma} : \dot{\epsilon} - \dot{U} \geq 0 \tag{3.7}$$

or

$$\boldsymbol{\sigma} : \dot{\epsilon} - \frac{\partial U}{\partial \epsilon} : \dot{\epsilon} - \frac{\partial U}{\partial \epsilon^p} : \dot{\epsilon}^p \geq 0 \tag{3.8}$$

With the constitutive relation

$$\boldsymbol{\sigma} = \frac{\partial U}{\partial \epsilon} = \mathbf{E} : (\epsilon - \epsilon^p) \tag{3.9}$$

and the following expression for the mechanical dissipation rate, $\dot{D}$,

$$\dot{D} = -\frac{\partial U}{\partial \epsilon^p} : \dot{\epsilon}^p = \boldsymbol{\sigma} : \dot{\epsilon}^p \tag{3.10}$$

the Clausius-Duhem inequality can be simply expressed as

$$\dot{D} \geq 0 \tag{3.11}$$

which indicates that the dissipation of mechanical energy is an irreversible process.

Plasticity models are characterized by a yield function, Ψ, which defines a surface in stress space separating elastic and plastic regimes and an evolution equation for the plastic strain which is also referred to as a flow rule. Yield functions are often written as follows

$$\Psi(\boldsymbol{\sigma}, \epsilon^p) = g(\boldsymbol{\sigma}) - h(\epsilon^p) \tag{3.12}$$

where g is a function of stress invariants and h is a positive function of ϵ^p. Information about the load history is stored in ϵ^p or often some invariant of ϵ^p and the effects of

the load history on the yield surface are incorporated through $h(\epsilon^p)$. The yield surface represented by this yield function is given by $\Psi = 0$ and the normal to the yield surface, $\mathbf{f}$, is given by

$$\mathbf{f} = \frac{\partial \Psi}{\partial \boldsymbol{\sigma}} \tag{3.13}$$

A typical flow rule is given by

$$\dot{\epsilon}^p = \dot{\rho} \mathbf{g} \tag{3.14}$$

where ρ is a monotonically increasing parameter and $\mathbf{g}$ is a second-order tensor that represents the orientation of the plastic strain increment. By substituting this expression for the plastic strain rate into the dissipation rate equation we obtain

$$\dot{D} = \dot{\rho} \boldsymbol{\sigma} : \mathbf{g} \tag{3.15}$$

For elastic processes, $\dot{\rho}$ equals zero and for plastic processes $\dot{\rho}$ is positive. Thus, Equation 3.15 indicates that mechanical dissipation will be generated when plastic deformation occurs and the tensor product $\boldsymbol{\sigma} : \mathbf{g}$ is positive. In other words, to ensure that dissipation accompanies plastic deformation, one should select yield functions and flow laws such that the tensor product $\boldsymbol{\sigma} : \mathbf{g}$ is positive whenever plastic deformation is generated.

The flow rule is referred to as an associated flow rule when the normal to the yield surface and orientation of the plastic strain increment are equal, i.e., $\mathbf{f} = \mathbf{g}$. This condition is also referred to as normality because the plastic strain increment is oriented in a direction normal to the yield surface. Maximum plastic dissipation results when associated flow rules are used (Simo and Hughes, 1986). Yield functions and flow rules are not thermodynamically required to be associated; however, they should always be chosen such that dissipation and plastic deformation are coincident events for all possible load paths. In other words, flow rules and yield functions cannot be chosen independently. Several existing plasticity theories that may be used to describe the behavior of cellular solids are presented in the next few sections.

3.2.1 Drucker-Prager

The Drucker-Prager model was developed to capture the behavior of geologic materials such as sands and soils. This model has a yield function given by

$$\Psi = \sqrt{J_2} + \frac{\mu}{3} I_1 - c \tag{3.16}$$

where μ is an internal friction parameter and c is a material constant. J_2 is the second invariant of the deviatoric stress tensor and I_1 is the first invariant of the total stress tensor:

$$J_2 = \frac{1}{2} \boldsymbol{\sigma}^d : \boldsymbol{\sigma}^d, \qquad I_1 = \boldsymbol{\sigma} : \mathbf{i} \tag{3.17}$$

where $\boldsymbol{\sigma}^d$ is the stress deviator. The yield surface given by this function is a cone in principal stress space as shown in Figure 3.1.
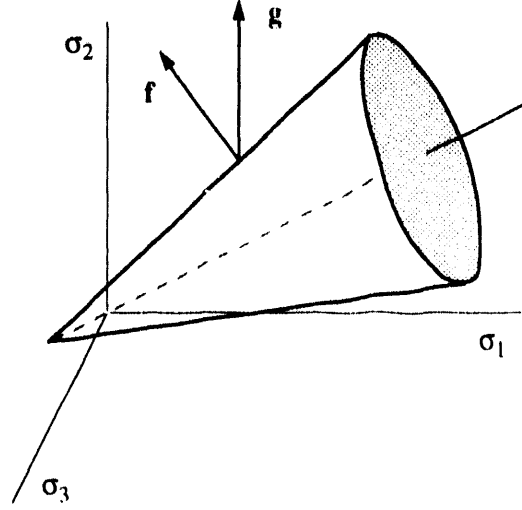
Figure 3.1. Drucker-Prager Yield Surface.

The normal to the yield surface, **f**, is given by

$$\mathbf{f} = \frac{\boldsymbol{\sigma}^d}{(2\sqrt{J_2})} + \frac{\mu}{3}\mathbf{i} \tag{3.18}$$

and the orientation of the plastic strain increment is chosen to be

$$\mathbf{g} = \frac{\boldsymbol{\sigma}^d}{(2\sqrt{J_2})} + \frac{\beta}{3}\mathbf{i} \tag{3.19}$$

where β is the dilatancy parameter. When μ is equal to β the flow is associated with the yield function.

3.2.2 von Mises

Next, consider a von Mises plasticity model with associated flow and linear strain hardening. The model was originally developed to describe the plastic deformation of metals. The yield function, Ψ, is as follows:

$$\Psi = \sqrt{J_2} - (H_0 + H_1 \epsilon^p) \tag{3.20}$$

where H_0 is the initial yield strength, H_1 is the hardening modulus, and ϵ^p is the equivalent plastic strain which is a monotonically increasing invariant given by

$$\epsilon^p = \int (d\boldsymbol{\epsilon}^p : d\boldsymbol{\epsilon}^p)^{\frac{1}{2}} \tag{3.21}$$

26
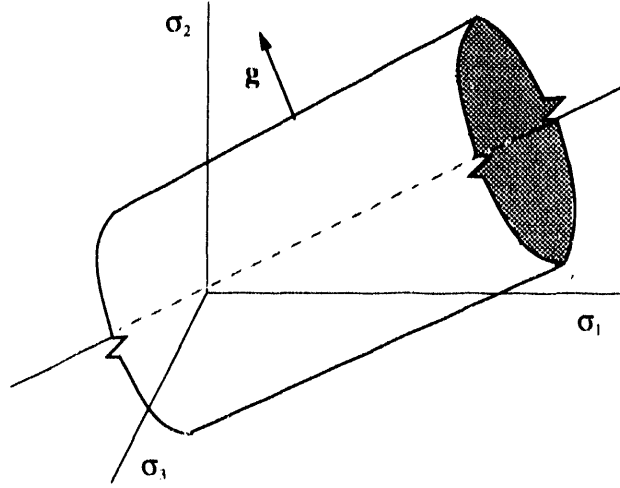
Figure 3.2. von Mises Yield Surface.

This yield function represents a yield surface that is an infinitely long cylinder in stress space as shown in Figure 3.2. The corresponding orientation of the plastic strain increment is normal to the yield surface and is given by

$$\mathbf{f} = \mathbf{g} = -\frac{\sigma_i^d}{(2\sqrt{J_2})} .$$

(3.22)

Equation 3.22 indicates that this model predicts only deviatoric or shape changing plastic strains. Since rigid polyurethane foams and aluminum honeycombs exhibit significant volumetric plastic strains, a von Mises plasticity model is not appropriate for these materials.

3.2.3 Mohr-Coulomb

Next, consider a simple Mohr-Coulomb model which has been used to describe the behavior of sand and other geologic materials. This model has a yield function given by

$$\Psi = \tfrac{1}{2}(\sigma_1 - \sigma_2) + \tfrac{1}{2}(\sigma_1 + \sigma_2)sin\phi - c\,cos\phi$$

(3.23)

where ϕ is the internal friction angle, c is the cohesion, and the coordinate system is chosen such that σ_1 and σ_2 are the maximum and minimum principal stresses, respectively. Then for an associated flow law the components of $\mathbf{f}$ and $\mathbf{g}$ in the principal coordinate system are

$$\mathbf{f} = \mathbf{g} \Rightarrow \tfrac{1}{2} \begin{bmatrix} 1 + sin\phi & 0 & 0 \\ 0 & -1 + sin\phi & 0 \\ 0 & 0 & 0 \end{bmatrix}$$

(3.24)

A Tresca model with associated flow is identical to a Mohr-Coulomb model with the internal friction angle set equal to zero.

3.2.4 Principal Stress

Finally, consider the principal stress theory of Rankine that was recently used by Neilsen, Morgan and Krieg (1987) in a plasticity model for rigid polyurethane foam. This criterion has a yield function given by

$$\Psi^i = \tfrac{1}{2}\boldsymbol{\sigma} : \mathbf{P}^i : \boldsymbol{\sigma} - h(\epsilon^p) \qquad i = 1,2,3 \tag{3.25}$$

where $\mathbf{P}^i$ is a fourth-order principal projection operator given by

$$\mathbf{P}^i = \mathbf{n}^i \otimes \mathbf{n}^i \otimes \mathbf{n}^i \otimes \mathbf{n}^i \tag{3.26}$$

and $\mathbf{n}^i$ is a unit vector oriented in a principal stress direction. This yield function actually represents six different yield surfaces with normals to the principal stress axes as shown in Figure 3.3.

The flow law is given by

$$\dot{\epsilon}^p = \dot{\rho}^i \mathbf{P}^i : \boldsymbol{\sigma} \tag{3.27}$$

where the repeated indices imply summation. This flow law indicates that plastic strain increments may be associated with each principal stress direction.

Cellular solids generally exhibit both plastic deformation and stiffness changes. Plasticity models predict permanent deformations but assume that the stiffness of the material does not change. Thus, a combination of plasticity theories and continuum damage theories, which predict stiffness changes, are needed for cellular materials. In the next section, continuum damage theories which have a structure similar to existing plasticity theories are presented.
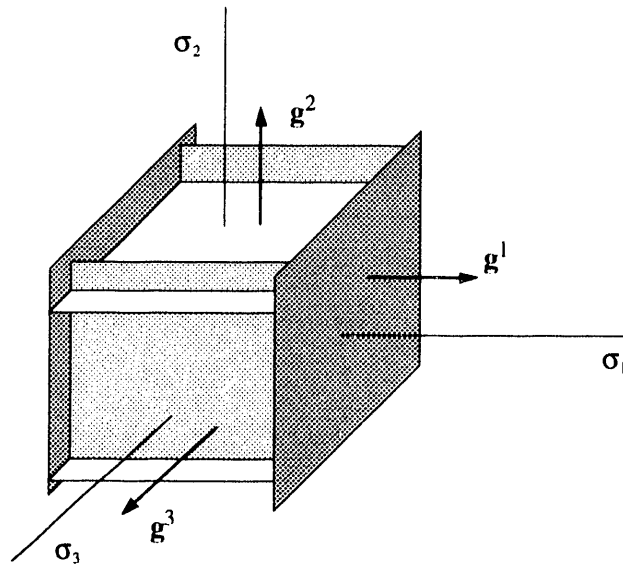
Figure 3.3. Principal Stress Yield Surface.

3.3 Continuum Damage

Continuum damage theories were developed to mathematically describe the progressive reduction in stiffness and strength of brittle materials resulting from the initiation and growth of microcracks and microvoids. These theories have been used to describe the nucleation and growth of microcracks and microvoids in metals and the formation of microcracks in concrete, rocks and ceramics (Kachanov, 1986; Krajcinovic, 1989). An important assumption implicit in these models is that the cracks are small and distributed such that the cracked material can be logically represented by an equivalent continuum with damage. When the cracks are large, fracture mechanics is used to predict the formation and growth of large individual cracks. However, when there are a large number of small cracks it rapidly becomes impossible to follow the formation and growth of each crack; thus, a continuum damage theory is used.

For the development of continuum damage theories, consider the following expression for the strain energy function, U,

$$U = U(\epsilon, \mathbf{S}) = \tfrac{1}{2}\epsilon : \mathbf{S} : \epsilon \tag{3.28}$$

where $\mathbf{S}$ is the fourth-order damaged elastic stiffness tensor which is equal to the elasticity tensor, $\mathbf{E}$, when the material is undamaged and changes as the material is damaged. The Clausius-Duhem dissipation inequality can be written as

$$\sigma : \dot{\epsilon} - \frac{\partial U}{\partial \epsilon} : \dot{\epsilon} - \frac{\partial U}{\partial \mathbf{S}} :: \dot{\mathbf{S}} \geq 0 \tag{3.29}$$

Using the constitutive relation

$$\sigma = \frac{\partial U}{\partial \epsilon} = \mathbf{S} : \epsilon \tag{3.30}$$

and an expression for the dissipation rate, $\dot{D}$,

$$\dot{D} = -\frac{\partial U}{\partial \mathbf{S}} :: \dot{\mathbf{S}} = -\tfrac{1}{2}\epsilon : \dot{\mathbf{S}} : \epsilon \tag{3.31}$$

the Clausius-Duhem inequality is again given by $\dot{D} \geq 0$. Next, if we introduce an evolution equation for the rate of change in elastic stiffness

$$\dot{\mathbf{S}} = -\dot{\omega}\mathbf{R} \tag{3.32}$$

where $\dot{\omega}$ in some sense represents the increment in damage and $\mathbf{R}$ represents the orientation of the damage increment. The dissipation rate is then given by

$$\dot{D} = \frac{\dot{\omega}}{2}\epsilon : \mathbf{R} : \epsilon \tag{3.33}$$

Using a procedure analogous to that of plasticity, we assume that a damage surface exists and separates elastic and damaging processes. The damage surface is mathematically described by a damage function, Ψ,

$$\Psi = \frac{1}{2}\epsilon : \mathbf{Q} : \epsilon - g(\mathbf{S}, \epsilon) \tag{3.34}$$

29

where $\mathbf{Q}$ is some fourth-order tensor and g is some positive function. When Ψ is less than zero the behavior is elastic and when Ψ is equal to zero the behavior may be damaging. As with plasticity, the thermodynamical constraint for dissipation to accompany damage can be satisfied with appropriate selections for the damage function and damage evolution equation. For example, if we use the damage evolution equation given by Equation 3.32 and let $\mathbf{Q}$ equal $\mathbf{R}$ in the damage function, Equation 3.34, then dissipation will always accompany damage.

The damage function given by Equation 3.34 is expressed in terms of strain which implies that the damage function represents a surface in strain space; however, if one is opposed to working in strain space the damage function can always be expressed in terms of stress. For example, choose

$$\mathbf{Q} = \mathbf{S} : \mathbf{P} : \mathbf{S} \tag{3.35}$$

then

$$\Psi = \frac{1}{2}\boldsymbol{\sigma} : \mathbf{P} : \boldsymbol{\sigma} - g(\mathbf{S}, \epsilon) \tag{3.36}$$

We could also use an evolution equation for the compliance of the material, $\mathbf{C}$, in place of the evolution equation for the stiffness given by Equation 3.32. Since $\mathbf{C} : \mathbf{S} = \mathbf{I}$, the evolution equations for stiffness and compliance must be related as follows

$$\dot{\mathbf{C}} = -\mathbf{C} : \dot{\mathbf{S}} : \mathbf{C} \tag{3.37}$$

Evolution equations which would be appropriate for the damage function given by Equation 3.36 are

$$\dot{\mathbf{S}} = -\dot{\omega}\mathbf{S} : \mathbf{P} : \mathbf{S} \qquad or \qquad \dot{\mathbf{C}} = \dot{\omega}\mathbf{P} \tag{3.38}$$

Thus, for damage functions in stress space it may be easier to use evolution equations for compliance. At this point, we have placed no restrictions on the forms for $\mathbf{Q}$ and $\mathbf{R}$ and have simply stated that they should be chosen such that the thermodynamical restriction for dissipation to accompany damage is satisfied.

3.3.1 Simple Scalar Damage

Most existing continuum damage models are scalar damage models. For these models the orientation of the damage is given by some fixed fourth-order tensor. One of the simplest scalar damage models has a damage function given by

$$\Psi = \frac{1}{2}\epsilon : \mathbf{E} : \epsilon - h(\mathbf{S}, \epsilon) \tag{3.39}$$

and an evolution equation for the elastic stiffness tensor given by

$$\dot{\mathbf{S}} = -\dot{\omega}\mathbf{E} \tag{3.40}$$

where $\mathbf{E}$ is the isotropic elastic stiffness tensor given by Equation 3.3. This evolution equation indicates that the damage orientation is given by the original undamaged elastic

30

stiffness tensor. With this evolution equation, the current elastic stiffness tensor, $\mathbf{S}$, is related to the undamaged elastic stiffness tensor, $\mathbf{E}$, as follows

$$\mathbf{S} = (1 - \omega)\mathbf{E} \qquad (3.41)$$

Since the elastic stiffness tensor, $\mathbf{E}$, is isotropic, the damaged elastic stiffness tensor, $\mathbf{S}$, is also isotropic. As the material is damaged, the elastic modulus is degraded as follows

$$E = (1 - \omega)E^o \qquad (3.42)$$

where E and E^o are the elastic moduli for the damaged and original undamaged material, respectively. With this model, information about the current damaged state is stored in a single scalar, E. This continuum damage model is quite simple; however, the appropriateness of this model for any damaging materials has not been demonstrated because Equation 3.41 implies that Poisson's ratio remains unchanged.

3.3.2 von Mises Damage

Next consider a scalar damage model which has the same yield function as a von Mises plasticity model written as follows

$$\Psi = \tfrac{1}{2}\boldsymbol{\sigma} : \mathbf{P}^d : \boldsymbol{\sigma} - g^2(\mathbf{S}) \qquad (3.43)$$

On the surface, this yield function looks different than the yield function given by Equation 3.20. However, both Equation 3.20 and this equation represent a yield surface that is an infinitely long cylinder in principal stress space as shown in Figure 3.2. An appropriate damage evolution equation for this model is given by

$$\dot{\mathbf{S}} = -\dot{\omega}\mathbf{S} : \mathbf{P}^d : \mathbf{S} = -4\dot{\omega}G^2\mathbf{P}^d \qquad (3.44)$$

where G represents the damaged shear modulus for the material. For this model the damage history is stored in the single scalar G. A von Mises plasticity model is characterized by deviatoric plastic strains and no change in the volumetric response of the material. Likewise, a von Mises damage model is characterized by reductions in the shear stiffness of the material and no change in the volumetric stiffness of the material.

3.3.3 Principal Stress Damage

Next, consider the principal stress criterion of Rankine which has damage functions given by

$$\Psi^i = \tfrac{1}{2}\boldsymbol{\sigma} : \mathbf{P}^i : \boldsymbol{\sigma} - h(\mathbf{S}) \qquad i = 1, 2, 3 \qquad (3.45)$$

where $\mathbf{P}^i$ is again the fourth-order principal projection operator. The damage evolution equations for this model are chosen to be

$$\dot{\mathbf{S}} = -\dot{\omega}^i\mathbf{S} : \mathbf{P}^i : \mathbf{S} \qquad or \qquad \dot{\mathbf{C}} = \dot{\omega}^i\mathbf{P}^i \qquad (3.46)$$

where the repeated indices imply summation. This model is not a simple scalar damage model and information about damage is not stored in a single scalar because the orientation of the damage, specifically, $\mathbf{P}^i$, can change during a loading process. For this model, information about the current damaged state is stored in the damaged elastic stiffness tensor, $\mathbf{S}$, or the damaged compliance tensor, $\mathbf{C}$.

3.3.4 Principal Strain Damage

Finally, consider a principal strain criterion which has recently been used by Bazant and Lin (1988) to describe the behavior of concrete. This model is able to predict the formation of vertical cracks in concrete specimens subjected to uniaxial compression. This model has damage functions given by

$$\Psi^i = \tfrac{1}{2}\epsilon : \mathbf{P}^i : \epsilon - h(\mathbf{S}) \qquad i = 1,2,3 \tag{3.47}$$

where $\mathbf{P}^i$ is again the fourth-order principal projection operator; however, now the $\mathbf{n}^i$ used in the definition of $\mathbf{P}^i$ in Equation 3.26 are vectors oriented in a principal strain direction. Bazant and Lin's (1988) crack band model uses a damage evolution equation given by

$$\dot{\mathbf{C}} = \dot{\omega}^i \mathbf{P}^i \tag{3.48}$$

The interesting characteristic of this model is that for certain load paths this model will predict damage without dissipation. For example, under uniaxial compression lateral tensile strains are generated and damage is predicted but the dissipation equation

$$\dot{D} = \dot{\omega}^i \tfrac{1}{2}\sigma : \mathbf{P}^i : \sigma \tag{3.49}$$

indicates that no dissipation is generated. This model could be improved by simply using a different damage evolution equation. For example, if one of the following damage evolution equations is used with the damage function given by Equation 3.47, then dissipation will accompany damage for all load paths.

$$\dot{\mathbf{S}} = -\dot{\omega}^i \mathbf{P}^i \qquad or \qquad \dot{\mathbf{C}} = \dot{\omega}^i \mathbf{C} : \mathbf{P}^i : \mathbf{C} \tag{3.50}$$

This brief review of principal strain models clearly shows that evolution equations and damage functions cannot be selected arbitrarily. The examples in this section show that damage theories which are analogous to plasticity theories can be developed using a similar framework. In the next section, we explore theories in which continuum damage is coupled with plasticity.

3.4 Coupled Theories

If both damage and plastic deformation are generated then the developments presented in the previous sections must be modified to capture the coupling. The strain energy function is now given by

$$U = U(\epsilon, \epsilon^p, \mathbf{S}) = \tfrac{1}{2}(\epsilon - \epsilon^p) : \mathbf{S} : (\epsilon - \epsilon^p) \tag{3.51}$$

The Clausius-Duhem inequality becomes

$$\boldsymbol{\sigma} : \dot{\epsilon} - \frac{\partial U}{\partial \epsilon} : \dot{\epsilon} - \frac{\partial U}{\partial \epsilon^p} : \dot{\epsilon}^p - \frac{\partial U}{\partial \mathbf{S}} :: \dot{\mathbf{S}} \geq 0 \tag{3.52}$$

The constitutive relation is given by

$$\boldsymbol{\sigma} = \frac{\partial U}{\partial \epsilon} \tag{3.53}$$

and the dissipation rate by

$$\dot{D} = -\frac{\partial U}{\partial \mathbf{S}} :: \dot{\mathbf{S}} - \frac{\partial U}{\partial \epsilon^p} : \dot{\epsilon}^p = -\frac{1}{2}(\epsilon - \epsilon^p) : \dot{\mathbf{S}} : (\epsilon - \epsilon^p) + \boldsymbol{\sigma} : \dot{\epsilon}^p \tag{3.54}$$

If we introduce evolution equations for both the fourth-order elastic stiffness tensor and the second-order plastic strain tensor as follows:

$$\dot{\mathbf{S}} = -\dot{w}\mathbf{R} \qquad \dot{\epsilon}^p = \dot{\rho}\mathbf{g} \tag{3.55}$$

then the dissipation rate is given by

$$\dot{D} = \dot{\rho}\boldsymbol{\sigma} : \mathbf{g} + \frac{\dot{w}}{2}(\epsilon - \epsilon^p) : \mathbf{R} : (\epsilon - \epsilon^p) \tag{3.56}$$

At this point we could choose a yield surface for the plasticity part that is independent from the damage surface and require that both terms in Equation 3.56 satisfy the dissipation inequality. This would certainly be a sufficient condition. However for many materials, it seems reasonable to expect that damage will only be generated when permanent strains are generated which implies that for such materials the damage and yield surfaces are the same. Even with this assumption, there is still a significant amount of latitude in choosing appropriate evolution equations for permanent strain and damage.

For example, if we choose a yield function given by

$$\Psi = \boldsymbol{\sigma} : \mathbf{P} : \boldsymbol{\sigma} - g(\epsilon, \epsilon^p, \mathbf{S}) \tag{3.57}$$

where g is some positive function, and a damage evolution equation and flow law given by

$$\dot{\mathbf{S}} = -\dot{w}\mathbf{S} : \mathbf{P} : \mathbf{S} \qquad \dot{\epsilon}^p = \dot{\rho}\mathbf{P} : \boldsymbol{\sigma} \tag{3.58}$$

then the dissipation rate is given by

$$\dot{D} = (\dot{\rho} + \dot{\omega})\boldsymbol{\sigma} : \mathbf{P} : \boldsymbol{\sigma} \qquad (3.59)$$

Use of the yield function given by Equation 3.57 and the evolution equations given by Equation 3.58 will ensure that mechanical dissipation is generated whenever damage or plastic deformation is generated. An interesting feature of this coupled theory is that ρ and ω are not required to monotonically increase as long as the sum of the two terms does. What this means is that stiffness of the material could actually be increasing while plastic deformation is being generated and the theory would still be thermodynamically acceptable. The requirement that damage monotonically increases is only applicable to damage only theories; however, for most materials that exhibit both damage and permanent strain it may still be appropriate based on physical arguments to assume that damage is not a reversible process even though the assumption of irreversibility is not required.

To complete this coupled theory we need an additional equation to determine the relative amounts of damage and plastic strain generated during a given step. For example, we could postulate a relationship of the form

$$M\dot{\rho} = (1 - M)\dot{\omega} \qquad (3.60)$$

where M is some material parameter obtained from experimental observations. When M is equal to zero the theory represents a plasticity only theory since $\dot{\omega}$ is equal to zero and when M is equal to one, the theory reduces to a damage only theory. When M is between zero and one both permanent strains and damage are generated when the material is loaded into the inelastic regime.

3.4.1 Simple Scalar Damage Coupled with Plasticity

Most damage models are simple isotropic, scalar damage models. One of the simplest scalar damage models has a damage function give by Equation 3.39 which can also be written as

$$\Psi = \boldsymbol{\sigma} : \mathbf{C} : \boldsymbol{\sigma} - g(\mathbf{S}, \boldsymbol{\epsilon}, \boldsymbol{\epsilon}^p) \qquad (3.61)$$

where $\mathbf{C}$ is the compliance tensor and is equal to the inverse of the damaged elasticity tensor, $\mathbf{S}$. For this model, the evolution equations for plastic strain and damage are given by

$$\dot{\boldsymbol{\epsilon}}^p = \dot{\rho}\mathbf{C} : \boldsymbol{\sigma} = \dot{\rho}(\boldsymbol{\epsilon} - \boldsymbol{\epsilon}^p) \qquad \dot{\mathbf{S}} = -\dot{\omega}\mathbf{E} \qquad (3.62)$$

where the relationship between $\dot{\rho}$ and $\dot{\omega}$ is given by Equation 3.60. With this model, the orientation of the plastic strain increment is given by the elastic strain tensor, $\boldsymbol{\epsilon}^E = (\boldsymbol{\epsilon} - \boldsymbol{\epsilon}^p)$.

34

3.4.2 von Mises

Next consider a coupled von Mises theory with a damage (yield) function given by

$$\Psi = \tfrac{1}{2}\boldsymbol{\sigma} : \mathbf{P}^d : \boldsymbol{\sigma} - g^2(\epsilon^p) \tag{3.63}$$

The flow rule and damage evolution equation are given by

$$\dot{\boldsymbol{\epsilon}}^p = \dot{\rho}\mathbf{P}^d : \boldsymbol{\sigma} \qquad \dot{\mathbf{E}} = -\dot{\omega}4G^2\mathbf{P}^d \tag{3.64}$$

As expected, this coupled model is characterized by deviatoric plastic strains, reductions in the shear stiffness, and a linear elastic volumetric response.

3.4.3 Principal Stress

Finally, consider a principal stress criterion of Rankine that was recently used in a plasticity model for polyurethane foams by Neilsen, Morgan and Krieg (1987). If we wanted to develop a coupled model based on this same criterion we would use a damage (yield) function given by

$$\Psi^i = \tfrac{1}{2}\boldsymbol{\sigma} : \mathbf{P}^i : \boldsymbol{\sigma} - h(\boldsymbol{\epsilon}, \boldsymbol{\epsilon}^p, \mathbf{S}) \tag{3.65}$$

where $\mathbf{P}^i$ is again the fourth-order principal projection operator. One possible choice for the plastic and damage flow rules would be

$$\dot{\boldsymbol{\epsilon}}^p = \dot{\rho}^i\mathbf{P}^i : \boldsymbol{\sigma} \qquad \dot{\mathbf{S}} = -\dot{\omega}^i\mathbf{S} : \mathbf{P}^i : \mathbf{S} \tag{3.66}$$

These examples show that coupled theories can be easily developed using the general framework presented in this section.

4. BIFURCATIONS AND LOCALIZATION

When materials are loaded into an inelastic regime, small regions of intense deformation often develop at some point in the loading process. This intense localized deformation limits the formability of materials and will often quickly lead to failure with continued loading. Localization is often associated with satisfaction of the classical discontinuous bifurcation criterion (Hill, 1962; Rice, 1976). Here we propose that the loss of strong ellipticity criterion should be used in place of the classical discontinuous bifurcation criterion as a necessary condition for localization. The application of the strong ellipticity criterion implies that a bifurcation mode associated with loss of positive definiteness of the symmetric part of the acoustic tensor must be identified rather than a mode associated with the first zero eigenvalue of the acoustic tensor itself. The eigensystem for the symmetric part of the tangent stiffness tensor is obtained for several different plasticity and continuum damage models. This eigensystem provides information about deformation modes associated with both diffuse and discontinuous bifurcations. Material properties, boundary conditions, and body geometry are all shown to affect the diffuse and localized deformation modes that are generated. Numerous experimental observations of necking and localization in metal specimens subject to various boundary conditions are explained with a bifurcation analysis of a von Mises plasticity model. Finally, bifurcation analyses are performed on constitutive theories which may be appropriate for cellular solids.

4.1 Introduction to Bifurcation Criteria

Necessary but not sufficient conditions for general and discontinuous bifurcations, loss of uniqueness, and localized deformation of elastic-plastic materials have been previously developed. A necessary condition for loss of material stability, loss of uniqueness and a general bifurcation in the solution is the loss of positive definiteness of the rate of second order work (Drucker, 1950; Hill, 1958). This general bifurcation criterion can also be expressed as loss of positive definiteness of the symmetric part of the tangent stiffness tensor. In general, the strain eigentensor, or mode, associated with a general bifurcation will not have a kinematically compatible form. Thus, the mode can only exist in a zone described as a point or surface, i.e., a domain of measure zero. Such a mode cannot exist in any real sense without affecting the stress state in the surrounding material and is usually referred to as a diffuse mode which initiates smooth changes in the deformation field such as necking.

Valanis (1989) states that loss of material stability should be associated with the limit point where the tangent stiffness tensor obtains a zero eigenvalue. This would be appropriate if one considers only statically determinate specimens with force prescribed

systems. For materials with symmetric tangent stiffness tensors, the Valanis (1989) and Drucker (1950) interpretations both identify the limit point as the point at which necessary conditions for loss of material stability are first satisfied. For materials with unsymmetric tangent stiffness tensors, loss of positive definiteness of the symmetric part of the tangent stiffness tensor and satisfaction of the necessary condition for a general bifurcation can occur prior to the limit point.

Hill (1962), Mandel (1966), and Rudnicki and Rice (1975) have suggested that loss of material stability and localization does not occur until the acoustic tensor has a zero eigenvalue. This acoustic tensor is dependent on both an orientation vector and on the material. There are two reasons why this definition is more appropriate than the one involving only the tangent stiffness tensor. First, this condition identifies the point where the character of the differential equations changes (loss of ellipticity) and, second, the mode is associated with a strain rate jump within a planar band that does not lead to any kinematic incompatibilities with the surrounding material. Since the mode can be interpreted as a jump in strain rate within a band over the strain rate in the surrounding material, the mode is called a discontinuous bifurcation. Localized deformations associated with discontinuous bifurcations may initiate on a domain indefinite in extent. Evolution of the domain can only be controlled if additional constraints such as that provided by a non-local constitutive theory are present (Schreyer, 1990b). A spectral analysis of the acoustic tensor is rather difficult, although recent work in this area by Ottosen and Runesson (1991), Bigoni and Hueckel (1991), and Runesson, Ottosen and Peric (1991) appears encouraging.

Ottosen and Runesson (1991) state that loss of strong ellipticity of the governing differential equations occurs whenever positive definiteness of the symmetric part of the acoustic tensor is lost. When the tangent stiffness tensor and thus the acoustic tensor are symmetric, loss of strong ellipticity and satisfaction of the classical necessary condition for a discontinuous bifurcation will first occur at the same point. However, for non-symmetric acoustic tensors, loss of strong ellipticity will precede satisfaction of the necessary condition for a classical discontinuous bifurcation. In addition to the loss of positive definiteness of the acoustic tensor, loss of strong ellipticity can also be interpreted as satisfaction of the general bifurcation condition with an associated strain rate which is of a form suitable for providing a kinematically compatible velocity field (Bigoni and Hueckel, 1991). Here we postulate that localization should be associated with the loss of strong ellipticity.

An eigenanalysis of the symmetric part of the tangent stiffness tensor provides a wealth of information about deformation modes associated with both diffuse and discontinuous bifurcations. The necessary condition for a general bifurcation is first satisfied when the fundamental eigenvalue of the symmetric part of the tangent stiffness tensor obtains a value of zero. The deformation mode associated with this bifurcation is characterized by the fundamental eigentensor. Discontinuous bifurcations are investigated by choosing a mode which satisfies the general bifurcation criterion and is restricted to be of a form

normally associated with a discontinuous bifurcation. The mode is expressed as a linear combination of the eigentensors associated with the symmetric part of the tangent stiffness tensor. With this approach there is no need to explicitly determine or analyze the acoustic tensor. By interpreting the problem of material stability as an eigensystem problem in the presence of a constraint, we automatically establish the structure for incorporating additional constraints, such as plane strain, which may be present because of external loading and boundary conditions. The presence of additional constraints automatically infer that the usual procedure of finding the first zero eigenvalue of the acoustic tensor may not be an indicator of localization.

The approach used is to determine the spectral decomposition of the symmetric part of the tangent stiffness tensor. For conventional elastic-plastic models this decomposition is straightforward and explicit linear combinations of eigentensors can be obtained to show satisfaction of constraints which reduce to linear algebraic equations of the eigentensors. Some of the constraints can only be satisfied if the fundamental eigenvalue is negative which only occurs when plasticity models with associated flow rules exhibit strain softening. The degree of softening, if any, required to meet the constraint condition depends on the particular loading path being considered.

With the insight provided by this approach, we show that features exhibited by a number of classical experiments can be easily explained using simple constitutive models. The failure modes of a material subject to various constraints can provide valuable confirmation of the suitability of a constitutive model. For simplicity, we confine our attention to rate and temperature independent material behavior and infinitesimal deformations.

4.1.1 General Bifurcations

Drucker (1950, 1959) postulated that the stability of a material could be evaluated by considering the work done by an external agency. A material is stable (will remain in equilibrium) if a) positive work is done by the external agency during the application of the set of stresses and b) the net work done by it over a cycle of application and removal is zero or positive. If plastic deformation is generated during the cycle then the net work must be non-zero. These statements indicate that a necessary condition for loss of material stability is

$$\dot{\epsilon} : \dot{\sigma} = 0 \qquad (4.1)$$

where $\dot{\sigma}$ and $\dot{\epsilon}$ are perturbations to the stress and strain rate fields at some point or region in the body due to the external agency. Equation 4.1 was shown by Hill (1958) to be a necessary condition for a bifurcation and loss of uniqueness. This general bifurcation criterion, Equation 4.1, can also be written as

$$\dot{\epsilon} : \mathbf{D}^s : \dot{\epsilon} = 0 \qquad (4.2)$$

where $\mathbf{D}^s$ is the symmetric part of the tangent stiffness tensor, $D^s_{ijkl} = \frac{1}{2}(D_{ijkl} + D_{klij})$. Equation 4.2 indicates that general bifurcations may occur whenever $\mathbf{D}^s$ is not positive definite.

4.1.2 Limit Point Bifurcations

General bifurcations are usually associated with changes in the stress state both inside and outside the bifurcation zone. The subset of general bifurcations associated with no change in the stress state occur only at the limit point when

$$\mathbf{D} : \dot{\epsilon} = 0 \qquad or \qquad det(\mathbf{D}) = 0 \qquad (4.3)$$

or, in other words, when the tangent stiffness tensor $\mathbf{D}$ has a zero eigenvalue. Valanis (1989) recently suggested that Equation 4.3 is a necessary and sufficient condition for loss of material stability. His interpretation assumes that the general bifurcation associated with the limit point is always activated. This interpretation is only valid when the tangent stiffness tensor is symmetric and tractions are prescribed everywhere on the boundary of a specimen. If constraints are present, the general bifurcation associated with the limit point may not be activated, and it becomes necessary to evaluate other potential general and discontinuous bifurcations. Here we adopt the classical necessary condition for a general bifurcation given by Equation 4.2.

4.1.3 Classical Discontinuous Bifurcations

Criteria for discontinuous bifurcations in elastic-plastic materials with associated flow rules follow from Hadamard's (1903) studies of elastic stability and were developed by Hill (1962). Later, Mandel (1966), Rice (1976), Rice and Rudnicki (1975, 1980), Raniecki and Bruhns (1981), and Ottosen and Runesson (1991) used Hill's criterion to investigate discontinuous bifurcations in elastic-plastic materials with non-associated flow rules.

Consider a homogeneous solid subjected to monotonic, proportional loading. We wish to determine at what point in the loading process a discontinuous bifurcation can occur such that subsequent strain rates become discontinuous across parallel planes of orientation n that separate a zone of localized deformation from the rest of the body. Maxwell's compatibility conditions require that the strain rate in the localized zone, $\dot{\epsilon}^l$, be of the form

$$\dot{\epsilon}^l = \dot{\epsilon}^o + \dot{\epsilon}^k \qquad with \qquad \dot{\epsilon}^k = \tfrac{1}{2}(\mathbf{m} \odot \mathbf{n} + \mathbf{n} \odot \mathbf{m}) \qquad (4.4)$$

where $\dot{\epsilon}^o$ is the strain rate outside the localized zone, $\dot{\epsilon}^k$ is a kinematically admissible discontinuous mode, and $\mathbf{m}$ can be interpreted as a vector that represents the orientation of the relative velocity of regions on opposite sides of the localized deformation zone due to the introduction of the localized deformation.

Assume that the entire body is being plastically deformed, the stress and strain components are uniform throughout, and the body is at the onset of localization. With the assumption of rate-independent behavior, the stress rates inside and outside the localized zone are given by

$$\dot{\sigma}^l = \mathbf{D}^l : \dot{\epsilon}^l \qquad and \qquad \dot{\sigma}^o = \mathbf{D}^o : \dot{\epsilon}^o \qquad (4.5)$$

40

where $\mathbf{D}^i$ and $\mathbf{D}^o$ are the tangent stiffness tensors for material inside and outside the localized deformation zone, respectively. For continuing equilibrium, the traction rates must be continuous across the boundaries of the localized deformation zone:

$$\dot{\mathbf{t}}^i = \dot{\mathbf{t}}^o \qquad or \qquad \mathbf{n} \cdot (\dot{\boldsymbol{\sigma}}^i - \dot{\boldsymbol{\sigma}}^o) = \mathbf{0} \tag{4.6}$$

By combining these equations, Rice (1976) shows that the requirement for continuing equilibrium is given by

$$\mathbf{n} \cdot (\mathbf{D}^i - \mathbf{D}^o) : \dot{\boldsymbol{\epsilon}}^o + \mathbf{Q} \cdot \mathbf{m} = \mathbf{0} \tag{4.7}$$

where

$$\mathbf{Q} = \mathbf{n} \cdot \mathbf{D}^i \cdot \mathbf{n} \tag{4.8}$$

is the acoustic tensor.

Suppose the body is loaded such that the strain rate $\dot{\boldsymbol{\epsilon}}^o$ is constrained to evolve continuously. Then it is reasonable to assume that the tangent stiffness tensor for material outside the localized zone, $\mathbf{D}^o$, is identical to the tangent stiffness tensor for material inside the localized zone, $\mathbf{D}^i$, at the initiation of the bifurcation. The classical necessary condition for a discontinuous bifurcation is then obtained from Equation 4.7:

$$\mathbf{Q} \cdot \mathbf{m} = \mathbf{0} \qquad or \qquad det(\mathbf{Q}) = 0 \tag{4.9}$$

In other words, the classical criterion for a discontinuous bifurcation is that the acoustic tensor, $\mathbf{Q}$, has a zero eigenvalue, a necessary condition for loss of ellipticity (Rice, 1976).

4.1.4 Loss of Strong Ellipticity

The classical discontinuous bifurcation criterion is based on two important assumptions. The first assumption is that the discontinuity in the strain rate field is constrained to have a special form so that material in the localized zone will remain kinematically compatible with the surrounding material. The second assumption is that the strain rates evolve continuously such that the tangent stiffness tensor for material inside the localized zone is identical to the tangent stiffness tensor for material outside the localized zone during the initiation of the localized zone. The general bifurcation criterion requires neither of these assumptions. Specifically, a general bifurcation will not necessarily be associated with a mode which has the special form of $\dot{\boldsymbol{\epsilon}}^k$ in Equation 4.4 and the active tangent stiffness tensors for material inside and outside the bifurcation zone will not necessarily be identical.

The general bifurcation criterion, Equation 4.2, is a necessary condition for any type of bifurcation. A necessary condition for a general bifurcation with a kinematically compatible mode, $\dot{\boldsymbol{\epsilon}}^k$, is the loss of strong ellipticity criterion (Bigoni and Hueckel, 1991)

$$\dot{\boldsymbol{\epsilon}}^k : \mathbf{D}^s : \dot{\boldsymbol{\epsilon}}^k = 0 \qquad \Rightarrow \qquad \mathbf{m} \cdot \mathbf{Q}^s \cdot \mathbf{m} = 0. \tag{4.10}$$

41

We adopt loss of strong ellipticity as a necessary condition for localization because this criterion identifies the first possible bifurcation with a kinematically compatible mode.

The requirement for continuing equilibrium, Equation 4.7, may be satisfied when loss of strong ellipticity occurs if the continuity constraint (in time) on $\dot{\epsilon}^o$ is relaxed. For example, let $\mathbf{Q}$ be decomposed into its symmetric, $\mathbf{Q}^s$, and antisymmetric, $\mathbf{Q}^u$, parts:

$$\mathbf{Q} = \mathbf{Q}^s + \mathbf{Q}^u \tag{4.11}$$

Loss of strong ellipticity, Equation 4.10, will first occur when

$$\mathbf{Q}^s \cdot \mathbf{m} = \mathbf{0} \qquad or \qquad det(\mathbf{Q}^s) = 0 \tag{4.12}$$

since $\mathbf{Q}^s$ is positive, semi-definite at this point. This criterion, Equation 4.12, will be satisfied prior to or at the same time as the classical discontinuous bifurcation criterion of Equation 4.9. If no external constraint is placed on $\dot{\epsilon}^o$ other than compatibility, then $\dot{\epsilon}^o$ is free to adjust such that the continuing equilibrium equation

$$\mathbf{n} \cdot (\mathbf{D}^i - \mathbf{D}^o) : \dot{\epsilon}^o + \mathbf{Q}^u \cdot \mathbf{m} = \mathbf{0} \tag{4.13}$$

is satisfied when the loss of strong ellipticity criterion is satisfied. This means that a discontinuous bifurcation may occur when the loss of strong ellipticity criterion is satisfied and $\dot{\epsilon}^o$ is not constrained.

4.1.5 Summary of Bifurcation Criteria

The criteria for diffuse and discontinuous bifurcations are summarized in Table 4.1. The general bifurcation criterion is first satisfied when the determinant of the symmetric part of the tangent stiffness tensor is equal to zero. For materials with associated flow, the tangent stiffness tensor is symmetric and the general and limit point bifurcation criteria both identify the limit point as the first point at which a diffuse bifurcation may occur. However, for materials with non-associated flow the general bifurcation criterion indicates that diffuse bifurcations may occur in the hardening regime.

Table 4.1. Summary of Bifurcation Criteria.

CRITERIA	EQUATION	MODE
General	$\dot{\epsilon} : \mathbf{D}^s : \dot{\epsilon} = 0$	Diffuse, Necking
Limit Point	$\mathbf{D} : \dot{\epsilon} = \mathbf{0}$	Diffuse, Necking
Strong Ellipticity	$\mathbf{m} \cdot \mathbf{Q}^s \cdot \mathbf{m} = 0$	Localized
Classical Discontinuous	$\mathbf{Q} \cdot \mathbf{m} = \mathbf{0}$	Localized

The strong ellipticity criterion is first satisfied when the determinant of the symmetric part of the acoustic tensor is equal to zero. For materials with associated flow rules, the strong ellipticity and classical discontinuous bifurcation criteria identify the same

first discontinuous bifurcation point. However, for materials with non-associated flow the strong ellipticity criterion will predict that localization may occur prior to the point identified by the classical discontinuous bifurcation criterion.

Discontinuous bifurcations are a subset of general bifurcations and classical discontinuous bifurcations are a subset of those discontinuous bifurcations which satisfy the loss of strong ellipticity criterion. Constraints may inhibit the activation of certain possible bifurcation modes for which the necessary but not sufficient conditions given in the previous section have been satisfied.

4.2 Characterization of Bifurcation Modes

Bifurcation modes, $\dot{\epsilon}$, represent perturbations to a homogeneous strain rate field that may be activated whenever the necessary conditions presented in the previous section are satisfied. Any bifurcation mode, $\dot{\epsilon}$, can be characterized by its three eigenvalues, $\lambda_1 \leq \lambda_2 \leq \lambda_3$. Modes associated with discontinuous bifurcations are restricted to be of the kinematically compatible form, $\dot{\epsilon}^k$, given in Equation 4.4. Suppose we choose a local coordinate system with coordinate x_1 parallel and coordinates x_2 and x_3 perpendicular to n such that the components of n and m are

$$\mathbf{n} \Rightarrow \left\{ \begin{array}{c} 1 \\ 0 \\ 0 \end{array} \right\} \qquad \mathbf{m} \Rightarrow \left\{ \begin{array}{c} \alpha \\ 2\beta \\ 0 \end{array} \right\} \tag{4.14}$$

The components of the corresponding discontinuous bifurcation mode, $\dot{\epsilon}^k$, are

$$\dot{\epsilon} \Rightarrow \begin{bmatrix} \alpha & \beta & 0 \\ \beta & 0 & 0 \\ 0 & 0 & 0 \end{bmatrix} \tag{4.15}$$

When β is equal to zero, the relative velocity of the bodies is oriented in a direction normal to the zone, and the strain rate jump in the zone represents an opening mode (Figure 4.1). When α is equal to zero, the strain rate jump represents a shearing mode. Also, note that $\dot{\epsilon}$ has eigenvalues of $\alpha/2 \pm \sqrt{\alpha^2/4 + \beta^2}$ and zero. Thus, a discontinuous bifurcation mode has a fundamental eigenvalue, λ_1, that is less than or equal to zero, an intermediate eigenvalue, λ_2, that is equal to zero, and a third eigenvalue, λ_3, that is greater than or equal to zero.

Modes associated with general bifurcations can be any symmetric second-order tensor as long as the necessary condition for a general bifurcation, Equation 4.2, is satisfied. For example, a general bifurcation mode could have components obtained as a slight generalization of Equation 4.15:

$$\dot{\epsilon} \Rightarrow \begin{bmatrix} \alpha & \beta & 0 \\ \beta & 0 & 0 \\ 0 & 0 & \rho \end{bmatrix} \tag{4.16}$$

43

(a) opening mode   (b) shearing mode
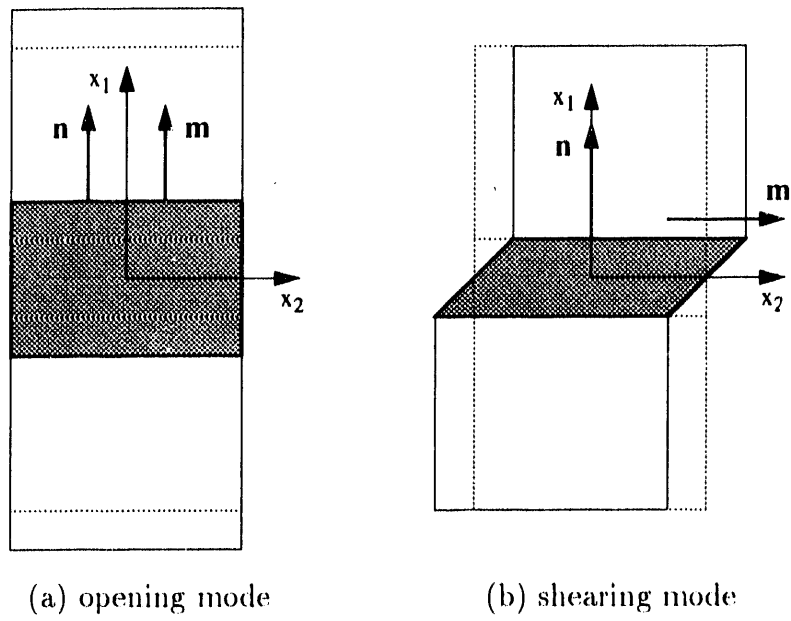
Figure 4.1. Discontinuous Bifurcation Modes.
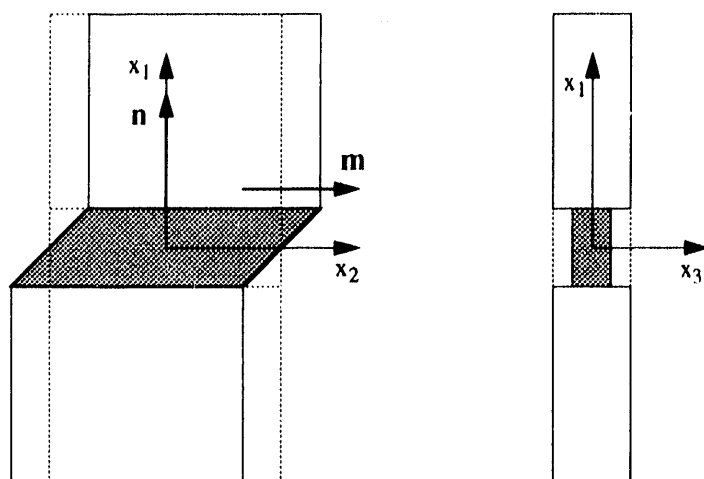
Figure 4.2. General Bifurcation Mode.

An analysis in the $x_1 - x_2$ plane can be performed as before for a discontinuous bifurcation with the origin of x_3 at the surface of a possible discontinuity; however, now an incompatibility in the velocity field exists for points $x_3 \neq 0$ which are not in the $x_1 - x_2$ plane (Figure 4.2). There are two ways to interpret this situation. In brittle materials, some experimental specimens exhibit microcracking in a specific orientation which could be considered a manifestation of the incompatible velocity field. In ductile materials, the potential development of an incompatible mode will lead to changes in the local stress state and the evolution of smooth changes in the deformation field such as necking.

The construction given above displays a compatible mode in the $x_1 - x_2$ plane with the possibility of an incompatible component in the x_3 direction. Of course, a compatible mode could possibly exist in other planes. The actual orientation of the necked region might be based on the geometry of the specimen. For example, if the dimensions of a specimen in the x_1 and x_2 directions are much larger than the dimension in the x_3 direction, then there might be a preference for most materials to neck with the direction of the potential incompatibility oriented towards the minimum dimension of the specimen.

In general, for a localized zone to form and remain compatible in some plane with the surrounding material, there must be some orientation in the plane such that the normal component of the localized mode is equal to zero. In terms of the eigenvalues associated with a bifurcation mode, compatibility can only exist in principal planes for which $\lambda_i \lambda_j \leq 0$. Recall, that a discontinuous bifurcation mode has a zero intermediate principal value and is thus compatible in all three principal planes. General bifurcation modes with one positive and two negative eigenvalues are compatible only in the principal planes with eigenvalues of opposite sign. Finally, general bifurcation modes that are positive or negative definite are compatible only at a single point and are not compatible in any principal plane.

4.3 Bifurcation Criteria and the Eigensystem for $\mathbf{D}^s$

In this section, we investigate the relationship between the bifurcation criteria presented in the previous section and the eigensystem associated with the symmetric part of the tangent stiffness tensor, $\mathbf{D}^s$. Consider the eigenvalue problem

$$\mathbf{D}^s : \mathbf{x}_i = \omega_i \mathbf{x}_i \tag{4.17}$$

in which $\mathbf{x}_i$ denotes an eigentensor for $\mathbf{D}^s$ and ω_i the corresponding eigenvalue. Due to its minor symmetries, $\mathbf{D}^s$ has six symmetric and three skew-symmetric eigentensors. Since the bifurcation modes, $\dot{\epsilon}$, are symmetric second-order tensors, we confine our attention to only the symmetric eigentensors associated with $\mathbf{D}^s$ and refer to them simply as the eigentensors associated with $\mathbf{D}^s$ throughout the remainder of this paper. For convenience, we normalize the eigentensors so that

$$\mathbf{x}_i : \mathbf{x}_j = \delta_{ij} \tag{4.18}$$

and order the eigenvalues such that $\omega_1 \leq \omega_2 \leq ...\omega_6$. The strain rate perturbation, or any symmetric second-order tensor, can be written as a linear combination of the eigentensors associated with $\mathbf{D}^s$ as follows:

$$\dot{\epsilon} = \sum_{i=1}^{6} \alpha_i \mathbf{x}_i \tag{4.19}$$

and the necessary condition for a general bifurcation from Equation 4.2 can be written as

$$\dot{\epsilon} : \mathbf{D}^s : \dot{\epsilon} = \sum_{i=1}^{6} \alpha_i^2 \omega_i = 0 \tag{4.20}$$

The necessary condition for a general bifurcation is first satisfied when $\omega_1 = 0$, and the corresponding bifurcation mode is characterized by the fundamental eigentensor.

If constraints from the geometry or boundary conditions are present, the bifurcation mode given by the fundamental eigentensor may not be activated. If the material strain softens with continued loading, the fundamental eigenvalue will become negative and the necessary condition, Equation 4.20, for numerous other diffuse and discontinuous bifurcation modes will be satisfied. A discontinuous bifurcation associated with loss of strong ellipticity may be activated when the general bifurcation criterion is satisfied and the corresponding $\dot{\epsilon}$ has a special form. Specifically, the intermediate eigenvalue for this second-order tensor, $\dot{\epsilon}$, must equal zero. Finally, localization will only occur when the necessary condition for a discontinuous bifurcation mode that is not constrained by the boundary conditions is satisfied.

4.4 Eigenanalysis of the Elastic Tangent Stiffness Tensor

Eigenanalyses of the tangent stiffness tensors provide a wealth of information about both diffuse and discontinuous bifurcation modes and aid in the identification of constrained bifurcation modes. Here, it is shown that the eigensystem for an elastic tangent stiffness tensor can be easily obtained. In subsequent sections, eigensystems for tangent stiffness tensors associated with plastic and damaging processes are obtained.

For an elastic increment in an isotropic material, the tangent stiffness tensor is equal to the elasticity tensor, $\mathbf{E}$, which is repeated here for convenience:

$$\mathbf{E} = 3K\mathbf{P}^{sp} + 2G\mathbf{P}^d \tag{4.21}$$

where K is the bulk modulus and G is the shear modulus for the elastic material. The bulk and shear moduli are related to Young's modulus, E, and Poisson's ratio, v, as follows:

$$K = \frac{E}{3(1 - 2v)} \qquad G = \frac{E}{2(1 + v)} \tag{4.22}$$

46

The fourth-order spherical projection operator, $\mathbf{P}^{sp}$, and the deviatoric projection operator, $\mathbf{P}^d$, are given by

$$\mathbf{P}^{sp} = \frac{1}{3}\mathbf{i} \otimes \mathbf{i} \qquad\qquad \mathbf{P}^d = \mathbf{I} - \mathbf{P}^{sp} \qquad\qquad (4.23)$$

Here $\mathbf{I}$ is the symmetric fourth-order identity tensor and $\mathbf{i}$ is the second-order identity. The spherical projection operator, $\mathbf{P}^{sp}$, has only one nonzero eigenvalue of one with a corresponding eigentensor equal to the second-order identity. All of the other eigentensors for $\mathbf{P}^{sp}$ are in a deviatoric space, a space of symmetric second-order tensors orthogonal to $\mathbf{i}$. The deviatoric projection operator, $\mathbf{P}^d$, has an eigenvalue of one with a multiplicity of five. The corresponding five eigentensors are orthogonal to $\mathbf{i}$ and span the deviatoric space. The second-order identity is also an eigentensor for $\mathbf{P}^d$ with a corresponding eigenvalue of zero. With this information and the expression for $\mathbf{E}$, one observes that $\mathbf{E}$ has an eigenvalue of $3K$ with a multiplicity of one and an eigenvalue of $2G$ with a multiplicity of five. The corresponding eigentensors are the second-order identity and any set of five tensors which are orthogonal to the identity and span the deviatoric space, respectively. Specifically, the components in a Cartesian coordinate system of the normalized eigentensors, $\mathbf{e}_i$, for $\mathbf{E}$ can be chosen to be the following:

$$\frac{1}{\sqrt{6}}\begin{bmatrix} -1 & 0 & 0 \\ 0 & 2 & 0 \\ 0 & 0 & -1 \end{bmatrix}, \frac{1}{\sqrt{2}}\begin{bmatrix} -1 & 0 & 0 \\ 0 & 0 & 0 \\ 0 & 0 & 1 \end{bmatrix}, \frac{1}{\sqrt{2}}\begin{bmatrix} 0 & 1 & 0 \\ 1 & 0 & 0 \\ 0 & 0 & 0 \end{bmatrix}, \frac{1}{\sqrt{2}}\begin{bmatrix} 0 & 0 & 1 \\ 0 & 0 & 0 \\ 1 & 0 & 0 \end{bmatrix}, \frac{1}{\sqrt{2}}\begin{bmatrix} 0 & 0 & 0 \\ 0 & 0 & 1 \\ 0 & 1 & 0 \end{bmatrix}, \frac{1}{\sqrt{3}}\begin{bmatrix} 1 & 0 & 0 \\ 0 & 1 & 0 \\ 0 & 0 & 1 \end{bmatrix}$$

$$(4.24)$$

with corresponding eigenvalues of $\lambda_i = 2G$ for $i = 1,5$ and $\lambda_6 = 3K$. The set of eigentensors given above is not unique; however, the set must always span the space of symmetric second-order tensors. Also, note that if Poisson's ratio equals zero then $2G = 3K = E$ and all of the eigenvalues are equal to E and $\mathbf{E} = E\mathbf{I}$. Since, the elastic tangent stiffness tensor, $\mathbf{E}$, is symmetric and positive definite, bifurcations cannot occur during elastic loading or unloading.

4.5 Eigenanalysis of the Plastic Tangent Stiffness Tensor

A plasticity model is characterized by a yield function, Ψ, which defines a surface in stress space separating elastic and plastic regimes and a flow rule

$$\dot{\epsilon}^p = \dot{\rho}\mathbf{g} \qquad\qquad (4.25)$$

where $\mathbf{g}$ is a second-order tensor which defines the orientation of the plastic strain increment and ρ is a monotonically increasing parameter. The tangent stiffness tensor for a plastic increment is given by

$$\mathbf{D} = \mathbf{E} - \frac{1}{A}\mathbf{E} : \mathbf{g} \otimes \mathbf{f} : \mathbf{E} \qquad\qquad (4.26)$$

where $\mathbf{f}$ is the normal to the yield surface defined by the yield function Ψ:

$$\mathbf{f} = \frac{\partial \Psi}{\partial \boldsymbol{\sigma}} \qquad (4.27)$$

The scalar A is given by

$$A = H + \mathbf{g} : \mathbf{E} : \mathbf{f} \qquad (4.28)$$

where H is the generalized strain hardening modulus given by

$$H = \frac{\partial \Psi}{\partial \boldsymbol{\epsilon}^p} : \dot{\boldsymbol{\epsilon}}^p \qquad (4.29)$$

which is positive, zero, or negative for strain hardening, perfect, and strain softening plasticity, respectively. Plastic loading occurs when $\Psi = 0$ and $\mathbf{f} : \mathbf{E} : \dot{\boldsymbol{\epsilon}} > 0$.

Consider the eigensystems of $\mathbf{E} : (\lambda_i, \mathbf{e}_i)$ and $\mathbf{D}^s : (\omega_i, \mathbf{x}_i)$ as presented previously. The elastic tangent stiffness tensor, $\mathbf{E}$, is symmetric and positive definite. Also, the eigenvectors for $\mathbf{E}$ span the space of symmetric second-order tensors. The eigenvalues and eigenvectors for the symmetric part of the plastic tangent stiffness tensor, $\mathbf{D}^s$, will depend on the specific plasticity model being used. Since, the eigentensors of $\mathbf{E}$ span the space of symmetric second-order tensors, we can express $\mathbf{f}$ and $\mathbf{g}$ as a linear combination of the eigentensors of $\mathbf{E}$. Suppose $\mathbf{f}$ and $\mathbf{g}$ can be expressed as a linear combination of two of the elastic eigentensors (say the first and second to be specific). Then

$$\mathbf{f} = f_1 \mathbf{e}_1 + f_2 \mathbf{e}_2 \qquad \mathbf{g} = g_1 \mathbf{e}_1 + g_2 \mathbf{e}_2 \qquad (4.30)$$

and

$$\mathbf{E} : \mathbf{f} = f_1 \lambda_1 \mathbf{e}_1 + f_2 \lambda_2 \mathbf{e}_2 \qquad \mathbf{E} : \mathbf{g} = g_1 \lambda_1 \mathbf{e}_1 + g_2 \lambda_2 \mathbf{e}_2 \qquad (4.31)$$

Postulate an eigentensor for $\mathbf{D}^s$ of the form

$$\mathbf{x} = \xi_1 \mathbf{e}_1 + \xi_2 \mathbf{e}_2 \qquad (4.32)$$

Then

$$\mathbf{D}^s : \mathbf{x} = \mathbf{E} : \mathbf{x} - \frac{\mathbf{f} : \mathbf{E} : \mathbf{x}}{2A} \mathbf{E} : \mathbf{g} - \frac{\mathbf{g} : \mathbf{E} : \mathbf{x}}{2A} \mathbf{E} : \mathbf{f} = \omega(\xi_1 \mathbf{e}_1 + \xi_2 \mathbf{e}_2) \qquad (4.33)$$

which shows that the postulated form of Equation 4.32 is valid. After equating the coefficients of $\mathbf{e}_1$ and $\mathbf{e}_2$, the result is

$$\begin{bmatrix} (2A\omega - 2A\lambda_1 + 2g_1 f_1 \lambda_1^2) & (g_1 f_2 \lambda_1 \lambda_2 + g_2 f_1 \lambda_1 \lambda_2) \\ (g_2 f_1 \lambda_1 \lambda_2 + g_1 f_2 \lambda_1 \lambda_2) & (2A\omega - 2A\lambda_2 + 2g_2 f_2 \lambda_2^2) \end{bmatrix} \begin{Bmatrix} \xi_1 \\ \xi_2 \end{Bmatrix} = \begin{Bmatrix} 0 \\ 0 \end{Bmatrix} \qquad (4.34)$$

For a nontrivial solution to exist, the determinant of the coefficient matrix must equal zero. The quadratic characteristic equation yields the two eigenvalues ω_1, ω_2 and the corresponding normalized eigentensors $\mathbf{x}_1$ and $\mathbf{x}_2$ are obtained by determining the associated values of ξ_1 and ξ_2. The remaining four eigenvalues and eigentensors of $\mathbf{D}^s$ coincide with those of $\mathbf{E}$ and span the remaining space of symmetric second-order tensors. The procedure can be extended in a similar manner to the case where $\mathbf{f}$ and $\mathbf{g}$ are members of any subspace of the space spanned by the eigentensors of $\mathbf{E}$.

48

4.6 Bifurcation Analysis of Plasticity Models

In this section, bifurcation analyses are performed on several existing plasticity models to characterize the nature of the bifurcations predicted by these models and determine if any existing models can capture the bifurcations exhibited by cellular solids.

4.6.1 Drucker-Prager

Consider a Drucker-Prager plasticity model with a yield function given by

$$\Psi = \sqrt{J_2} + \frac{\mu}{3}I_1 - k \tag{4.35}$$

where J_2 is the second invariant of the deviatoric stresses and I_1 is the first invariant of the total stress tensor as follows:

$$J_2 = \frac{1}{2}\sigma^d : \sigma^d, \qquad I_1 = \sigma : i \tag{4.36}$$

where σ^d is the stress deviator. The normal to the yield surface, $\mathbf{f}$ is given by

$$\mathbf{f} = \frac{\sigma^d}{(2\sqrt{J_2})} + \frac{\mu}{3}i \tag{4.37}$$

and the orientation of the plastic strain increment is

$$\mathbf{g} = \frac{\sigma^d}{(2\sqrt{J_2})} + \frac{\beta}{3}i \tag{4.38}$$

The tangent stiffness tensor for a plastic step is given by Equation 4.26.

Unfortunately, an eigenanalysis of the plastic tangent stiffness tensor for this material is rather difficult because two of the eigenvalues and two of the eigentensors depend on the hardening modulus. However, using the procedure outlined in Section 4.5, we can obtain values for the critical hardening moduli for various bifurcation criteria. For any loading, the tensors $\mathbf{f}$ and $\mathbf{g}$ can be written as a linear combination of two of the elastic eigentensors, one from the deviatoric space and one from the spherical space. For example, for uniaxial tension in the x_2 direction $\mathbf{f}$ and $\mathbf{g}$ can be written as linear combinations of $\mathbf{e}_1$ and $\mathbf{e}_6$ from Equation 4.24 as follows:

$$\mathbf{f} = f_1\mathbf{e}_1 + f_6\mathbf{e}_6 \qquad \mathbf{g} = g_1\mathbf{e}_1 + g_6\mathbf{e}_6 \tag{4.39}$$

Two of the eigentensors associated with $\mathbf{D}^s$ can also be written as linear combinations of $\mathbf{e}_1$ and $\mathbf{e}_6$ as follows:

$$\mathbf{x}_1 = \gamma_1\mathbf{e}_1 + \gamma_6\mathbf{e}_6 \qquad \mathbf{x}_6 = \rho_1\mathbf{e}_1 + \rho_6\mathbf{e}_6 \tag{4.40}$$

The remaining four eigentensors for $\mathbf{D}^s$ have corresponding eigenvalues of $2G$ and are given by

$$\mathbf{x}_i = \mathbf{e}_i \qquad i = 2, 3, 4, 5 \tag{4.41}$$

From Equation 4.34, we obtain the eigenvalues associated with $\mathbf{x}_1$ and $\mathbf{x}_6$. The necessary condition for a general bifurcation is first satisfied when the fundamental eigenvalue, ω_1, obtains a value of zero, which occurs when the generalized hardening modulus obtains a value of

$$H^{gb} = \tfrac{1}{2}\sqrt{G^2 + \mu^2\beta^2 K^2 + KG(\mu^2 + \beta^2)} - \tfrac{1}{2}G - \tfrac{1}{2}\mu\beta K \tag{4.42}$$

Any diffuse or discontinuous bifurcation mode can be written as a linear combination of the eigentensors associated with $\mathbf{D}^s$. For a discontinuous bifurcation to occur in the $x_1 - x_2$ plane, $\dot{\epsilon}_{13}$, $\dot{\epsilon}_{23}$ and $\dot{\epsilon}_{33}$ must all equal zero. The conditions $\dot{\epsilon}_{13} = 0$ and $\dot{\epsilon}_{23} = 0$ imply that α_4 and α_5 equal zero in Equation 4.19 and that the mode is restricted to the following form

$$\dot{\epsilon} = \mathbf{x}_1 + \alpha_2\mathbf{x}_2 + \alpha_3\mathbf{x}_3 + \alpha_6\mathbf{x}_6 \tag{4.43}$$

or

$$\dot{\epsilon} = (\gamma_1 + \alpha_6\rho_1)\mathbf{e}_1 + \alpha_2\mathbf{e}_2 + \alpha_3\mathbf{e}_3 + (\gamma_6 + \alpha_6\rho_6)\mathbf{e}_6 \tag{4.44}$$

subject to the following constraint which is needed to satisfy the requirement that $\dot{\epsilon}_{33}$ equals zero

$$-\tfrac{1}{\sqrt{6}}(\gamma_1 + \alpha_6\rho_1) + \tfrac{1}{\sqrt{2}}\alpha_2 + \tfrac{1}{\sqrt{3}}(\gamma_6 + \alpha_6\rho_6) = 0 \tag{4.45}$$

The general bifurcation condition, Equation 4.20, provides the following additional constraint:

$$\omega_1 = -\alpha_2^2\omega_2 - \alpha_3^2\omega_3 - \alpha_6^2\omega_6 \tag{4.46}$$

Using the above equations and maximizing ω_1 with respect to the independent variables, α_2, α_3 and α_6, we obtain equations for the fundamental eigenvalue associated with loss of strong ellipticity. Then by iteratively solving the eigenvalue problem and the above equations with monotonically decreasing values for the hardening modulus, we identify the critical hardening modulus for the loss of strong ellipticity.

For this material and loading, Rudnicki and Rice (1975) have obtained the following expression for the hardening modulus associated with a classical discontinuous bifurcation

$$H^{db} = E\left[\frac{(\mu - \beta)^2}{18(1 - \nu)} - \frac{(\mu + \beta - \sqrt{3})^2}{36}\right] \tag{4.47}$$

The critical hardening moduli predicted by the various criteria for uniaxial tension are plotted as a function of μ for various values of β in Figure 4.3. Figure 4.3a shows critical values of the dimensionless hardening modulus, (H/E), as a function of the internal friction parameter μ with the dilatancy parameter β fixed at -0.3. Loading is characterized by decreasing values of (H/E). Throughout this chapter, a value of 0.3 is used for Poisson's ratio. The general bifurcation condition is always reached first for all values of $\mu \neq \beta$. When $\mu = \beta = -0.3$, the general bifurcation and limit point bifurcation criteria coincide as they should for an associated law. Similarly, the strong ellipticity condition is always attained prior to the classical discontinuous bifurcation condition unless $\mu = \beta = -0.3$ where the two discontinuous bifurcation criteria coincide

50
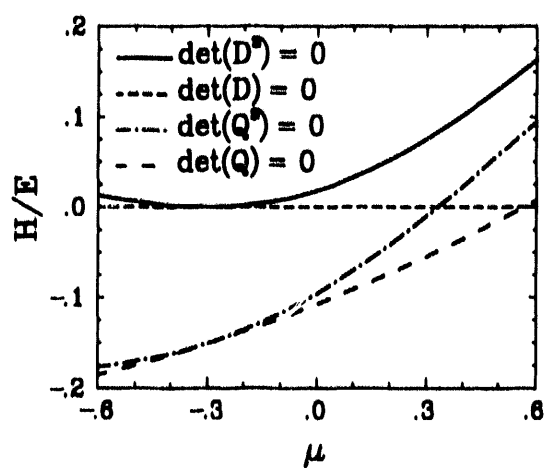
(a) $\beta = -0.3$
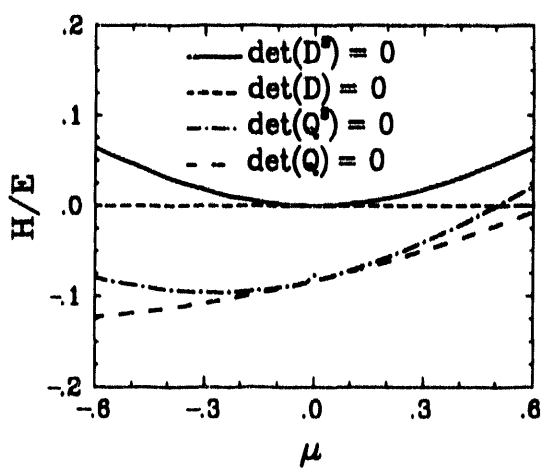
(b) $\beta = 0.0$
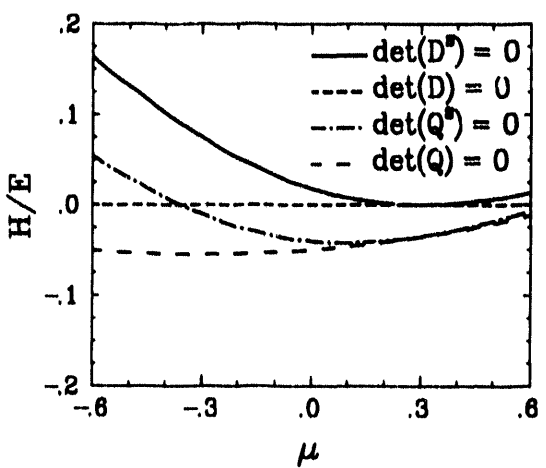
(c) $\beta = 0.3$

Figure 4.3. Critical Hardening Moduli for a Drucker-Prager Material with Non-Associated Flow.

51

as they should for an associated law. Figures 4.3b and 4.3c show similar results when the dilatancy parameter β is fixed at 0.0 and 0.3, respectively.

All of these results indicate that the first general bifurcation point is reached in the hardening regime when the flow is non-associative $\mu \neq \beta$. When the flow is associative, the tangent stiffness tensor is symmetric, $\mathbf{D} = \mathbf{D}^s$, and the general bifurcation criterion and the limit point bifurcation criterion both identify the limit point as the first general bifurcation point. Likewise, when the flow is associative, the classical discontinuous bifurcation criterion and the loss of strong ellipticity criterion identify the same point in the softening regime as the first discontinuous bifurcation point. To reach a discontinuous bifurcation point, the material must exhibit either strain-softening or non-associative flow. When the flow is non-associative, the loss of strong ellipticity criterion is satisfied prior to the classical discontinuous bifurcation criterion, as expected.

To analyze a Drucker-Prager material with associated flow for a general stress path, we can simply repeat the process used in the first part of this section and let $\mu = \beta$. For an associated flow rule, we find that the fundamental eigenvalue for $\mathbf{D}^s$ obtains a value of zero when H equals zero and that a negative H, strain-softening, leads to a negative fundamental eigenvalue. The fundamental eigentensor corresponding to the zero eigenvalue at the limit point is

$$\mathbf{x}_1 = \mathbf{g} = \frac{\sigma^d}{(2\sqrt{J_2})} + \frac{\mu}{3}\mathbf{i} \tag{4.48}$$

Four of the eigentensors of $\mathbf{D}^s$ are orthogonal to $\mathbf{i}$ and σ^d and span the remaining deviatoric space. These eigentensors have corresponding eigenvalues of $2G$. The remaining eigentensor is given by

$$\mathbf{x}_6 = \mathbf{i} - \frac{\mu\sigma^d}{\sqrt{J_2}} \tag{4.49}$$

and has a corresponding eigenvalue of

$$\omega_6 = \frac{(3KG + 2\mu^2 KG)}{(G + \mu^2 K)} \tag{4.50}$$

Note that when μ obtains a value of zero, $\mathbf{x}_6 = \mathbf{i}$ and $\omega_6 = 3K$. Variations in the hardening modulus, H, lead to changes in ω_1 and ω_6 and their corresponding eigentensors. A negative H leads to a negative fundamental eigenvalue.

The critical hardening moduli predicted by the various criteria for uniaxial tension are plotted as a function of μ in Figure 4.4. Note that for an associated flow rule, the general bifurcation and limit point bifurcation criteria both predict the limit point as the first bifurcation point independent of μ. Also, when the flow is associative, the strong ellipticity criterion and the classical discontinuous bifurcation criterion generate identical predictions for the amount of strain-softening needed for localization. For localization to occur, the material must strain-soften or exhibit a significant amount of pressure dependence. Specifically, μ must equal $\sqrt{3}/2$ for a discontinuous bifurcation to occur without strain-softening.
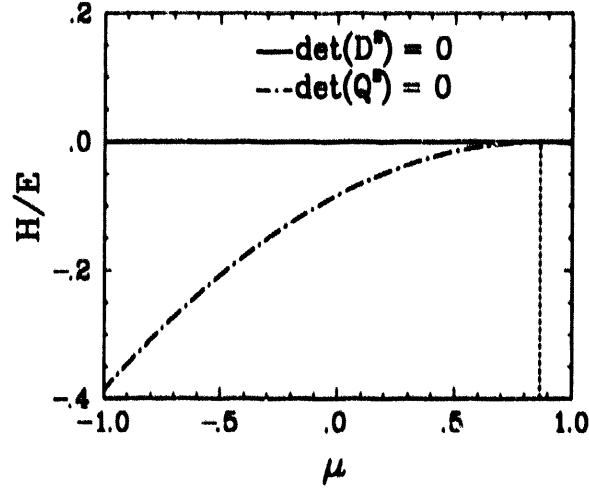
Figure 4.4. Critical Hardening Moduli for a Drucker-Prager Material with Associated Flow.

4.6.2 von Mises

In this section, we analyze a simple von Mises plasticity model with associated flow and a yield function given by

$$\Psi = \sqrt{J_2} - k \tag{4.51}$$

Then

$$f = g = \frac{\sigma^d}{(2\sqrt{J_2})} \tag{4.52}$$

and the tangent stiffness tensor for a plastic step is given by

$$D = E - \frac{2G^2}{(H + G)} \frac{\sigma^d \odot \sigma^d}{\sigma^d : \sigma^d} \tag{4.53}$$

The plastic tangent stiffness tensor is symmetric, $D = D^s$.

The fundamental eigentensor for D is

$$x_1 = \frac{\sigma^d}{(\sigma^d : \sigma^d)^{\frac{1}{2}}} \tag{4.54}$$

with a corresponding eigenvalue of

$$\omega_1 = 2G \left(\frac{H}{H + G} \right) \tag{4.55}$$

which varies from $2G$ to 0 as H varies from ∞ to 0 and becomes negative for negative H. The remaining eigentensors for D are a set of four tensors which span the remaining space of symmetric second-order deviatoric tensors with corresponding eigenvalues of $2G$ and the second-order identity with a corresponding eigenvalue of $3K$. Note that for this

53

model none of the eigentensors and only one eigenvalue, the fundamental one, depend on the hardening modulus, H. The fundamental eigentensor does, however, depend on the current stress state.

A general bifurcation may first occur when the fundamental eigenvalue obtains a value of zero. At this point, the hardening modulus, H, equals zero. The character of the bifurcation is given by the fundamental eigentensor. For example, when the material is subjected to uniaxial tension,

$$\mathbf{x}_1 \Rightarrow \frac{1}{\sqrt{6}} \begin{bmatrix} -1 & 0 & 0 \\ 0 & 2 & 0 \\ 0 & 0 & -1 \end{bmatrix} \qquad (4.56)$$

which represents a general bifurcation since $\mathbf{x}_1$ has no zero eigenvalues. If constraints are present, the material may be loaded into a strain-softening regime without exhibiting localized deformation associated with the first general bifurcation mode. In the strain-softening regime, the fundamental eigenvalue is negative, and numerous alternate bifurcation modes may be activated.

Any bifurcation mode can be written as a linear combination of the eigentensors as given in Equation 4.19. For a discontinuous bifurcation to occur in the $x_1 - x_2$ plane, $\dot{\epsilon}_{13}$, $\dot{\epsilon}_{23}$ and $\dot{\epsilon}_{33}$ must all equal zero. This implies that α_4 and α_5 equal zero and the mode is restricted to the following form:

$$\dot{\epsilon} \Rightarrow \frac{1}{\sqrt{6}} \begin{bmatrix} -1 & 0 & 0 \\ 0 & 2 & 0 \\ 0 & 0 & -1 \end{bmatrix} + \frac{\alpha_2}{\sqrt{2}} \begin{bmatrix} -1 & 0 & 0 \\ 0 & 0 & 0 \\ 0 & 0 & 1 \end{bmatrix} + \frac{\alpha_3}{\sqrt{2}} \begin{bmatrix} 0 & 1 & 0 \\ 1 & 0 & 0 \\ 0 & 0 & 0 \end{bmatrix} + \frac{\alpha_6}{\sqrt{3}} \begin{bmatrix} 1 & 0 & 0 \\ 0 & 1 & 0 \\ 0 & 0 & 1 \end{bmatrix} \qquad (4.57)$$

subject to the constraint

$$\frac{-1}{\sqrt{6}} + \frac{\alpha_2}{\sqrt{2}} + \frac{\alpha_6}{\sqrt{3}} = 0 \qquad (4.58)$$

which is an equation for a straight line in the $\alpha_2 - \alpha_6$ plane. Note that α_3 is arbitrary. The general bifurcation condition, Equation 4.20, gives the following additional constraint

$$2G\alpha_2^2 + 2G\alpha_3^2 + 3K\alpha_6^2 = -\omega_1 \qquad (4.59)$$

which is the equation for an ellipse in the $\alpha_2 - \alpha_6$ plane. Note that when ω_1 equals zero, the general bifurcation regime is a single point with $\alpha_2 = \alpha_3 = \alpha_6 = 0$. As H and ω_1 become negative, the size of the general bifurcation regime grows. The first discontinuous bifurcation mode is reached when H obtains a value of $-E/12$. At this point, $\alpha_2 = \sqrt{3}(1 + v)/(5 - v)$, $\alpha_6 = \sqrt{2}(1 - 2v)/(5 - v)$, and $\alpha_3 = 0$ (Figure 4.5). Ottosen and Runesson (1991) analyzed the acoustic tensor and also showed that the first discontinuous bifurcation mode is reached at this point for a von Mises material subjected to uniaxial tension. If the hardening modulus decreases beyond $-E/12$ additional discontinuous bifurcation modes may be activated.
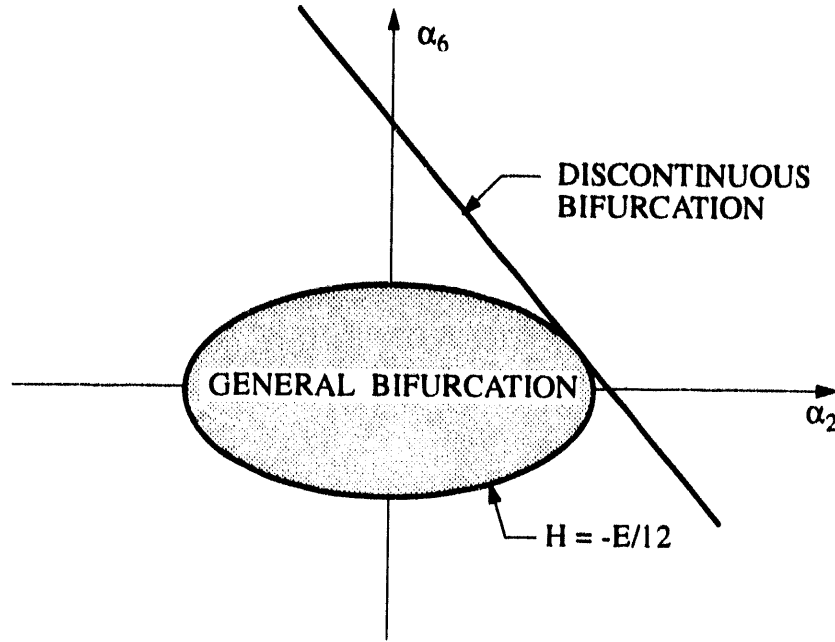
Figure 4.5. Bifurcation Regimes for a von Mises Material Subject to Uniaxial Tension.

Since the fundamental eigentensor depends on the stress state, the amount of softening needed to reach a discontinuous bifurcation will also depend on the stress state. For example, when the von Mises material is subjected to a pure shear stress in the $x_1 - x_2$ plane, the components of the fundamental eigentensor are

$$x_1 \Rightarrow \tfrac{1}{\sqrt{2}} \begin{bmatrix} -1 & 0 & 0 \\ 0 & 1 & 0 \\ 0 & 0 & 0 \end{bmatrix} \tag{4.60}$$

which indicates that the necessary condition for a discontinuous bifurcation is satisfied at the limit point when $H = 0$. The important point here is that by altering the stress path, the amount of strain-softening needed to satisfy the necessary conditions for a discontinuous bifurcation can be significantly changed. This occurs because the fundamental eigentensor for this material model depends on the stress state.

4.6.3 Mohr-Coulomb

Next, consider a simple Mohr-Coulomb model with a yield function given by

$$\Psi = \tfrac{1}{2}(\sigma_1 - \sigma_2) + \tfrac{1}{2}(\sigma_1 + \sigma_2)sin\phi - ccos\phi \tag{4.61}$$

where ϕ is the internal friction angle, c is the cohesion, and the coordinate system is chosen such that σ_1 and σ_2 are the maximum and minimum principal stresses, respectively. Then

for an associated flow law

$$\mathbf{f} = \mathbf{g} \Rightarrow \tfrac{1}{2} \begin{bmatrix} 1 + sin\phi & 0 & 0 \\ 0 & -1 + sin\phi & 0 \\ 0 & 0 & 0 \end{bmatrix} \tag{4.62}$$

and the tangent stiffness tensor for a plastic step is again given by Equation 4.26. For this model, the bifurcation at the limit point, $H = 0$, is always a discontinuous bifurcation since the fundamental eigentensor for $\mathbf{D}^s$ is equal to $\mathbf{f}$ which has the characteristics required for a discontinuous mode. The nature of the discontinuous bifurcation, as given by the eigentensor, indicates that the components of $\mathbf{n}$ and $\mathbf{m}$ are as follows:

$$\mathbf{n} \Rightarrow \left\{ \begin{array}{c} \sqrt{1+sin\phi} \\ \sqrt{1-sin\phi} \\ 0 \end{array} \right\} = c \left\{ \begin{array}{c} 1 \\ tan(\frac{\pi}{4}+\frac{\phi}{2}) \\ 0 \end{array} \right\}, \qquad \mathbf{m} \Rightarrow \tfrac{1}{2} \left\{ \begin{array}{c} \sqrt{1+sin\phi} \\ -\sqrt{1-sin\phi} \\ 0 \end{array} \right\} \tag{4.63}$$

It is not surprising that the Mohr-Coulomb model predicts a discontinuous bifurcation at the limit point and that the orientation of the localized zone depends on the internal friction angle because this model was developed to capture this type of failure. A shear localization is obtained when $\phi = 0$ and a discontinuous opening mode is obtained when $\phi = \pi/2$. This analysis indicates that a Mohr-Coulomb model is appropriate for materials that exhibit localization at the limit point with an orientation that is dependent on an internal friction angle.

A Tresca model with associated flow is identical to a Mohr-Coulomb model with the internal friction angle set equal to zero. Thus, the previous results indicate that a Tresca model is appropriate for materials that display localization at the limit point with an orientation of 45 degrees in the plane of maximum and minimum principal stresses. This model does not predict the generation of necking or diffuse bifurcation modes that are sometimes observed experimentally in metals and is, therefore, not appropriate for metals.

4.6.4 Principal Stress

In this section, we consider the principal stress theory of Rankine which uses a yield function given by

$$\Psi = \tfrac{1}{2}(\boldsymbol{\sigma} : \mathbf{P}^i : \boldsymbol{\sigma})^{\frac{1}{2}} - h(\epsilon^p) \tag{4.64}$$

where $\mathbf{P}^i$ is the principal projection operator. This model has a flow law given by

$$\epsilon^p = \dot{\omega}\mathbf{g} = \dot{\omega}(\mathbf{n} \cdot \boldsymbol{\sigma} \cdot \mathbf{n})\mathbf{n} \otimes \mathbf{n} \tag{4.65}$$

For proportional loading, the first possible bifurcation occurs at the limit point and is characterized by the fundamental eigentensor for $\mathbf{D}^s$. The fundamental eigentensor for $\mathbf{D}^s$ is equal to $\mathbf{g}$ which has the characteristics of a discontinuous opening mode bifurcation. Thus, this model predicts localization at the limit point with the orientation of localization given by the orientation of the maximum principal st. ss.

4.7 Evaluation of von Mises Plasticity for Metals

A von Mises plasticity model with associated flow has been used extensively to describe the plastic deformation of metals. This model does an excellent job of capturing the initiation of plastic deformation in metals. In this section, we use the previous analyses to determine if there is any relationship between the bifurcations predicted by this model and experimentally observed necking and localized deformations in metals. Several different experimental investigations that may enhance an understanding of the necking and localized deformation in metals are reviewed.

### 4.7.1 Axisymmetric Rod Subjected to Uniaxial Tension

First consider a metallic, axisymmetric rod subjected to uniaxial tension. The first type of bifurcation that is generated in metal rods is necking at some section along the length of the rod. In some rods, for example aluminum rods tested at high temperature, (Nadai, 1950), the applied load slowly decreases as the rods continue to neck until the cross-sectional area in the necked region is reduced to a point. In other materials, the initiation of necking is quickly followed by the formation of a crack either at an angle or perpendicular to the applied loading. Here we interpret a crack or the formation of very thin localized deformation zones as evidence of a discontinuous bifurcation, and necking as evidence of a diffuse bifurcation.

Needleman (1972), Hutchinson and Miles (1974) and Miles (1975) have all investigated the necking of rods subjected to uniaxial tension using Hill's (1958) general bifurcation criterion. These researchers have all shown that the initiation of necking is coincident with the attainment of maximum load. The necking in the rod is related to activation of the first general bifurcation mode and is characterized by the fundamental eigentensor, x_1, which is equal to the normalized deviatoric stress tensor (Figure 4.6).

Materials that neck until failure do not strain-soften and therefore do not allow for the activation of any other general or discontinuous bifurcation modes. The fundamental eigentensor associated with the tangent stiffness tensor for a von Mises material is dependent on the stress state. As the necked region evolves, the stress state in the necked region changes. This leads to a local change in the stress deviator and thus a change in the fundamental eigentensor. Specifically, as necking occurs, a shear stress component is introduced which directly leads to the introduction of a shear strain component in the fundamental eigentensor which explains the formation of a necked region without the generation of any incompatibilities in the neck.

In other materials, a small amount of necking is quickly followed by the formation of a crack either at an angle or perpendicular to the applied loading. The analyses given above indicates that a von Mises material subjected to a pure shear stress can localize without softening but that a von Mises material subjected to a uniaxial tensile stress must exhibit a significant amount of softening to localize. As the necked region evolves
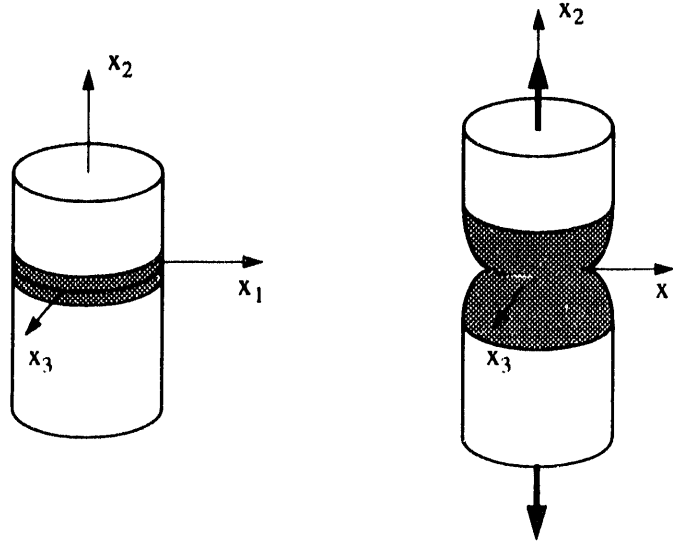
Figure 4.6. Activation of First General Bifurcation Mode in a Rod Subject to Uniaxial Tension.

in the bar, the stress state deviates from a homogeneous uniaxial tensile stress state and strictly speaking the results from the above analyses do not apply. However, if the amount of necking is not significant, then it seems reasonable to expect the stress state in the necked region to approach that of the original homogeneous uniaxial tensile stress state and to conclude that the material must exhibit strain softening for the localization to occur. Of course, the localization could also be due to pressure dependence of the yield surface, non-associated flow, or a combination of softening, pressure dependence, and non-associativity. An accurate study of the evolution of the necked region and subsequent potential localization would require a numerical study similar to that of Needleman (1972) which would allow a characterization of the stress state in the evolving necked region.

4.7.2   Axisymmetric Rod with Lateral Displacements Constrained

Next, consider the same axisymmetric rod subjected to uniaxial tension with the artificial constraint that lateral displacements be identical along the entire length of the bar as shown in Figure 4.7. This constraint will not allow the bar to neck and will thus constrain the first general bifurcation mode. Furthermore, the first discontinuous bifurcation mode given by Equation 4.57, which is characterized by the formation of a localized zone at an angle of 48.8 degrees from the loading axis will also be constrained. With continued softening of the material, the first unconstrained discontinuous bifurcation that will actually lead to localization is an opening mode discontinuous bifurcation with an orientation, n, parallel to the loading axis. To activate this mode, α_6 in Equation 4.57 is equal to $\frac{1}{\sqrt{2}}$, α_2 and α_3 are equal to zero, and $H = -E/(6-6v)$. This example shows that when the first possible discontinuous bifurcation is constrained, the localization that is ultimately generated is not characterized by the mode associated with the first possible discontinuous bifurcation but rather by the first unconstrained discontinuous bifurcation.
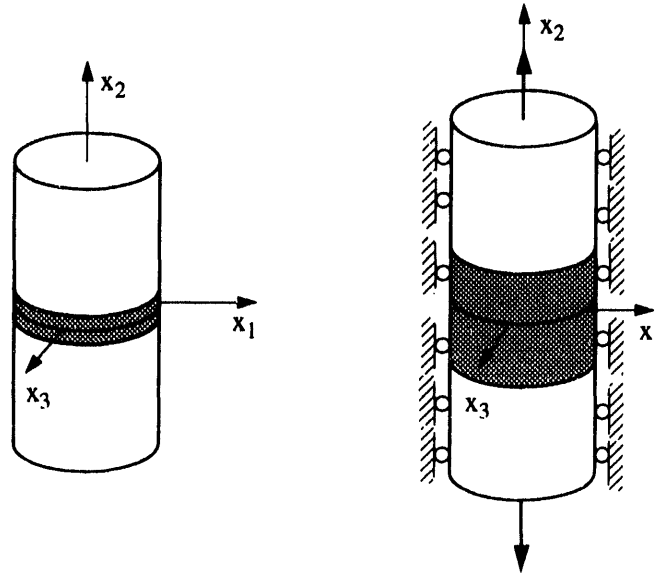
Figure 4.7. Localization in Rod with Lateral Displacements Constrained to be Identical.

4.7.3 Thin Plate Subjected to Uniaxial Tension

Experiments on thin metal plates subjected to uniaxial in-plane tension indicate that necked regions form at angles of between 55 and 65 degrees from the loading axis (Nadai, 1950; Aronofsky, 1951) and not perpendicular to the applied loading as with axisymmetric rods. Again, the formation of the neck is sometimes followed by the formation of a crack plane, and at other times the material just continues to neck until failure.

Necking in a thin plate is again associated with the activation of the first general bifurcation and characterized by the fundamental eigentensor. In the rotated coordinate system shown in Figure 4.8, the components of the fundamental eigentensor for $\mathbf{D}^s$ based on Equation 4.54 are

$$\bar{\mathbf{x}}_1 \Rightarrow \frac{1}{\sqrt{6}} \begin{bmatrix} 2sin^2(\theta) - cos^2(\theta) & 3cos(\theta)sin(\theta) & 0 \\ 3cos(\theta)sin(\theta) & 2cos^2(\theta) - sin^2(\theta) & 0 \\ 0 & 0 & -1 \end{bmatrix} \qquad (4.66)$$

For a thin necked region to form in the plane of the plate, the x_1 - x_2 plane, and to remain compatible with the surrounding material, the perturbation to the strain field in the necked region is subject to the constraint that the 11 component of the fundamental eigentensor in the rotated coordinate system must equal zero. This requirement would be that of a discontinuous bifurcation if the third eigenvalue of $\mathbf{x}_1$ is zero instead of -1. Therefore, there is a potential incompatibility in the x_3 direction. The in-plane constraint yields $2sin^2(\theta) - cos^2(\theta) = 0$ or $\theta = 35.3$ degrees. In other words, the predicted necked region is oriented at an angle of 54.7 degrees from the loading axis which corresponds to many experimental observations and is identical to the orientation predicted by Nadai (1950) and Thomas (1961) using similar in-plane compatibility arguments. However, these authors did not address the potential incompatibility in the x_3 direction. The

(a) lateral displacement at end   (b) no lateral displacement at end
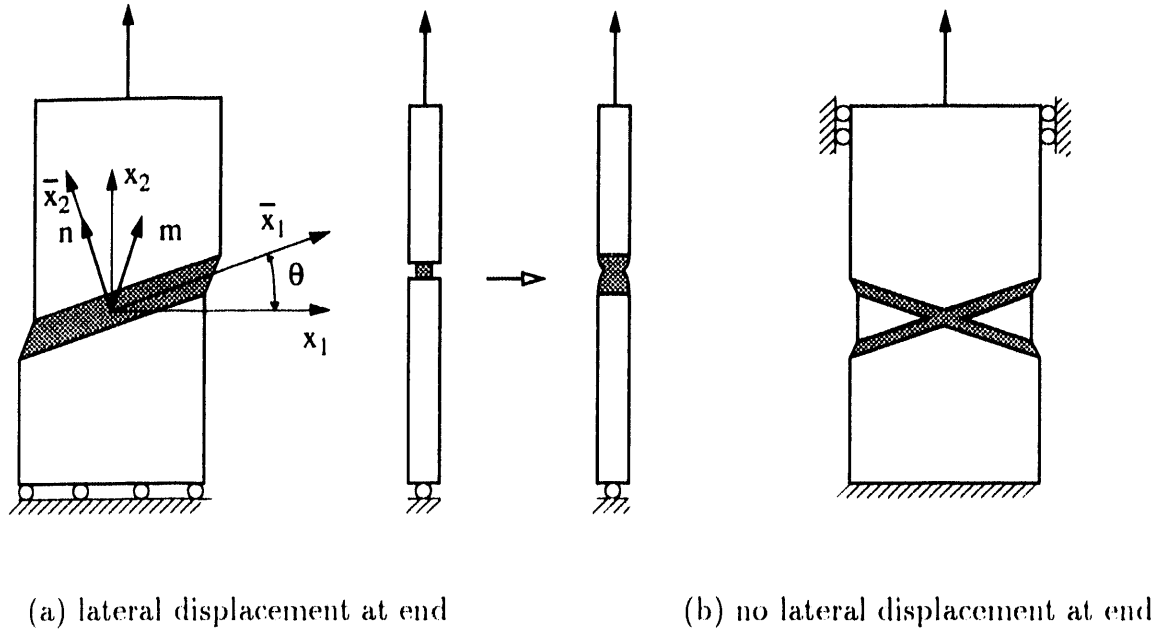
Figure 4.8.   Activation of General Bifurcation Mode in a Plate Subject to Uniaxial
                   Tension.

neck is characterized by the fundamental eigentensor which, for a von Mises material, is
dependent on the stress state. As the neck evolves, the stress state in the neck and thus
the fundamental eigentensor change. The components of the fundamental eigentensor are
expected to vary continuously as a function of location within the neck which explains
the formation of the neck without the generation of any incompatibilities which were
introduced and left unexplained in Thomas' (1961) analysis of this thin plate problem.

As shown in Figure 4.8a, the orientation of **m** which represents the orientation of relative
velocities of regions on opposite sides of the necked region indicates that at least one end
of the specimen must be free to move in the x_1 direction for the neck to occur as shown.
Vardoulakis (1978) has developed a device that allows for this lateral displacement; how-
ever, many specimens are tested in devices that do not allow lateral displacement. This
leads to the formation of two necked regions and relative motion of the bodies on opposite
sides of the necks as shown in Figure 4.8b.

Aronofsky (1951) shows that the variation in the orientation of the necked region from
25 to 35 degrees could be due to material anisotropy. The analysis presented in the
previous sections allows an alternative explanation of this phenomenon if the loading
device provides a constraint which allows the material to be loaded into a strain softening
regime. For example, consider the strain perturbation given by

$$\dot{\epsilon} = \mathbf{x}_1 + \frac{1}{\sqrt{2}}\beta\mathbf{x}_6 \qquad\qquad (4.67)$$

which satisfies the instability condition of Equation 4.20. Components of the strain

60
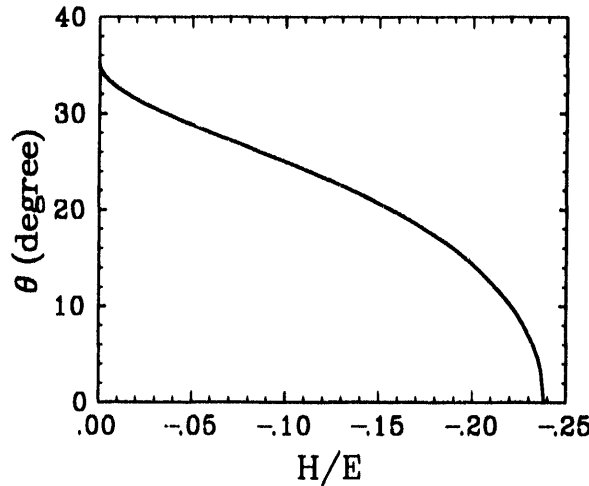
Figure 4.9. Effect of Strain-Softening on the Predicted Orientation of Localization.

perturbation in the rotated coordinate system become

$$
\dot{\epsilon} \Rightarrow \frac{1}{\sqrt{6}}
\begin{bmatrix}
2sin^2(\theta) - cos^2(\theta) + \beta & 3cos(\theta)sin(\theta) & 0 \\
3cos(\theta)sin(\theta) & 2cos^2(\theta) - sin^2(\theta) + \beta & 0 \\
0 & 0 & -1 + \beta
\end{bmatrix}
\tag{4.68}
$$

The predicted orientation of the necked region is plotted as a function of the amount of softening needed to satisfy the general bifurcation condition in Figure 4.9.

When the hardening modulus, H, has a value of $-E/10$ an orientation of 25 degrees (65 degrees from the loading axis) is predicted. Even less strain softening is needed to activate modes with orientations between 25 and 35 degrees. These results suggest that the experimentally observed variations in orientation could be caused by the combination of loading constraints and some strain-softening. Also, when the hardening modulus obtains a value of $-E/(6 - 6v)$ an orientation of 0 degrees and a discontinuous opening mode bifurcation is predicted which corresponds to lccalization perpendicular to the applied loading. Such a localization is sometimes observed experimentally which would suggest that some metals must exhibit a significant amount of strain softening, pressure dependence or non-associativity at failure.

4.7.4 Thin Plate Subjected to Equal Biaxial Tension

Metal sheets are often formed by subjecting them to equal biaxial tension with a hemispherical punch. At some point in the forming process intersecting shear bands form at angles through the thickness (Beaver, 1983) as shown in Figure 4.10. The necking that is generated prior to localization in thin plates subjected to uniaxial tension is not observed in thin plates subjected to equal biaxial tension. Thus, the change in load path to equal biaxial tension apparently inhibits the activation of any diffuse bifurcation modes prior to localization.
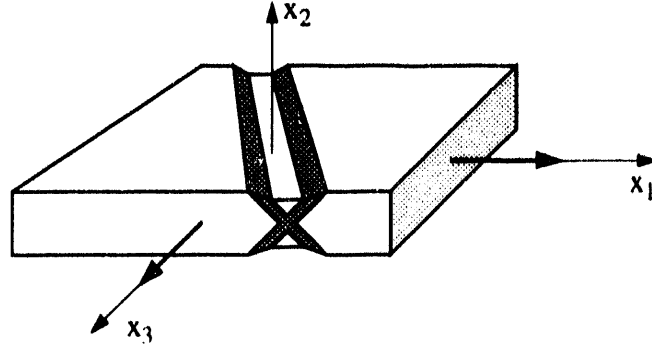
Figure 4.10. Activation of Discontinuous Bifurcation Mode in a Thin Plate Subject to Equal Biaxial Tension.

Storen and Rice (1975) suggest that that localization of plates subject to equal biaxial tension provides experimental evidence of the formation of vertices in the yield surface. Recently, Hill (1991) has shown that anisotropic hardening could also lead to the observed localization. Here we present an alternative explanation. For equal biaxial tension in the $x_1 - x_3$ plane (the plane of the plate), the components of the stress tensor and the stress deviator prior to localization are as follows:

$$\sigma \Rightarrow \sigma \begin{bmatrix} 1 & 0 & 0 \\ 0 & 0 & 0 \\ 0 & 0 & 1 \end{bmatrix}, \qquad \sigma^d \Rightarrow \frac{\sigma}{3} \begin{bmatrix} 1 & 0 & 0 \\ 0 & -2 & 0 \\ 0 & 0 & 1 \end{bmatrix} \qquad (4.69)$$

For this problem the fundamental eigentensor which is the normalized stress deviator is not compatible in the plane of the plate because the eigenvalues associated with the $x_1 - x_3$ plane are both positive. Thus, no orientation can be found for which a perturbation to the strain rate field given by the fundamental eigentensor is compatible in the $x_1 - x_3$ plane with the surrounding material. As the material begins to strain soften, numerous alternate bifurcation modes may be activated. However, by considering all linear combinations of the eigentensors associated with $\mathbf{D}^a$, we quickly find that the first bifurcation mode which satisfies the constraint to remain compatible in the $x_1 - x_3$ plane is a discontinuous bifurcation given by

$$\dot{\epsilon} \Rightarrow \frac{1}{\sqrt{6}} \begin{bmatrix} 1 & 0 & 0 \\ 0 & -2 & 0 \\ 0 & 0 & 1 \end{bmatrix} + \frac{\alpha_2}{\sqrt{2}} \begin{bmatrix} -1 & 0 & 0 \\ 0 & 0 & 0 \\ 0 & 0 & 1 \end{bmatrix} + \frac{\alpha_6}{\sqrt{3}} \begin{bmatrix} 1 & 0 & 0 \\ 0 & 1 & 0 \\ 0 & 0 & 1 \end{bmatrix} \qquad (4.70)$$

which satisfies the instability condition of Equation 4.20. This discontinuous bifurcation mode is activated when $H = -E/12$, $\alpha_2 = -\sqrt{3}(1+v)/(5-v)$ and $\alpha_6 = -\sqrt{2}(1 - 2v)/(5-v)$. This bifurcation mode represents shear bands forming at angles of 48.8 degrees from the x_2 axis which is exactly the type of localization that was observed by Beaver (1983). The formation of intersecting shear bands leads to an apparent necking due to the relative motion of material on opposite sides of the shear bands (Figure 4.10). Instead of the requirement of vertices (Storen and Rice, 1975) or of anisotropic hardening
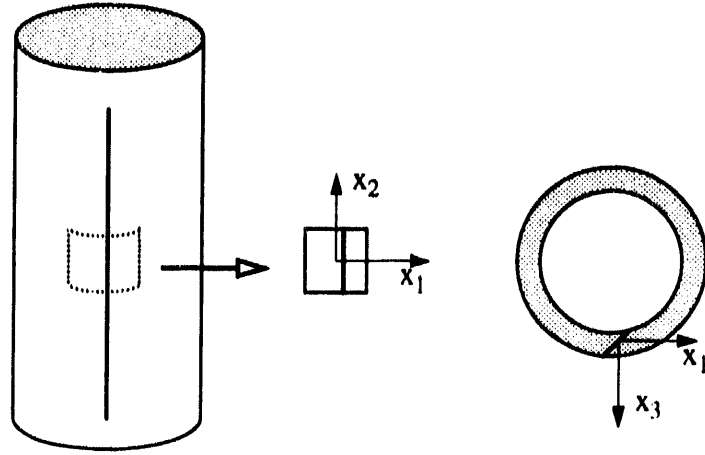
Figure 4.11. Activation of a Discontinuous Bifurcation at the Limit Point in a Pressurized Cylindrical Pressure Vessel.

(Hill, 1991), this analysis shows that with a sufficient degree of softening, conventional von Mises plasticity with associated flow can predict the localization in a plate subject to equal biaxial tension. Furthermore, this analysis helps to explain why the necking that is observed in thin plates subject to uniaxial tension is not observed in thin plates subjected to equal biaxial tension.

4.7.5   Thin-Walled Cylindrical Pressure Vessel

Several investigations (e.g., Needleman and Tvergaard, 1984), have involved thin-walled cylindrical pressure vessels subjected to internal pressure. These pressure vessels fail rather catastrophically, with cracks forming along the axis of the cylinder and at an angle through the thickness (discontinuous bifurcation) as shown in Figure 4.11.

Prior to localization the components of the stress tensor and the stress deviator are as follows:

$$\boldsymbol{\sigma} \Rightarrow \sigma \begin{bmatrix} 1 & 0 & 0 \\ 0 & .5 & 0 \\ 0 & 0 & 0 \end{bmatrix}, \qquad \boldsymbol{\sigma}^d \Rightarrow \frac{\sigma}{2} \begin{bmatrix} 1 & 0 & 0 \\ 0 & 0 & 0 \\ 0 & 0 & -1 \end{bmatrix} \tag{4.71}$$

We see that the stress deviator is different from the stress deviator found in the previous examples. For this example, the fundamental eigentensor for $\mathbf{D}^s$ which is equal to the normalized stress deviator represents a discontinuous bifurcation mode. Furthermore, the fundamental eigentensor indicates that a shear band oriented at 45 degrees through the thickness and along the axis of the specimen will occur at the limit point. This predicted localization was observed experimentally by Needleman and Tvergaard (1984). Comparing this result with the previous ones, we see that the stress state generated in the wall of a cylindrical pressure vessel has a detrimental effect on the apparent ductility of the material.

These examples show that the type of bifurcation, diffuse or discontinuous, exhibited by metals apparently depends not only on the material but also on the geometry and the pre-bifurcation stress state. A simple von Mises plasticity model with associated flow predicts both the necking and the localization that is observed experimentally. This analysis indicates that strain softening can account for many features observed in metals. Most previous analyses have focused primarily on pressure dependence, nonassociativity and vertex development in the yield surface to account for the experimental observations. A close correlation between theoretical predictions and experimental data is needed to provide answers concerning which effect is dominant for any given material.

4.8   Bifurcation Analysis of Continuum Damage Models

In this section, bifurcation analyses are performed on various continuum damage theories to evaluate the appropriateness of existing theories for cellular solids. Continuum damage theories have a constitutive relation of the form

$$\boldsymbol{\sigma} = \mathbf{S} : \boldsymbol{\epsilon} \tag{4.72}$$

where $\boldsymbol{\sigma}$ is the total stress tensor, $\mathbf{S}$ is the damaged elastic stiffness tensor and $\boldsymbol{\epsilon}$ is the total strain tensor. To determine if additional damage is being generated during the current load step, we postulate the existence of a damage function, Ψ, which defines a surface in stress or strain space separating the elastic and damaging processes

$$\Psi = \tfrac{1}{2}\boldsymbol{\sigma} : \mathbf{P} : \boldsymbol{\sigma} - g(\mathbf{S}) \qquad \Psi = \tfrac{1}{2}\boldsymbol{\epsilon} : \mathbf{R} : \boldsymbol{\epsilon} - g(\mathbf{S}) \tag{4.73}$$

where $\mathbf{P}$ is a positive-definite fourth-order tensor that defines the model and $\mathbf{R} = \mathbf{S} : \mathbf{P} : \mathbf{S}$. We also postulate the existence of an evolution equation for $\mathbf{S}$ which is analogous to a flow rule in plasticity. A possible damage evolution equation is given by

$$\dot{\mathbf{S}} = -\dot{\omega}\mathbf{R} \tag{4.74}$$

where $\mathbf{R}$ is a fourth-order tensor which defines the orientation of the damage increment and ω a monotonically increasing parameter that characterizes the magnitude of the damage increment. Note that both the damage function and the evolution equation have been chosen to use the fourth-order tensor $\mathbf{R}$.

Using the consistency condition, the tangent stiffness tensor, $\mathbf{D}$, for a damaging process such that $\dot{\boldsymbol{\sigma}} = \mathbf{D} : \dot{\boldsymbol{\epsilon}}$ is obtained

$$\mathbf{D} = \mathbf{S} - \frac{1}{A}(\mathbf{R} : \boldsymbol{\epsilon} \otimes \mathbf{f} : \mathbf{S}) \tag{4.75}$$

where $\mathbf{f}$ is the normal to the damage surface defined by the damage function Ψ:

$$\mathbf{f} = \frac{\partial \Psi}{\partial \boldsymbol{\sigma}} = \mathbf{P} : \boldsymbol{\sigma} \tag{4.76}$$

The scalar A and the generalized hardening modulus, H, are given by

$$A = H + \mathbf{f} : \mathbf{R} : \epsilon \qquad H = \frac{\partial \Psi}{\partial \mathbf{S}} :: \mathbf{R} \qquad (4.77)$$

The hardening modulus, H, is positive, zero or negative for strain hardening, perfect, and strain softening damage, respectively. Damage will occur when $\Psi = 0$ and $\mathbf{f} : \mathbf{S} : \dot{\epsilon} > 0$. The tangent stiffness tensor, $\mathbf{D}$, is symmetric when $\mathbf{R}$ is chosen such that $\mathbf{R} : \epsilon = \mathbf{f} : \mathbf{S}$. This is analogous to plasticity models that have symmetric tangent stiffness tensors when the flow rule is chosen to be associated with the yield function.

4.8.1 Simple Scalar Damage

In this section, we analyze a simple isotropic, scalar damage model with the following damage function:

$$\Psi = \tfrac{1}{2} \epsilon : \mathbf{E} : \epsilon - g(\mathbf{S}) \qquad (4.78)$$

and an evolution equation for the elastic stiffness tensor as follows:

$$\dot{\mathbf{S}} = -\dot{\omega} \mathbf{E} \qquad (4.79)$$

The tangent stiffness tensor for a damaging process is given by

$$\mathbf{D} = \mathbf{S} - \frac{1}{2H(1-w)^2 + \epsilon : \sigma}(\sigma \otimes \sigma) \qquad (4.80)$$

Since the tangent stiffness tensor is symmetric, bifurcations may first occur at the limit point when the hardening modulus, H, and the fundamental eigenvalue obtain a value of zero. The corresponding fundamental eigentensor for $\mathbf{D}$ is the strain tensor, ϵ, which means that the type of bifurcation that may be activated at the limit point depends on the strain state. For example, a scalar damaging material subject to a plane strain condition would exhibit a discontinuous bifurcation and localization at the limit point, but the same material subjected to uniaxial tensile stress would exhibit a diffuse bifurcation and necking at the limit point.

4.8.2 von Mises Damage

In this section, we analyze a simple von Mises damage model which has a damage function that is identical to the yield function for von Mises plasticity

$$\Psi = \tfrac{1}{2} \sigma : \mathbf{P}^d : \sigma - g(\mathbf{S}) \qquad (4.81)$$

The damage evolution equation is characterized by

$$\mathbf{f} = \mathbf{P}^d : \sigma = \sigma^d \qquad \mathbf{R} = 4G^2 \mathbf{P}^d \qquad (4.82)$$

65

and the tangent stiffness tensor is given by

$$\mathbf{D} = \mathbf{S} - \frac{4G^2}{(2G\sigma^d : \sigma^d + H)}(\sigma^d \odot \sigma^d) \qquad (4.83)$$

The tangent stiffness tensor is symmetric and has a fundamental eigenvalue and corresponding eigentensor given by

$$\omega_1 = \frac{2GH}{(H + 2G\sigma^d : \sigma^d)} \qquad \mathbf{x}_1 = \sigma^d \qquad (4.84)$$

For this model the first possible bifurcation is characterized by the stress deviator. The type of bifurcation that may occur at the limit point in this material will depend on the stress state. If the material is subjected to a pure shear stress then localization may occur at the limit point but if the material is subjected to uniaxial tension then a diffuse bifurcation leading to necking may be activated at the limit point. If the material strain softens with continued loading then numerous other bifurcation modes which are written as linear combinations of the eigentensors as in Equation 4.19 and which satisfy the general bifurcation criterion of Equation 4.20 may be activated.

4.8.3   von Mises Damage with Alternate Damage Evolution

In this section, consider a von Mises damage model which has a damage function which is identical to the yield function for von Mises plasticity

$$\Psi = \tfrac{1}{2}\sigma : \mathbf{P}^d : \sigma - g(\mathbf{S}) \qquad (4.85)$$

and

$$\mathbf{f} = \mathbf{P}^d : \sigma = \sigma^d \qquad (4.86)$$

If we choose the orientation of the damage increment to be given by

$$\mathbf{R} = \mathbf{S} \qquad (4.87)$$

then the tangent stiffness tensor is as follows:

$$\mathbf{D} = \mathbf{S} - \frac{2G}{(\sigma^d : \sigma^d + H)}(\sigma \odot \sigma^d) \qquad (4.88)$$

The tangent stiffness tensor for this model is not symmetric. An eigenanalysis of the symmetric part of this tangent stiffness tensor is more difficult than the eigenanalysis presented in the previous section. For this model, the necessary condition for a bifurcation is first satisfied in the hardening regime when H obtains a value of

$$H = \tfrac{1}{2}\sqrt{(\sigma^d : \sigma^d)^2 + \frac{2G}{3K}(\sigma^d : \sigma^d)(\sigma^{sp} : \sigma^{sp})} - \tfrac{1}{2}(\sigma^d : \sigma^d) \qquad (4.89)$$

With this model, bifurcations may occur in the hardening regime, $H > 0$, unless the stress state is purely deviatoric. When the stress state is purely deviatoric, bifurcations may first occur at the limit point.

4.8.4 Principal Stress Damage

In this section, we analyze a damage model which uses a principal stress projection operator and a damage evolution equation in which the compliance of the material is increased in the direction of maximum principal stress. Consider a model with the damage function

$$\Psi^i = \tfrac{1}{2}\sigma : P^i : \sigma - g(S) \tag{4.90}$$

where P^i is the principal projection operator given by

$$P^i = n^i \odot n^i \odot n^i \odot n^i \quad . \tag{4.91}$$

and n^i is a vector oriented in a principal stress direction. This yield function represents a cube in principal stress space. For proportional loading, the normal to one face of the damage surface is given by f^i and the flow rule is characterized by R^i where

$$f^i = P^i : \sigma = (n^i \cdot \sigma \cdot n^i)n^i \odot n^i \qquad R^i = S : P^i : S \tag{4.92}$$

The tangent stiffness tensor is as follows:

$$D = S - \frac{1}{(\sigma : P^i : S : P^i : \sigma + H)}(S : P^i : \sigma \odot \sigma : P^i : S) \tag{4.93}$$

The tangent stiffness tensor for this model is symmetric and at the limit point has a fundamental eigenvalue of zero with a corresponding fundamental eigentensor given by

$$x_1 = P^i : \sigma = (n^i \cdot \sigma \cdot n^i)n^i \odot n^i \tag{4.94}$$

This eigentensor, x_1, has the kinematically compatible form of $\dot{\epsilon}^k$ in Equation 4.4. Thus, this model predicts localization at the limit point in the form of a discontinuous opening mode bifurcation with an orientation in the direction of the principal stress.

4.8.5 Principal Strain Damage

In this section, we analyze a principal strain damage model with a damage function given by

$$\Psi^i = \epsilon : P^i : \epsilon - h(S) \quad \Psi^i = \sigma : C : P^i : C : \sigma - g(S) \tag{4.95}$$

where C is the compliance of the material, $C = S^{-1}$, and P^i is the principal projection operator. This yield function represents a cube in principal strain space. For proportional loading, the normal to one face of the damage surface is given by

$$f = C : P^i : C : \sigma \tag{4.96}$$

By selecting a damage evolution equation with the following form

$$R = P^i \tag{4.97}$$

we obtain a symmetric tangent stiffness tensor:

$$D = S - \frac{1}{(\epsilon : P^i : C : P^i : \epsilon + H)}(P^i : \epsilon \odot \epsilon : P^i) \qquad (4.98)$$

At the limit point, $H = 0$, this tangent stiffness tensor has a fundamental eigenvalue equal to zero with a corresponding fundamental eigentensor given by

$$x_1 = C : P^i : \epsilon \qquad (4.99)$$

An interesting feature of this model is that the character of the bifurcation depends on the elastic response of the material as reflected through C in Equation 4.99.

The bifurcation analyses presented in this chapter provide a connection between localization and constitutive theories. A bifurcation analysis along with careful observation of localization in material specimens subject to various loading conditions can provide valuable confirmation of the appropriateness of the constitutive theory chosen for a specific material.

5. NUMERICAL SIMULATION OF LOCALIZATION

A large number of researchers have used finite element methods to investigate localization phenomena (Bazant and Lin, 1988; Belytschko, Fish and Engelmann, 1988; deBorst, 1986; Larsson and Runesson, 1991; Leroy and Ortiz, 1989; Needleman, 1972; Needleman and Tvergaard, 1984; and Ortiz, Leroy and Needleman, 1987). These researchers show that diffuse bifurcations can be captured using standard finite element codes, but that mesh dependent solutions are obtained when localization occurs. The first section in this chapter includes finite element analyses of bifurcation problems using standard finite element codes. Following these analyses, modifications which enhance our ability to numerically simulate localization phenomena are discussed.

5.1 Analyses with Existing Finite Element Codes

In this section, several quasi-static, boundary value problems are numerically analyzed to determine if existing finite element codes can predict the general and discontinuous bifurcations which are predicted by the bifurcation analyses in the previous section. Several different combinations of geometry, loading and material are considered.

5.1.1 Rod Subjected to Uniaxial Tension - von Mises Plasticity

The first series of analyses was performed using three different two-dimensional, axisymmetric models of a rod (Figure 5.1). The rods were given an initial imperfection by reducing the radius of the finite element mesh one percent near the center. The analyses were performed using SANTOS (Stone, 1992) which is a finite element code that uses dynamic relaxation to solve non-linear, quasi-static problems. A von Mises, elastic, perfectly plastic material with the properties given in Table 5.1 were used in these analyses.

Three different analyses were performed using various element sizes to determine if the solution converged with mesh refinement. Plots of the deformed mesh subject to an axial displacement of 0.05 inches are shown in Figure 5.2. These plots show that the

Table 5.1. von Mises Material Parameters.

Young's Modulus = 30.0E+06 psi
Poisson's Ratio = 0.30
Yield Strength = 30.0E+03 psi
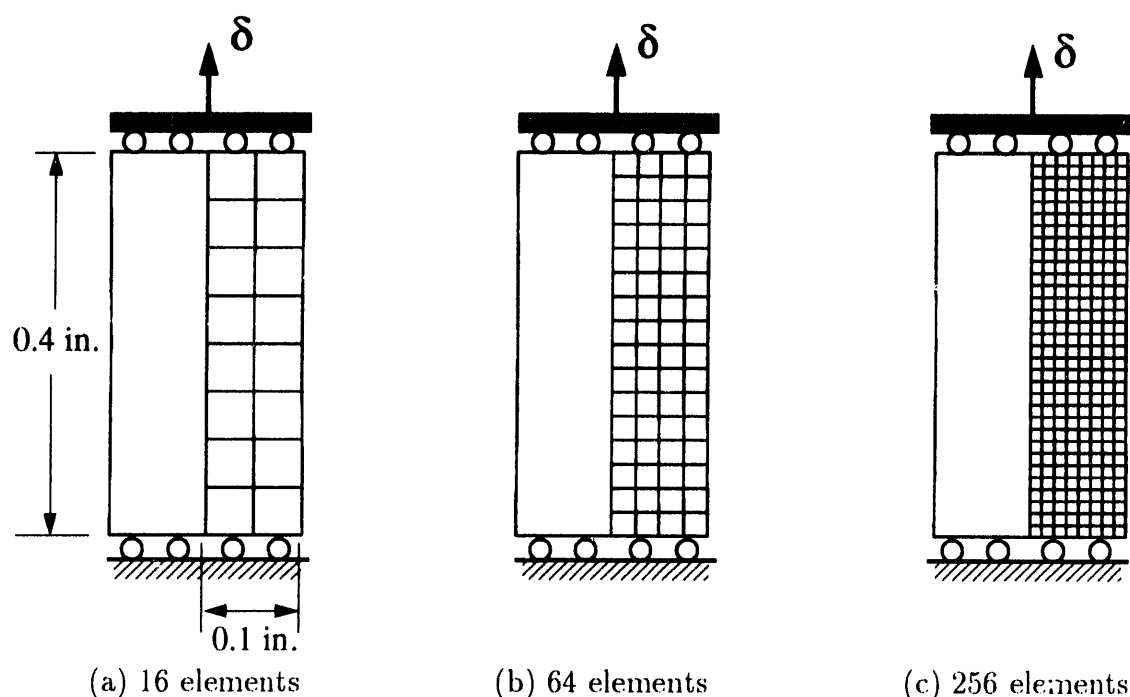
Figure 5.1. Axisymmetric Finite Element Models of a Rod.

necking associated with activation of the first general bifurcation mode is predicted by the finite element analyses. The bifurcation analyses presented in Section 4.7 also predicted activation of the first general bifurcation mode for this problem. Plots of applied load versus end displacement are shown in Figure 5.3. These plots indicate that the numerical results have converged to an accurate solution with mesh refinement.

Next, the effects of strain-softening on the numerical simulation were investigated by analyzing the behavior of rods constructed from strain-softening materials. Two analyses with different amounts of strain-softening were performed using the 256 element model shown in Figure 5.1. In the first softening analysis, the material was given a softening modulus of $-E/12$ which according to the bifurcation analysis is sufficient to initiate localization at the limit point. A plot of applied load versus end displacement and a plot of the deformed mesh at the last solution step are shown in Figure 5.4. These plots indicate that the solution algorithm remains stable well into the inelastic regime. The contour plots of equivalent plastic strain indicate that localized shear bands may be starting to form at the last stable solution step. The first possible bifurcation is not activated at the limit point in this analysis because it is associated with a mode which is not axisymmetric and this axisymmetric analysis will not allow deformations which are not axisymmetric. If the rod had been represented by a three dimensional model, this bifurcation mode may have been predicted. When the rod was given a softening modulus equal to $-E/(6 - 6v)$ the solution algorithm became unstable during the first load step
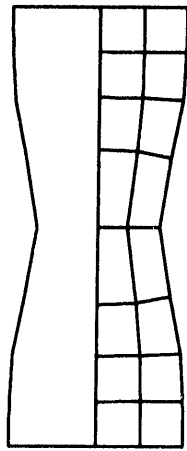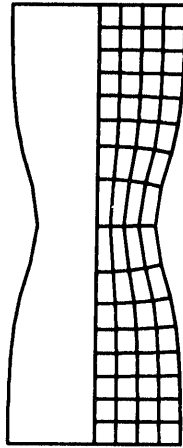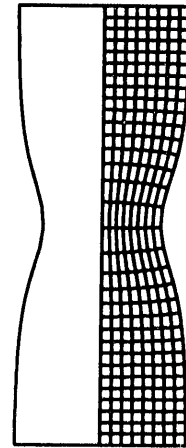
(a) 16 elements (b) 64 elements (c) 256 elements

Figure 5.2. Deformed Shape of Finite Element Models Subject to an Axial Displacement of 0.10 in. - Elastic, Perfectly Plastic von Mises Material.
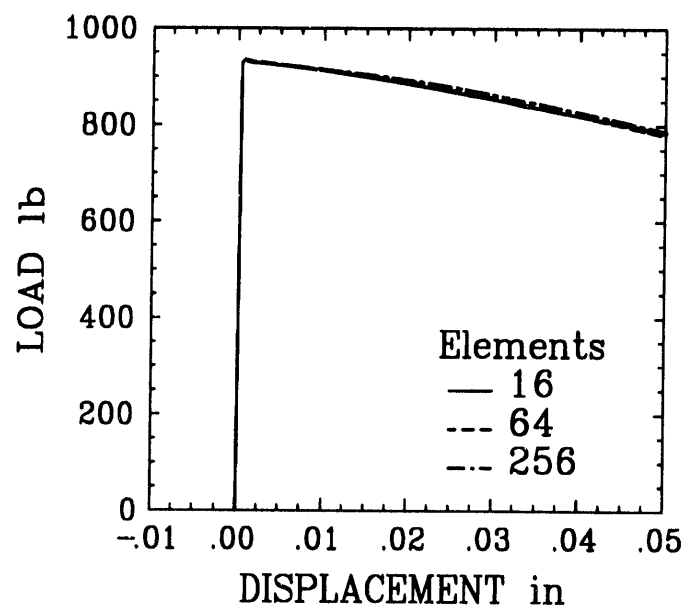
Figure 5.3. Applied Load vs. End Displacement - Elastic, Perfectly Plastic von Mises Material.

into the softening regime (Figure 5.5.) The contour plot of equivalent plastic strain or the deformed mesh plot at the last solution step provide little information about the reason for the instability. However, the bifurcation analysis presented in the previous section indicates that the initiation of a discontinuous opening mode bifurcation which is axisymmetric should be expected at the limit point in a rod with this amount of softening.

5.1.2 Rod Subjected to Uniaxial Tension - Principal Stress Plasticity

The next series of analyses was performed using the same models as in the previous analyses (Figure 5.1); however, in these analyses, an elastic strain-softening material which uses the principal stress criterion of Rankine was used. Material parameters given in Table 5.2 which are appropriate for a brittle foam were used.

Table 5.2. Principal Stress Material Parameters.

Young's Modulus = 3000 psi
Poisson's Ratio = 0.0
Tensile Strength = 300 psi
Softening Modulus = -100 psi

Plots of the deformed mesh are shown in Figure 5.6. The 16 and 64 element models have been subjected to an end displacement of 0.06 inches and the 256 element model has been subjected to an end displacement of 0.042 inches. At this point in the simulation, the axial stress in the 256 element model has been nearly reduced to zero due to the large amount of softening in the middle row of elements. These plots show the formation of a discontinuous opening-mode bifurcation in one row of elements. The width of the localized zone depends on the size of the elements being used. The bifurcation analysis of this problem also predicts the initiation of a discontinuous opening mode bifurcation at the limit point. Plots of applied load versus end displacement are shown in Figure 5.7. These plots show that the solution is not converging with mesh refinement and that the predicted applied load versus end displacement depends on the size of the elements used in the simulation.

5.1.3 Thin Plate Subjected to Uniaxial Tension - von Mises Plasticity

The next series of analyses were performed using JAC-3D (Biffle, 1989). JAC-3D is a three-dimensional finite element code which uses the conjugate gradient method to solve large deformation, quasi-static, solid mechanics problems. In these analyses, three-dimensional models of 3.0 inch square plates which are 0.30 inches thick (Figure 5.8) were subjected to uniaxial tension and equal biaxial tension to determine if the behavior predicted by the bifurcation analyses would be exhibited. The plates were given an initial imperfection by reducing the plate thickness near the center to 0.29 inches.

In the first analysis in this series, a von Mises plasticity theory with the properties given in Table 5.1 was used. The thin plate was subjected to uniaxial tension in the

72

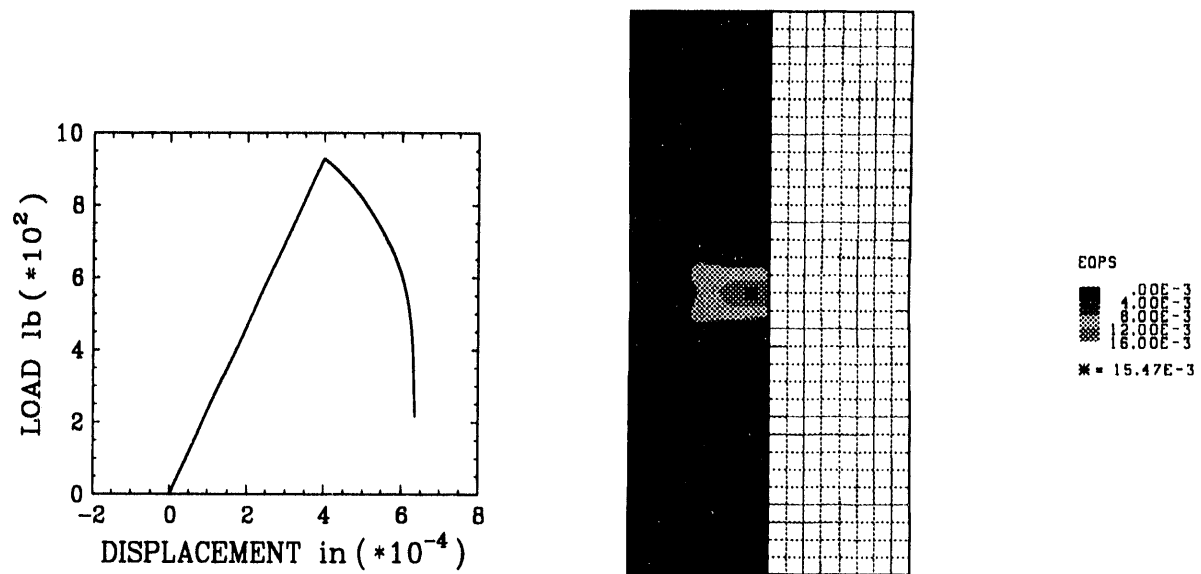**Figure 5.4.** Results from Finite Element Analysis with H = -E/12.

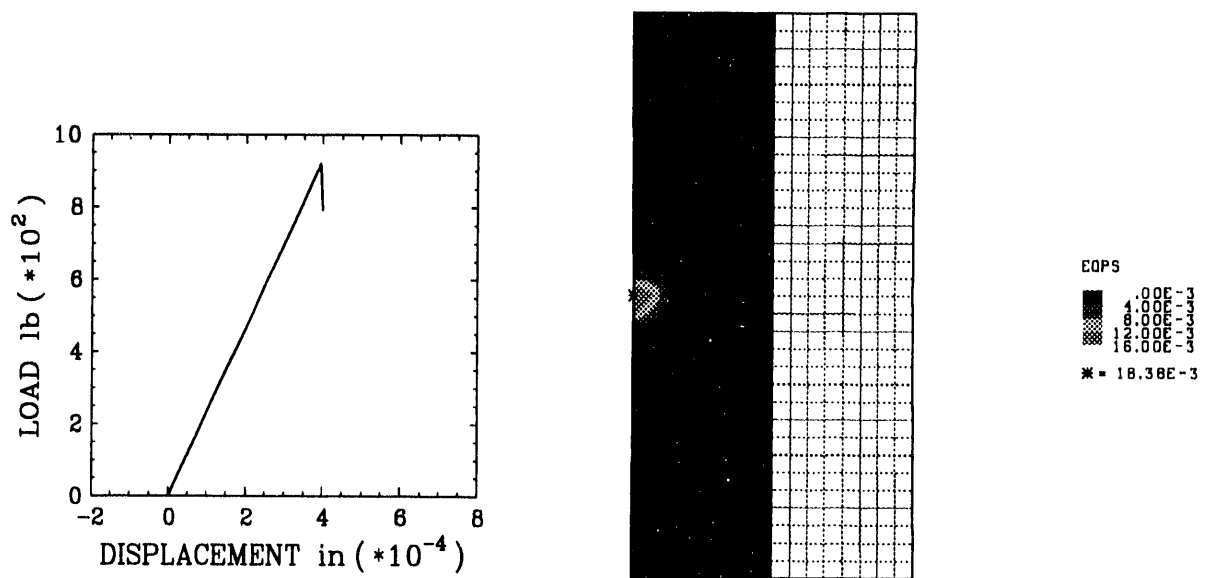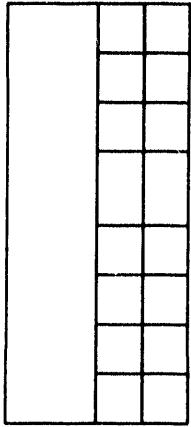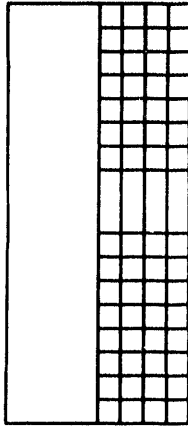**Figure 5.5.** Results from Finite Element Analysis with H = -E/(6-6v).
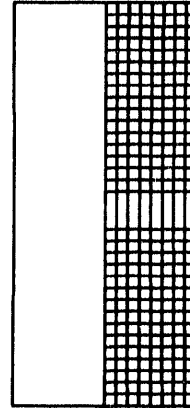
73

(a) 16 elements   (b) 64 elements   (c) 256 elements

Figure 5.6. Deformed Shape of Finite Element Models Subject to Uniaxial Tension - Principal Stress Plasticity.
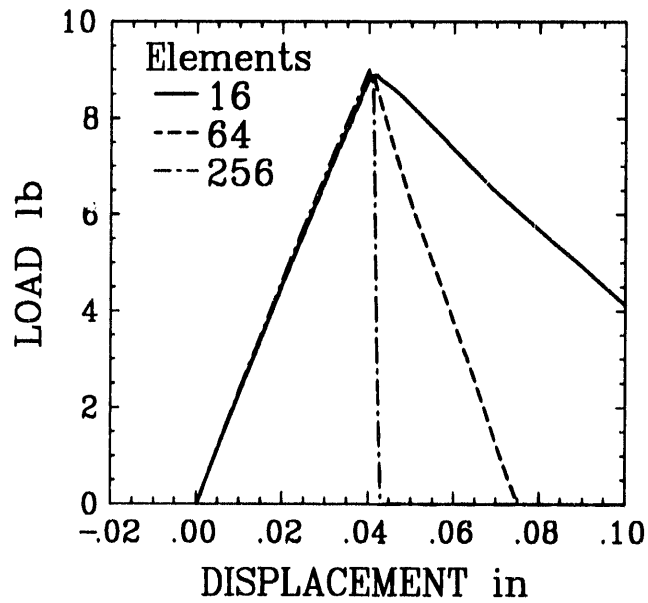
Figure 5.7. Applied Load vs. End Displacement - Principal Stress Plasticity.
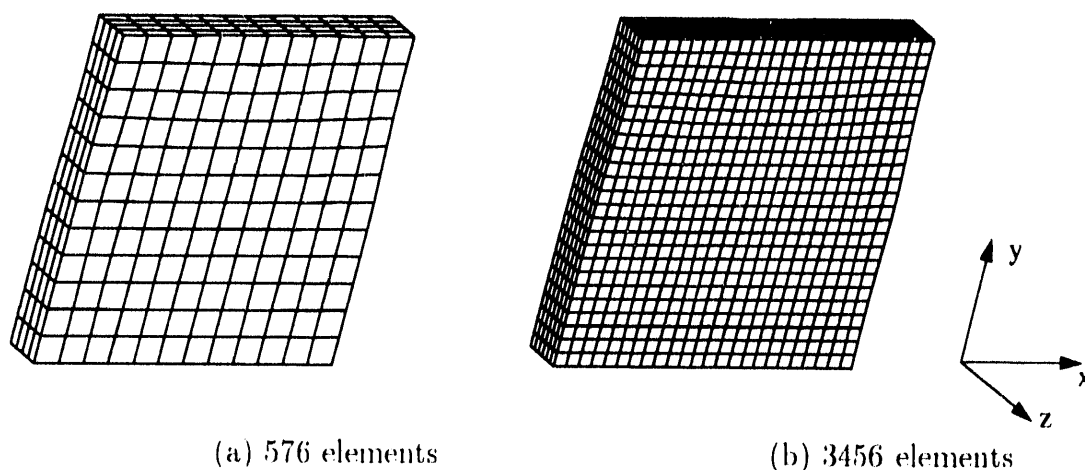
Figure 5.8. Finite Element Models of a Thin Plate.

y-direction shown in Figure 5.8. The deformed shape of the model and contours of out-of-plane displacement are shown in Figure 5.9. The displacement contours clearly show the initiation of necked regions oriented at an angle of approximately 60 degrees from the loading axis, which is very close to the orientation predicted by the bifurcation analysis. A second analysis of this problem was then performed using the fine mesh to evaluate the accuracy of the coarse mesh solution. A comparison of results from this analysis (Figure 5.10) with results obtained with the coarse mesh indicate that the coarse mesh solution is acceptably accurate.

5.1.4 Thin Plate Subjected to Equal Biaxial Tension

In the next analysis, the same plate was subjected to equal biaxial tension in the x-y plane. The deformed shape of this model and contours of out-of-plane displacement are shown in Figure 5.11. The numerical analysis indicates that bifurcations will not be generated for an elastic perfectly plastic, von Mises material. The theoretical bifurcation analysis performed previously indicates that plates subject to equal biaxial tension would have to be constructed from a material which exhibits a significant amount of strain-softening for bifurcations to occur. Thus, both the bifurcation analysis and the numerical analysis indicate that this material and loading will not generate any general or discontinuous bifurcations.

To simulate localization phenomena, we would like to be able to obtain solutions that are numerically stable beyond discontinuous bifurcation points. When the numerical procedure fails to converge, we really don't know if a discontinuous bifurcation point
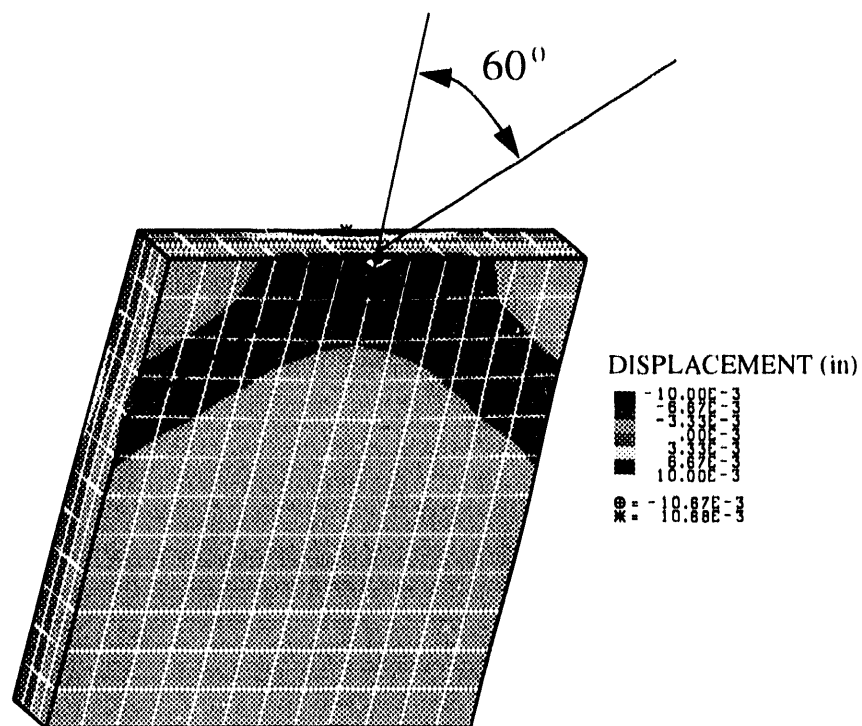
Figure 5.9. Normal Displacement Contours for a Thin Plate Subjected to Uniaxial Tension - 576 Element Mesh.
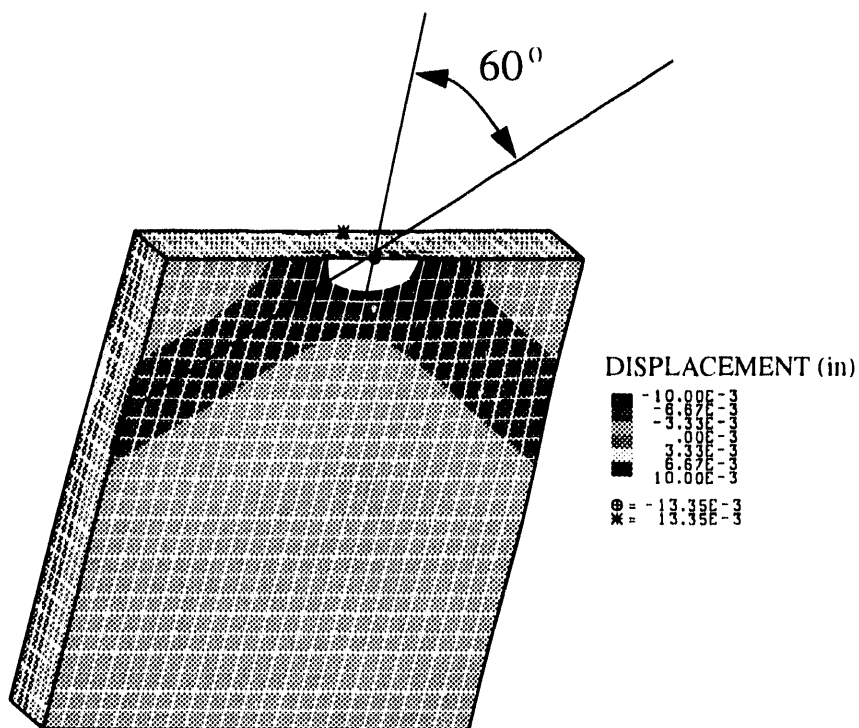
Figure 5.10. Normal Displacement Contours for a Thin Plate Subjected to Uniaxial Tension - 3456 Element Mesh.

76
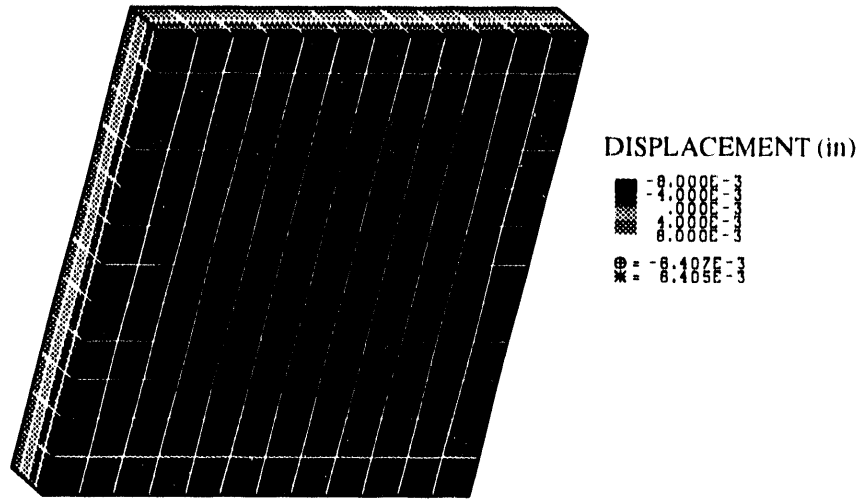
DISPLACEMENT (in)

Figure 5.11. Normal Displacement Contours for a Thin Plate Subjected to Equal Biaxial Tension.

has been reached or if the solution algorithm is unstable. To be able to say anything about the initiation and nature of the localization we must be able to obtain convergent solutions beyond the point of localization. The second problem which must be addressed is that of mesh dependence. To feel comfortable with solutions to localization problems or any problems we need solutions that converge with mesh refinement. In the next two sections, we briefly address these two problems associated with the numerical simulation of localization phenomena.

5.2 Modifications to Obtain Numerical Solutions

Localization phenomena are generally very difficult to simulate numerically. Localization occurs when the material is softening and the structure is unstable. The load generally does not monotonically increase; thus, it is generally not possible to solve localization problems in which the load is prescribed. In the example problems presented in the previous sections, solutions were obtained by prescribing displacements which monotonically increase. However in some localization problems, the load-displacement curve exhibits snap-back (Schreyer and Chen, 1986) which cannot be followed by simply prescribing displacements (Figure 5.12). To follow these paths we must resort to more complex procedures for advancing the problem. Riks (1979) and Crisfield (1981) have developed an arc-length control procedure which can solve some structural mechanics problems exhibiting softening. With this procedure, the solution is incremented a certain distance along the load-displacement curve during each load step and the prescribed loads or displace-
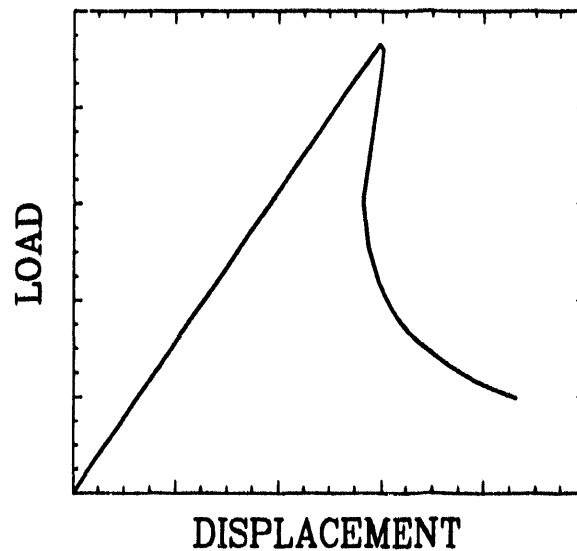
Figure 5.12. Load-Displacement Curve Exhibiting Snap-Back.

ments are functions of this constraint. However, de Borst (1986) and Chen, Neilsen and Schreyer (1991) have found that the arc-length control procedure is not robust enough to obtain solutions to many localization problems. Robustness of the arc-length control procedure is improved significantly by using a norm of the incremental displacements associated with nodes near the localized zone in place of a global norm as the constraint (de Borst, 1986). Chen, Neilsen and Schreyer (1991) propose a solution procedure in which the increment in damage or plastic deformation generated in some critical element is the constraint. With this procedure, the damage or plastic strain increment is prescribed to monotonically increase and the load needed to generate the prescribed increment in plastic strain or damage is computed. This solution procedure has been successfully used in the solution of a number of localization problems.

5.3   Modifications to Eliminate Mesh Dependence

Even if the solution algorithm is robust enough to solve the problem, we find that solutions to localization problems are mesh dependent as shown in Section 5.1.2. If the mesh is oriented along the localized zone, the size of the localized deformation zone will be equal to the dimension of the elements being used. The first and simplest approach for coping with the mesh dependence is to simply use elements that are the same size as the expected localized deformation zone. With this approach there is really no way to evaluate the accuracy of the solution with mesh refinement because the predicted size of the localized deformation zone is mesh dependent. The second approach is to use non-local constitutive theories which have some internal length scale as a material parameter. When this approach is used, elements which are smaller than the width of the localized deformation zone are usually required to capture the localization. The

78

third approach is to view localization and the size of the localized deformation zone as a structural property which is independent of the material or constitutive response and to assume that the localized deformation zone is embedded within an element. With this approach, elements which are larger than the width of the localized deformation zone can be used which is appealing because the size of localized deformation zones observed in experiments involving various materials are generally much smaller than the structure being analyzed. Pietruszcak and Mroz (1981), Ortiz, Leroy and Needleman (1987), Belytschko, Fish and Engelmann (1988), and Neilsen, Chen and Schreyer (1991) have used various approaches to embed localized deformations zones within elements. Pietruszcak and Mroz (1981) assume that material outside the localized deformation zone is rigid and that element deformations are governed by deformations within the localized deformation zone. Ortiz, Leroy and Needleman (1987) enhance the shape functions to allow for deformations associated with the first possible discontinuous bifurcation. Belytschko, Fish and Engelmann (1988) modify the strain nodal-displacement matrix to account for the existence of the localized deformation zone within the element. With this approach the standard mapping between element strains and nodal displacements is replaced by mappings between softening zone strains and nodal displacements and unloading zone strains and nodal displacements. Neilsen, Chen and Schreyer (1991) investigate the use of embedded elements with damaging materials. In the next section, we discuss the use of elements with embedded localized deformation zones and reanalyze the problem of Section 5.1.2. which was severely mesh dependent using standard finite elements.

5.4   Elements with Embedded Localized Deformation Zone

Consider a finite element of length a which is subjected to a uniaxial stress, σ, (Figure 5.13) and constructed from an elastic-plastic material with the constitutive relation shown in Figure 5.14. When the bar is loaded into the inelastic regime, softening is assumed to occur uniformly in a region of length s that extends through the bar (s is a material parameter). Material outside the softening zone elastically unloads. If the bar is modeled with finite elements and the elements are chosen such that the softening zone is modeled with a single element, then a conventional finite element approach can be used. The difficulty arises when the softening zone is smaller than a single element. The constitutive relation in Figure 5.14 describes the material behavior, but cannot completely describe the behavior of an element in which some of the material is strain-softening and the remaining material is elastically unloading.

If the material outside the softening zone is elastically unloading then the strain rate in the unloading region, $\dot{\epsilon}_u$, is given by

$$\dot{\epsilon}_u = \frac{\dot{\sigma}}{E} \tag{5.1}$$

where E is the elastic modulus. The strain rate in the softening zone, $\dot{\epsilon}_s$, is as follows:

$$\dot{\epsilon}_s = \frac{\dot{\sigma}}{E} + \frac{\dot{\sigma}}{H} \tag{5.2}$$
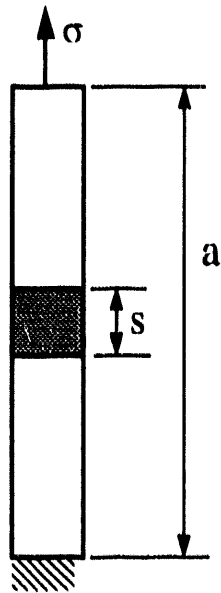
Figure 5.13. Softening Zone in Elastic-Plastic Rod Subjected to Uniaxial Tension.

Figure 5.14. Constitutive Relation for Elastic-Plastic Material.
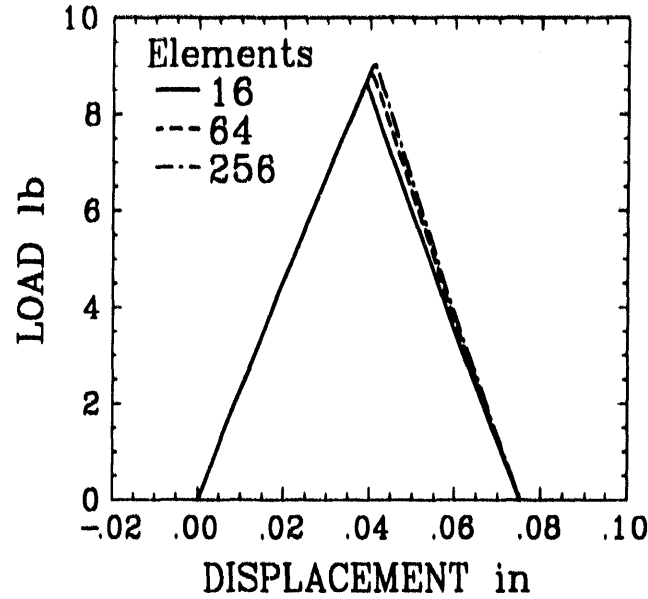
Figure 5.15. Applied Load vs. End Displacement Predictions Obtained Using Finite Elements with Embedded Softening Zones.

where H is the hardening modulus for the material. The average element strain rate, $\dot{c}_r$, is given by

$$\dot{c}_r = \frac{\dot{\sigma}}{E} + \frac{s\dot{\sigma}}{aH} \tag{5.3}$$

Equation 5.3 indicates that an element which is constructed entirely from a material with a hardening modulus, H_r, as follows:

$$H_r = \frac{Ha}{s} \tag{5.4}$$

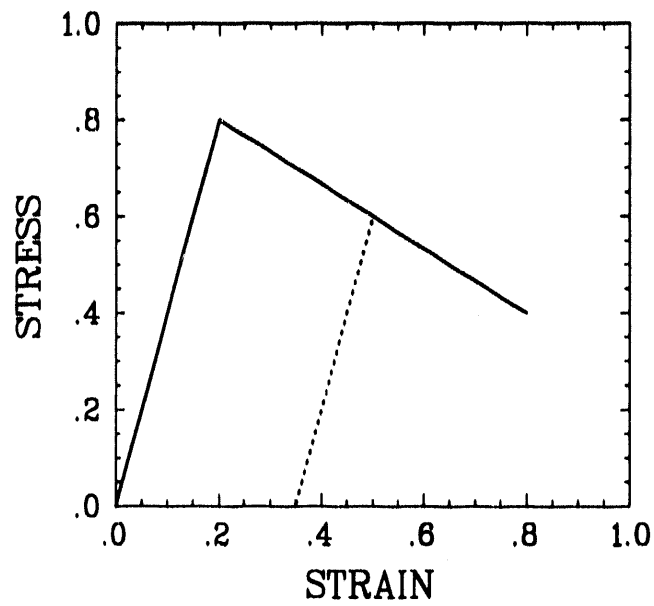will have the same axial response as the element with the embedded softening zone and a material softening modulus of H. Using this information, the problem of Section 5.1.2 was reanalyzed using element softening moduli which are mesh dependent. In this analysis, the material has a softening modulus of 50 psi and the softening zone is assumed to have a fixed length of 0.0125 inches. Thus, the 16 element mesh was analyzed with an element softening modulus of 200 psi, the 64 element mesh with an element softening modulus of 100 psi and the 256 element mesh with an element softening modulus of 50 psi. Results from these analyses (Figure 5.15) show that solutions which are not mesh dependent can be obtained by assuming that the softening zone has a fixed size and is embedded within a single element.

A similar approach can be used to relate the material response to the element response if the material is elastic-damaging with the constitutive relation shown in Figure 5.16. If we assume that material outside the softening zone is not damaged and is simply elastically unloading, then strain in the unloading region, c_u, is given by

$$c_u = \frac{\sigma}{E} \tag{5.5}$$

81
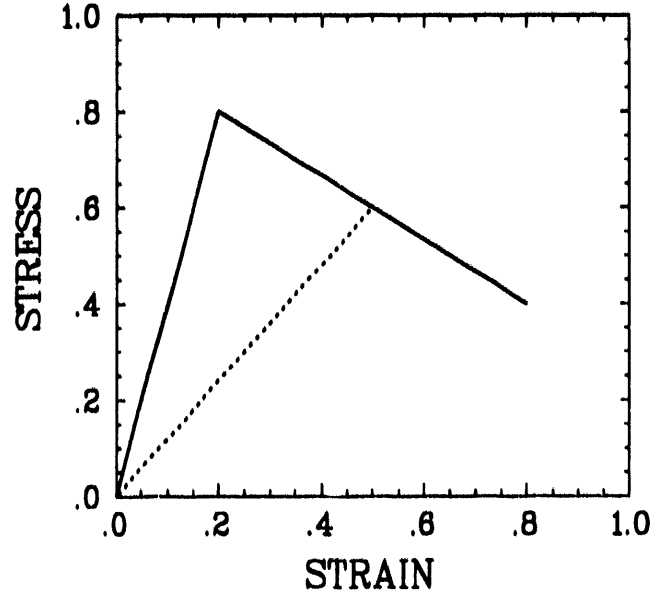
Figure 5.16. Constitutive Relation for Elastic-Damaging Material.

Strain in the softening zone, ϵ_s, is given by

$$\epsilon_s = \frac{\sigma}{E(1 - w)} \tag{5.6}$$

where w is damage in the softening zone material. The following expression for average element strain, ϵ_e, can be derived using the two previous equations

$$\epsilon_e = [1 - w + \frac{s}{a}w]\epsilon_s \tag{5.7}$$

If the element stress, σ, and strain, ϵ_e, are related by

$$\sigma = E(1 - w_e)\epsilon_e \tag{5.8}$$

where w_e is the equivalent element damage, then it can be shown that the element damage is related to damage in the softening zone material, w, by the following equation.

$$w_e = \frac{sw}{[a - aw + sw]} \tag{5.9}$$

As with plasticity, there is a relationship between inelastic material level parameters and equivalent inelastic element level parameters. This relationship depends on the size of the softening zone and on the size of the elements being used.

In the example plasticity problem presented in this section, the localized zone was an opening mode oriented across a single row of elements. For general applications in two

and three dimensions, the embedded localized deformation zone approach must be able to handle both opening and shearing localizations with various orientations and locations within an element. For example, the localized deformation zone may cross the center of the element or possibly only the corner. It is not clear that the current approaches for elements with embedded localized deformation zones are able to solve general localization problems. Larsson and Runesson (1991) and others have shown that using finite element meshes which are aligned along localized deformation zones significantly enhances our ability to solve general localization problems. Perhaps a combination of adaptive mesh refinement along with embedded localized zone techniques should be considered for the numerical solution of localization problems. A significant amount of research and development remains to be done in this area before localization problems can be solved routinely.

84

6. A MODEL FOR POLYURETHANE FOAM

Experimental investigations by Shaw and Sata (1966) and Patel and Finnie (1969) indicate that the initial yield surface for polyurethane foam can be described using a principal stress theory. Recent experiments (Donald and Maji, 1992) indicate that polyurethane foam exhibits localization, plastic deformation and damage when it is crushed. For compressive and tensile loads, the localized deformation zones are oriented in a direction normal to the principal stresses. The bifurcation analyses of principal stress plasticity models indicate that these models do predict the localized deformations exhibited by polyurethane foams. Thus, the principal stress plasticity model for polyurethane foam developed by Neilsen, Morgan and Krieg (1987) does capture the localized deformations exhibited by rigid polyurethane foams. The original polyurethane foam model along with modifications that reflect skeleton damage and improved behavior at lock-up are presented in this section.

6.1 Description of the Foam as a Mixture

The first step in the development of the constitutive theory for polyurethane foams was an examination of the individual components of the foam structure. Rigid polyurethane foams consists of closed polymer cells with air inside the cells. Therefore, each foam consists of two structural components: (1) the polymer structure or skeleton, and (2) a mixture of air and polymer particles. In applications where the air cannot escape from the skeleton during loading, the air contribution may be significant. For example, in hydrostatic and triaxial compression tests that were performed by Donald and Maji (1992), the samples were jacketed and the air could not escape. Thus, a model which considers the contribution of the air to the overall structural response of the foams is needed to capture the foam behavior exhibited in these tests. Total foam response can be decomposed into the response of the skeleton and the response of the air in series with the polymer wall material as shown in Figure 6.1.

Since, the air/polymer does not resist any shear deformation, the air/polymer contribution is completely volumetric. For convenience, the skeleton is assumed to occupy the same space as the foam. This implies that the skeleton strain is equal to the foam strain. Also, the foam stress, σ_f, is given by the following equation

$$\sigma^f = \sigma^{sk} - p\mathbf{i} \tag{6.1}$$

where σ^{sk} is the skeleton stress and $p\mathbf{i}$ represents the air/polymer contribution. The pressure in the mixture of air and polymer particles, p, is positive in compression. To better understand this equation, consider a hydrostatic compression test in which the
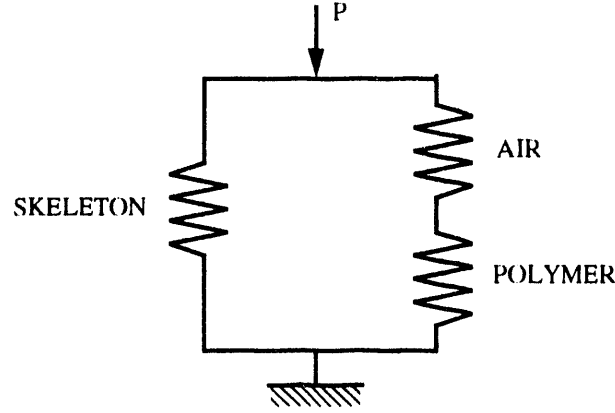
Figure 6.1. Decomposition of Foam Response into Skeleton and Air/Polymer Responses.

foam sample is jacketed and the air is not allowed to escape. If the foam consisted of loosely connected particles of polymer, then the skeleton contribution to the foam response would be negligible and the external pressure applied to the foam would equal the internal air/polymer pressure. This foam would not be able to resist any deviatoric loading. In most foams, however, the skeleton is structured so that it can carry load and the contribution of the skeleton must be added to the air/polymer contribution to determine how much load the foam can carry. In the next section, an expression for the air/polymer contribution as a function of the foam strain is derived.

6.2 Air/Polymer Response

An expression for the air/polymer pressure, p, was obtained by assuming that the air trapped within the cells is a perfect gas and that the foam compression is an isothermal process. The isothermal assumption is made because the air is in intimate contact with the polymer that makes up the cell walls and the thermal mass of the polymer is significantly larger than the thermal mass of the air. These equations indicate that the perfect gas equation of state can be used for the air and that

$$p^{air} V^{air} = p_o^{air} V_o^{air} \tag{6.2}$$

where p^{air} is the current air pressure, V^{air} the current air volume, p_o^{air} the original air pressure, and V_o^{air} the original air volume. The original air volume is related to the original foam volume, V_o by

$$V_o^{air} = V_o(1 - \Phi) \tag{6.3}$$

where Φ is the volume fraction of solid material. If we assume that the volume of the polymer is fixed when the foam is manufactured and merely changes its position as the foam deforms, an expression for the engineering volume strain, e_{vol}, is

$$e_{vol} = \frac{\Delta V^{air}}{V_o} \tag{6.4}$$

86

Prior to loading, we assume that the internal air pressure, p_0^{air}, is in equilibrium with the environment, i.e., $p_0^{air} = 14.7$ psi at sea level or $p_0^{air} \approx 12.5$ psi here in Albuquerque, New Mexico. The change in internal air pressure due to the loading $p = p^{air} - p_o^{air}$ is related to the change in air volume as follows

$$\Delta V^{air} = \frac{-pV_o(1 - \Phi)}{p_o^{air} + p} \tag{6.5}$$

Combining the above equations we obtain the following expression for the air contribution, p, in terms of the current engineering volume strain, e_{vol}

$$p = \frac{-p_o^{air} e_{vol}}{(e_{vol} + 1 - \Phi)} \tag{6.6}$$

This equation is used by Neilsen, Morgan and Krieg (1987) in their foam model and also by Gibson and Ashby (1988). In the development of Equation 6.6, a critical assumption is that the volume of the polymer does not change during loading. This assumption is only valid when the pressures are small. If the pressures are large, the volume of the polymer which makes up the cell walls will change according to the bulk modulus of the polymer, K^{poly}, as follows

$$\Delta V^{poly} = \frac{-pV_o\Phi}{K^{poly}} \tag{6.7}$$

The bulk modulus for polyurethane is approximately 150,000 psi. The expression for engineering volume strain is now given by

$$e_{vol} = \frac{\Delta V^{air} + \Delta V^{poly}}{V_o} \tag{6.8}$$

Finally, by combining the above equations the following quadratic equation is obtained

$$\Phi p^2 + [p_o^{air}\Phi + K^{poly}(1 - \Phi + e_{vol})]p + e_{vol}K^{poly}p_o^{air} = 0 \tag{6.9}$$

This equation can be easily solved and only one root is shown to be physically realistic. Plots of air pressure as a function of volume strain using Equations 6.6 and 6.9 are shown in Figure 6.2. This figure clearly shows that the effect of considering the elastic bulk response of the polymer is only significant for large pressures.

If the air is allowed to escape then the response of particle interaction is given by Equation 6.9 with the initial air pressure, p_0^{air} set equal to zero. With p_0^{air} equal to zero, Equation 6.9 reduces to

$$p = 0 \qquad or \qquad p = -\frac{K^{poly}}{\Phi}(1 - \Phi + e_{vol}) \tag{6.10}$$

These equations describe two intersecting lines. The response of the polymer when the air is allowed to escape can be approximated by simply prescribing a small value for the initial air pressure as shown in Figure 6.3.
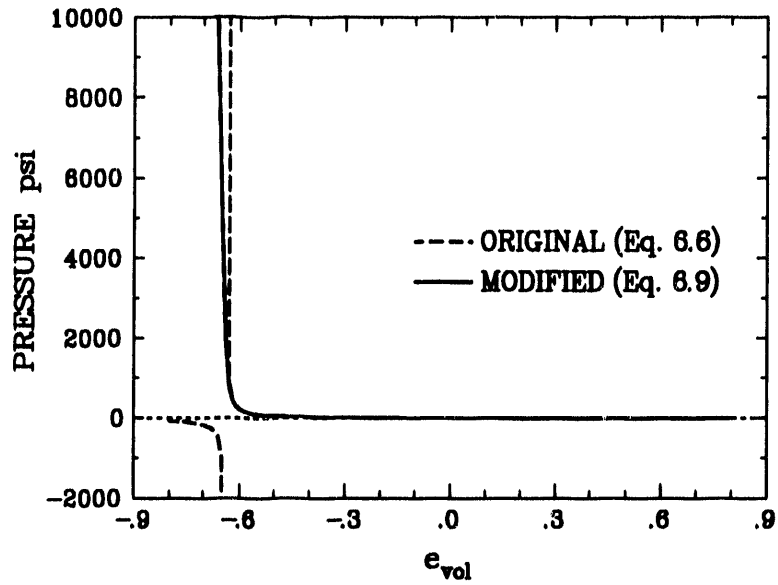
Figure 6.2. Air/Polymer Response for a 20 pcf Polyurethane Foam.
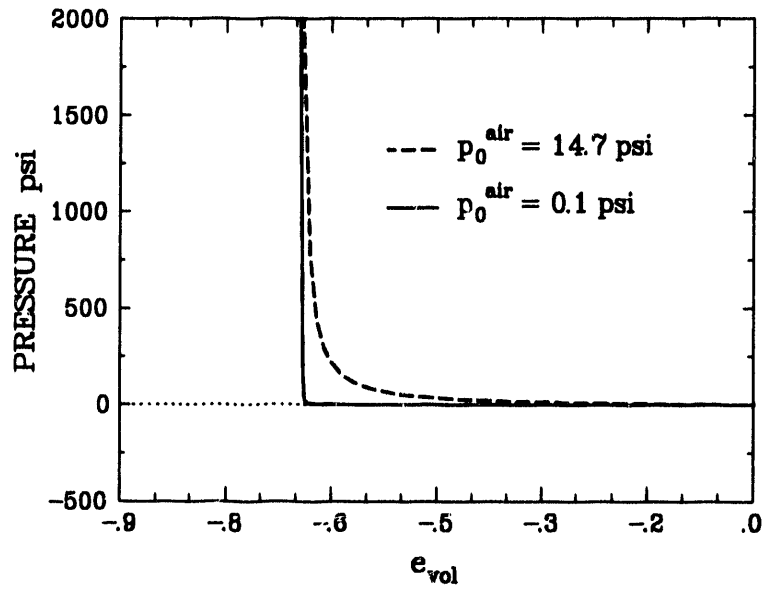

Figure 6.3. Air/Polymer Response for a 20 pcf Polyurethane Foam with Air Allowed to Escape.

6.3 Plasticity Theory for the Skeleton

Neilsen, Morgan, and Krieg (1987) developed a plasticity model to describe the contribution of the skeleton to the overall foam response. The yield function for their skeleton model is given by

$$\Psi^i = \tfrac{1}{2}(\boldsymbol{\sigma} : \mathbf{P}^i : \boldsymbol{\sigma})^{\tfrac{1}{2}} - A < II' > + B(1 + Ce_{vol})\qquad(6.11)$$

where $\mathbf{P}^i$ is the principal projection operator, II' is the second invariant of the deviatoric strains, $<>$ is the Heaviside step function, and e_{vol} is the engineering volume strain. The yield stress in each principal stress direction is a function of both the volume strain and the deviatoric strain. A, B, and C are material constants. The constant B is the yield stress of the skeleton for purely hydrostatic loading, and the product of B and C is the slope of the skeleton volumetric response after yielding for purely hydrostatic loading. The constant A is equal to the difference between the axial yield stress for hydrostatic loading and the axial yield stress for deviatoric loading. In Equation 6.11, the term $A < II' >$ is active only if the loading is deviatoric. This yield function was based on a series of uniaxial, hydrostatic and triaxial compression tests on low-density rigid polyurethane foams which were completed by the Civil Engineering Research Facility (CERF) at the New Mexico Engineering Research Institute (NMERI) in 1982. Results from this experimental investigation are documented by Neilsen, Morgan and Krieg (1987).

In triaxial compression tests, the material is subjected to some level of hydrostatic compression and subsequently additional load in one direction only. Results from NMERI's triaxial tests on foam indicated that the foam exhibited a higher strength when the additional axial load was applied as opposed to hydrostatic compression only. The application of additional axial load corresponds to the introduction of deviatoric strains which led to the assumption that the yield surface grows when deviatoric strains are introduced. A recent series of tests completed by Donald and Maji (1992) reveal that the apparent increase in strength associated with the application of the additional axial load is actually due to the anisotropic character of the low density foams. During the NMERI tests the additional axial load was always applied in the rise direction of the foam and the foam is generally stronger in the rise direction than in directions perpendicular to the rise direction. Therefore, for the improved model developed in the next section, we adopt an anisotropic yield function that does not include a jump associated with the introduction of deviatoric loading.

6.4 Coupled Theory for the Skeleton

Experiments completed by Donald and Maji (1992) indicate that the skeleton exhibits both plastic deformation and damage as it is crushed. Therefore, a coupled plasticity, continuum damage model for the skeleton would be more appropriate than the previously

developed plasticity model. The experimental evidence suggests that a principal stress based model is appropriate for polyurethane foams; thus, we adopt the following yield (damage) function

$$\Psi^i = \frac{1}{2}(\sigma : \mathbf{P}^i : \sigma)^{\frac{1}{2}} - (A + Be_{vol}) \tag{6.12}$$

where $\mathbf{P}^i$ is again the principal projection operator, A and B are material parameters that are dependent on the current amount of damage in the current principal stress orientation. Information about damage is stored in the damaged elastic stiffness tensor, $\mathbf{S}$. The evolution equations for plastic strain and damage are given by

$$\dot{\epsilon}^p = \dot{\rho}\mathbf{P}^i : \sigma \qquad \dot{\mathbf{S}} = -\dot{\omega}\mathbf{S} : \mathbf{P}^i : \mathbf{S} \qquad \dot{\mathbf{C}} = \dot{\omega}\mathbf{P}^i \tag{6.13}$$

The evolution equation for plastic strain indicates that plastic strains will be generated in principal stress directions. The damage evolution equation indicates that the compliance of the material will be increased in a direction parallel to the current maximum tensile stress. Even if the skeleton stiffness is isotropic prior to loading, the damage evolution equation indicates that the material will become anisotropic as it is damaged. Since the material stiffness is not isotropic it cannot simply be represented by two scalars and instead the entire stiffness or compliance matrix must be stored. However, by storing the compliance matrix we have implicitly stored information about load history.

To complete this model we need an additional equation that prescribes the relative amounts of damage and permanent strain generated during an inelastic step. The additional equation is given by

$$M\dot{\rho} = (1 - M)\dot{\omega} \tag{6.14}$$

In this equation, we allow the magnitude of the non-negative material parameter M to depend on the sign of the principal stress. Specifically, in compression the inelastic behavior is dominated by plasticity, whereas, in tension the inelastic behavior is dominated by damage.

6.5   Simplified Isotropic Theory for the Skeleton

Most existing finite element codes were developed using only isotropic plasticity models and generally do not have the architecture required for the easy implementation of anisotropic models. In this section, an isotropic, coupled plasticity damage model which captures at least most of the behavior exhibited by the foam skeleton is developed. This model uses the yield (damage) function given by Equation 6.12 and the flow law for plastic strain increments given by Equation 6.13. However, for the material to remain isotropic, we must adopt an isotropic evolution equation for damage.

If we assume that the skeleton has a Poisson's ratio equal to zero, then the undamaged elastic stiffness tensor for the skeleton, $\mathbf{E}$, is given by

$$\mathbf{E} = E_0\mathbf{I} \tag{6.15}$$

where E_0 is the initial or original elastic modulus and $\mathbf{I}$ is the fourth-order identity tensor. Thus, for this model we adopt a simple isotropic damage evolution equation given by

$$\dot{\mathbf{S}} = -\dot{\omega} E_0 \mathbf{I} \qquad (6.16)$$

With this simple scalar damage model, damage history is stored in a single scalar, the damaged elastic modulus, $E = (1 - w)E_0$.

6.6 Analysis of Material Characterization Tests

A series of tests were recently performed in the Civil Engineering Department at the University of New Mexico to characterize the behavior of rigid polyurethane foams and aluminum honeycombs (Donald and Maji, 1992). In this section, several finite element analyses of the material characterization tests are performed to determine if the constitutive model developed in this chapter will analytically predict the foam behavior which was observed during the experiments.

The constitutive model developed in this chapter was implemented in the finite element code SANTOS (Stone, 1992). In SANTOS, the constitutive relations are expressed in terms of the deformation rate and Cauchy stress in the unrotated configuration (Taylor and Flanagan, 1986). The analyses were performed using SANTOS and the finite element models of axisymmetric material specimens shown in Figure 6.4. The models were subject to uniaxial compression, hydrostatic compression and uniaxial tension. The predicted response of the foam from the finite element analyses was compared with the experimental observations. Properties that are appropriate for a 5 pound per cubic foot foam were used in this investigation (Table 6.1).

In the first analyses, the models were subject to uniaxial compression. A plot of the undeformed and deformed 200 element mesh is shown in Figure 6.5. The deformed shapes show that the model predicts only axial deformation when the material is compressed in the plateau regime and a combination of axial and radial deformation when the material is loaded into the lock-up regime. This deformation behavior is observed experimentally. Mesh refinement had no significant effect on the predicted compressive response of the material. A plot of the applied load versus end displacement predicted by the finite element analyses is compared with the experimental result in Figure 6.6. This plot shows that response predicted by the finite element analyses is qualitatively accurate;

Table 6.1. Material Parameters for a 5 pcf Polyurethane Foam.

Elastic Modulus (psi)	Poisson's Ratio	A Comp. (psi)	B Comp. (psi)	M Comp.	A Tens. (psi)	B Tens. (psi)	M Tens.	Φ
3,000	0.0	110	0	0.1	110	-100	1.0	0.09

91

however, the amount of crush required to lock-up the foam is smaller than the crush at lock-up predicted by the analyses. One possible explanation for this discrepancy is that the polymer particles which make up the cell walls actually begin to contact each other and carry load before the volume fraction of solid material is close to unity. To correct this discrepancy, an additional particle interaction contribution could be included or the material parameter, Φ, could be modified to account for particle interaction.

In the next analyses, the models were subject to uniaxial tension. A plot of the deformed meshes is shown in Figure 6.7. The deformed shapes show the formation of a discontinuous opening mode bifurcation which is also observed in polyurethane foam samples subject to uniaxial tension. A plot of the applied load versus end displacement predicted by the finite element analyses is compared with the experimental result in Figure 6.8. Both the loading and unloading responses predicted by the finite element analyses are shown. The behavior predicted during loading in the softening regime is clearly mesh-dependent. This result was expected because a non-local feature was not incorporated in the current model. As expected, the unloading curves pass through the origin which indicates that the model predicts only damage when the material is subjected to uniaxial tension.

In the final analyses, the models were subject to hydrostatic compression. Plots of the deformed meshes are shown in Figure 6.9. The size of the original undeformed sample is indicated by the dashed lines in Figure 6.9. These analyses predict the generation of rather unusual deformed shapes and localization during hydrostatic compression tests. A bifurcation analysis of this model and stress state indicates that localization is not expected since the fundamental eigentensor for the tangent stiffness tensor is equal to the second-order identity which has no zero eigenvalue. However, if the stress state is not purely hydrostatic due to numerical roundoff then the bifurcation analysis indicates that localization as exhibited by the finite element analyses may occur. Also, recent studies by Benallal, Billardon and Geymonat (1989, 1990) of instabilities at the boundary of a solid may help to explain these numerical results.

A plot of applied pressure versus engineering volume strain predicted by the finite element analyses is compared with the experimental result in Figure 6.10. This plot shows that response predicted by the finite element analyses matches the experimental result reasonably well. Even though the deformed shapes were rather mesh dependent the plots of applied pressure vs. volume strain were not mesh dependent.
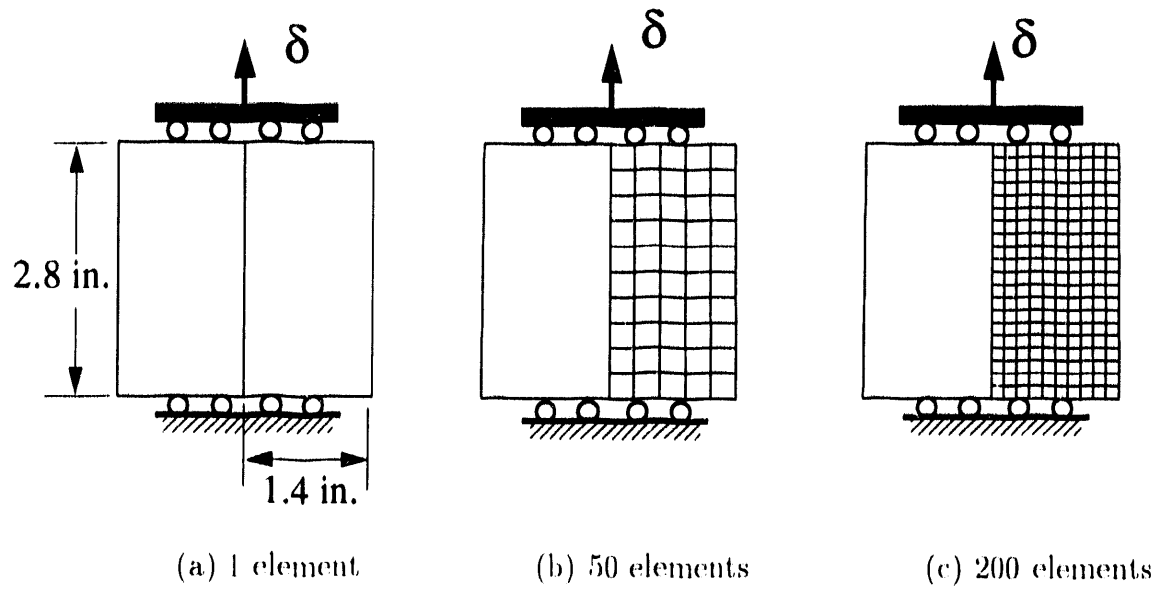
Figure 6.4. Axisymmetric Finite Element Models of Foam Specimens.
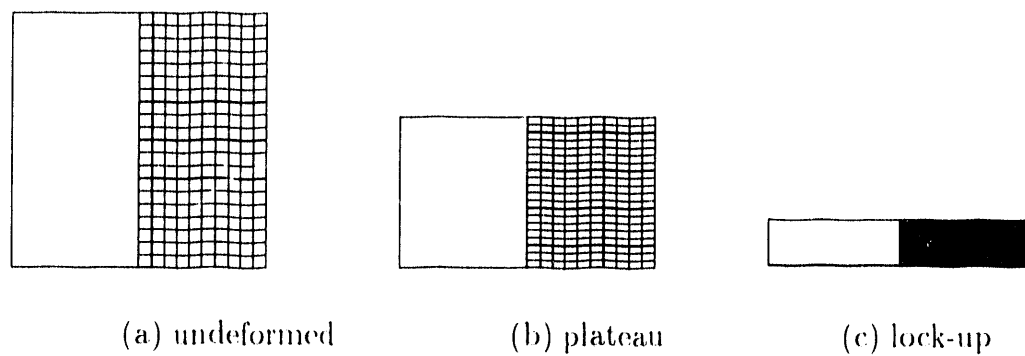
Figure 6.5. Deformed Shape of 200 Element Model Subject to Uniaxial Compression.
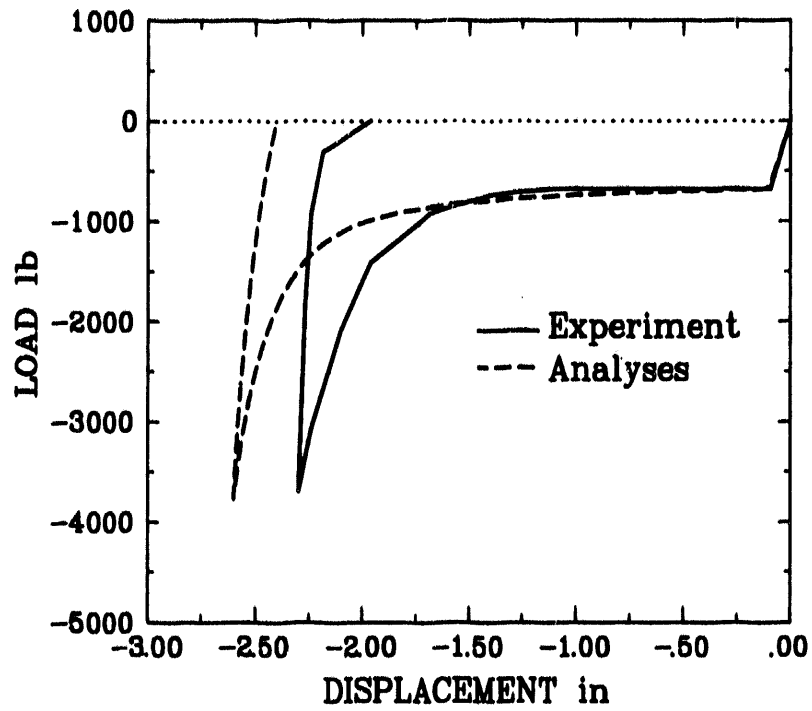
Figure 6.6. Applied Load vs. End Displacement - Uniaxial Compression -
Comparison of Finite Element Analyses Predictions with Experimental
Observations.

(a) 1 element   (b) 50 elements   (c) 200 elements
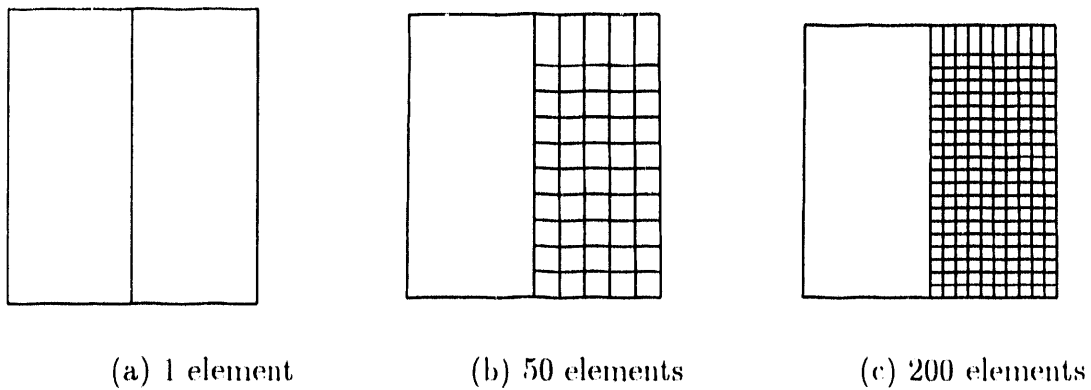
Figure 6.7. Deformed Shape of Models Subject to Uniaxial Tension.

94
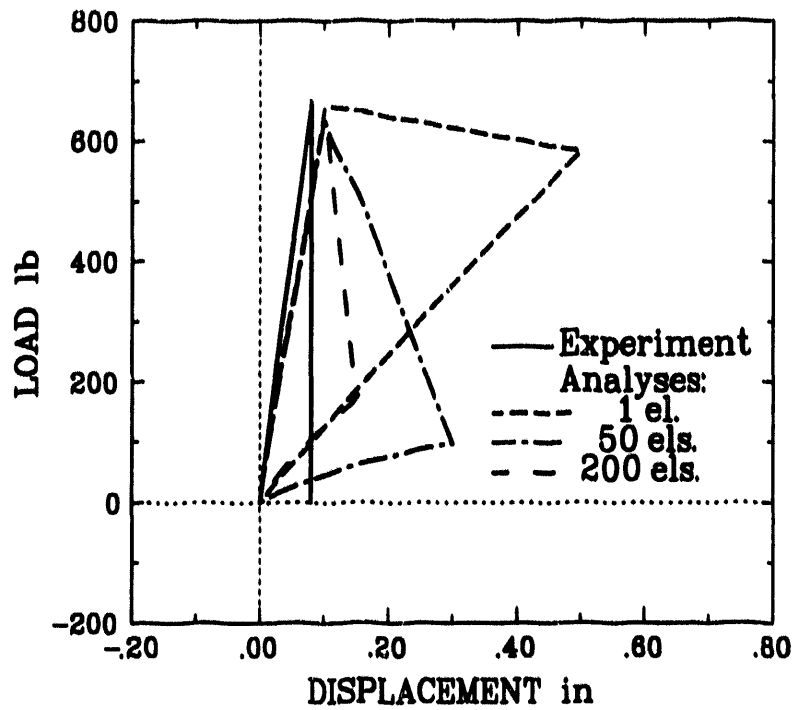
Figure 6.8. Applied Load vs. End Displacement - Uniaxial Tension - Comparison of Finite Element Analyses Predictions with Experimental Observations.
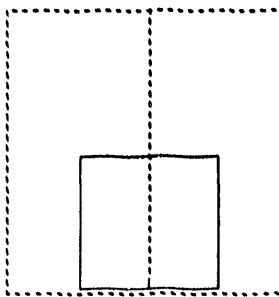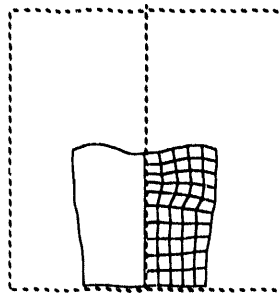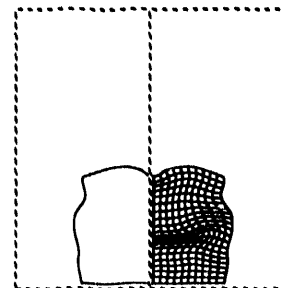
(a) 1 element   (b) 50 elements   (c) 200 elements

Figure 6.9. Deformed Shape of Models Subject to Hydrostatic Compression.

Figure 6.10. Applied Pressure vs. Engineering Volume Strain - Hydrostatic Compression - Comparison of Finite Element Analyses Predictions with Experimental Observations.

7. ALUMINUM HONEYCOMB MODEL

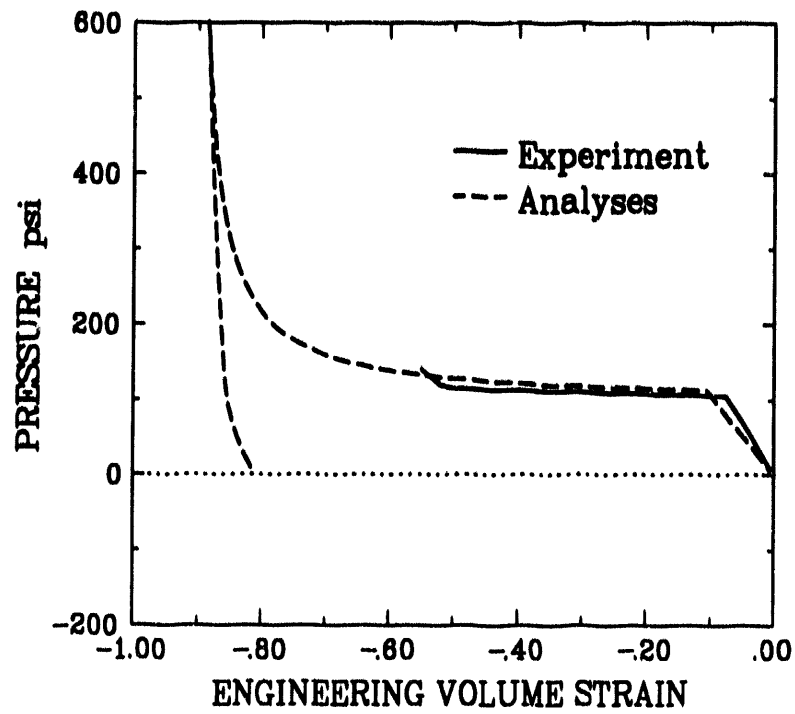Experiments on aluminum honeycomb indicate that localization and plastic deformation is generated when the material is crushed. Thus, a plasticity model developed for aluminum honeycomb should predict localization when the material is loaded into the plateau regime. The localization exhibited by honeycomb is oriented along geometric lines which is not a typical characteristic of other materials. The only existing model that predicts localizations which are similar to those observed in honeycomb is the Mohr-Coulomb model which predicts localization with an orientation which is dependent on the internal friction angle and the orientation of the principal stresses. A plasticity model which predicts localization with an orientation that is dependent on the geometry will require a yield function that is dependent on the geometry. Such a model was developed by Klintworth and Stronge (1988). Their model along with a bifurcation analysis is presented in the next section.

7.1 In-plane Response

A number of researchers have investigated the in-plane behavior of aluminum honeycomb (Klintworth and Stronge, 1988; Gibson and Ashby, 1988) and developed expressions for the initial yield surfaces for this material. Klintworth and Stronge (1988) have investigated the response of aluminum honeycomb subjected to in-plane stresses as shown in Figure 7.1. Their investigation indicates that the yield surface for in-plane loads consists of a family of intersecting yield surfaces with yield functions given by

$$\Psi = a\sigma_{xx} + b\sigma_{yy} + c(\sigma_{xy} + \sigma_{yx}) - d \qquad (7.1)$$

where a, b, c, and d are material parameters that depend on the cell geometry.

The experimental compression tests indicate that the yield surfaces do not change significantly in the plateau regime; thus, we can assume that the parameters a, b, c and d in the above yield functions are constant in the plateau regime. Furthermore, if we assume the material exhibits associated flow then

$$\mathbf{f} = \mathbf{g} = \frac{\partial \Psi}{\partial \boldsymbol{\sigma}} \Rightarrow \begin{bmatrix} a & c & 0 \\ c & b & 0 \\ 0 & 0 & 0 \end{bmatrix} \qquad (7.2)$$

The bifurcation analyses of plasticity theories with associated flow rules indicate that the first possible bifurcation occurs at the limit point. The mode associated with this bifurcation is characterized by the normal to the yield surface, $\mathbf{f}$, which is dependent on the
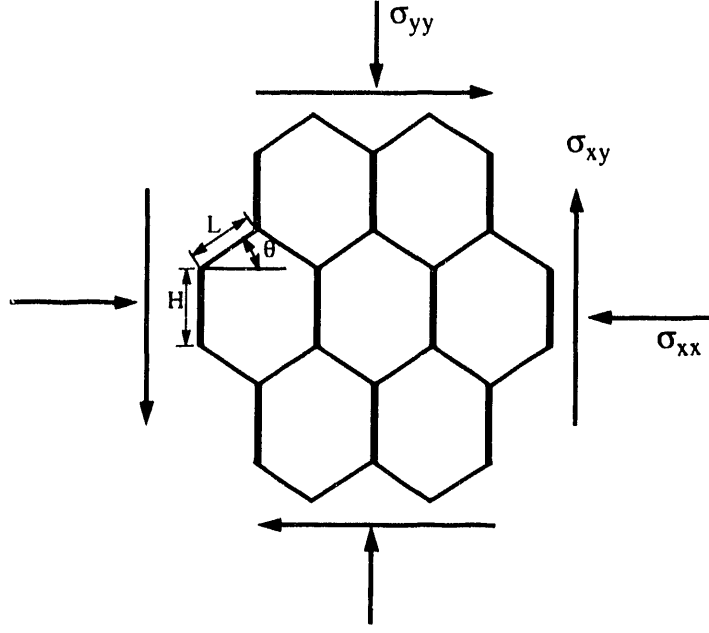
Figure 7.1. In-plane Loading of Aluminum Honeycomb Cells.

material parameters and thus cell geometry. For example, when the honeycomb is subjected to uniaxial compression in the x direction, the active yield surface is characterized by

$$a = -\frac{1}{\Sigma_x} - \frac{1}{\Upsilon_x}$$

$$b = -\frac{1}{\Sigma_y} + \frac{1}{\Upsilon_y}$$

$$c = -\frac{1}{2\Sigma_{xy}} + \frac{1}{2\Upsilon_{xy}}$$ (7.3)

$$d = 1$$

where Σ_x, Σ_y and Σ_{xy} are elastic buckling parameters and Υ_x, Υ_y and Υ_{xy} are plastic collapse parameters defined as follows:

$$\Sigma_x = \frac{\pi^2 E t^3}{12 L^2 (H + L\sin\theta)\cos\theta}$$

$$\Sigma_y = \frac{\pi^2 E t^3}{12 L^3 \cos\theta \sin\theta}$$

$$\Sigma_{xy} = \frac{\pi^2 E t^3}{12 L^2 (L + H\sin\theta)}$$ (7.4)

$$\Upsilon_x = \frac{t^2 \sigma_y}{2L(H + L\sin\theta)\sin\theta}$$

$$\Upsilon_y = \frac{t^2 \sigma_y}{2L^2 \cos^2\theta}$$

98

$$\Upsilon_{xy} = \frac{t^2\sigma_y}{2HL\cos\theta}$$

where L, H, t, and θ are the dimensions and angle that describe a typical cell as shown in Figure 7.1. E is the elastic modulus for the solid material and σ_y is the yield strength for the solid material. Parameters for a typical aluminum honeycomb are given in Table 7.1.

Table 7.1. Parameters for a 0.125-5052-.002 Aluminum Honeycomb.

E psi	σ_y psi	H in.	L in.	t in.	θ degree
10.0E6	24000	0.072	0.072	0.002	30

Using these material parameters we obtain the following values for the yield function constants: $a = -0.0884$ in^2/lb, $b = 0.0785$ in^2/lb, $c = 0.0425$ in^2/lb. By substituting these constants into the expression for f, Equation 7.2, and performing the bifurcation analysis we find that this plasticity model predicts localization at the limit point with an orientation of 30.0 degrees which is very close to the experimentally observed orientation (Figure 7.2.) Furthermore, the orientation of m indicates that the bifurcation is primarily a shearing type bifurcation which is also consistent with experimental observations.

When the foam is subjected to uniaxial compression in the y direction, the active yield surface is characterized by

$$a = -\frac{1}{\Sigma_x} + \frac{1}{\Upsilon_x}$$

$$b = -\frac{1}{0.346\Phi_y\Sigma_y} - \frac{1}{\Upsilon_y} \tag{7.5}$$

$$c = 0$$

$$d = 1$$

where

$$\Phi_y = \frac{L\sin\theta}{H} \tag{7.6}$$

Using the material parameters given in Table 7.1 we obtain the following yield function constants: $a = 0.0736$ in^2/lb, $b = -0.0952$ in^2/lb, $c = 0.0$ in^2/lb. By substituting these constants into the expression for f and performing the bifurcation analysis we find that this plasticity model predicts localization at the limit point with an n oriented at an angle of 48.7 degrees from the x axis which is again reasonably close to the orientation which is observed experimentally (Figure 7.3).

These bifurcation analyses indicate that the plasticity model developed by Klintworth and Stronge (1988) does capture the localized deformations for the load cases that were analyzed. It was beyond the scope of this paper to evaluate all of the yield surfaces required to describe all possible load paths.
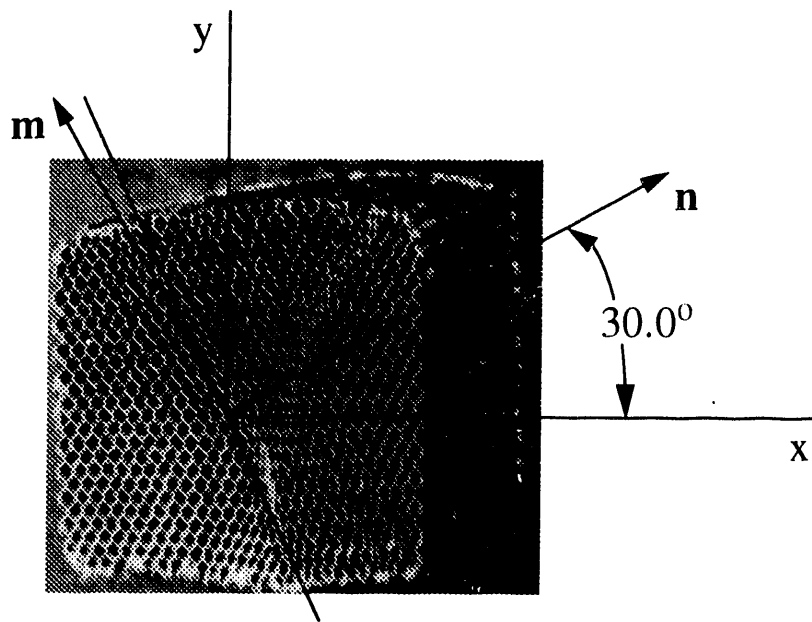
Figure 7.2. Comparison of Bifurcation Analysis Predictions with Experimental Observations of Localization in Aluminum Honeycomb Subjected to Uniaxial Compression in the x-Direction.
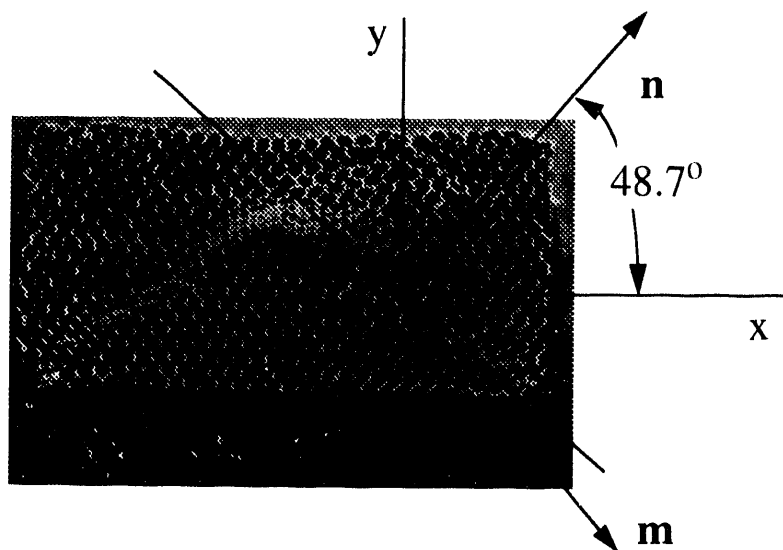
Figure 7.3. Comparison of Bifurcation Analysis Predictions with Experimental Observations of Localization in Aluminum Honeycomb Subjected to Uniaxial Compression in the y-Direction.

100
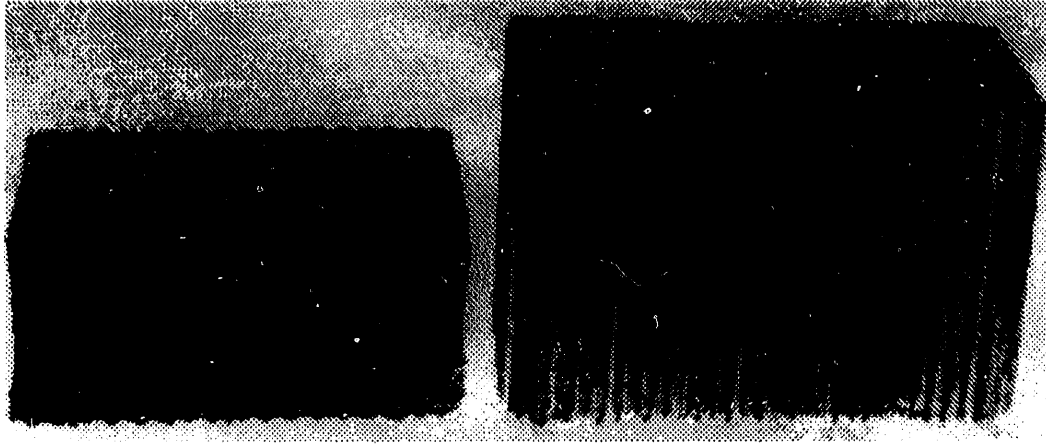
Figure 7.4. Localized Deformation Exhibit by Aluminum Honeycomb Subjected to Uniaxial Compression Along its Generator Axis.

7.2 Generator Axis Response

When aluminum honeycomb is used in impact limiters the material axes are usually oriented such that the material will be crushed along its generator axis during an accidental impact event. This material exhibits a significantly higher strength when it is loaded along its generator axis as opposed to in-plane. Uniaxial compression tests along the generator axis (Donald and Maji, 1992) indicate that this material exhibits localized deformation oriented in a direction normal to the loading axis when it is loaded into the plateau regime (Figure 7.4). This localized deformation can be captured with an associated flow law and a yield function which uses the principal projection operator, $\mathbf{P}^z$, as follows

$$\Psi^z = \boldsymbol{\sigma} : \mathbf{P}^z : \boldsymbol{\sigma} - e(\epsilon, \epsilon^p) \tag{7.7}$$

The bifurcation analysis of such a plasticity model presented in Section 4.6.4 indicates that this model will predict localization oriented normal to the principal stress direction at the limit point.

7.3 A Baseline Model

The analyses in the previous sections indicate that the rather complex combination of yield functions developed by Klintworth and Stronge (1988) would capture the localized deformations that are generated when the honeycomb is subjected to in-plane loads. In most impact limiter applications, the honeycomb is oriented such that the primary loads are oriented along the generator axis and the material is expected to absorb energy by crushing along the generator axis; thus, to simulate these impact events the most
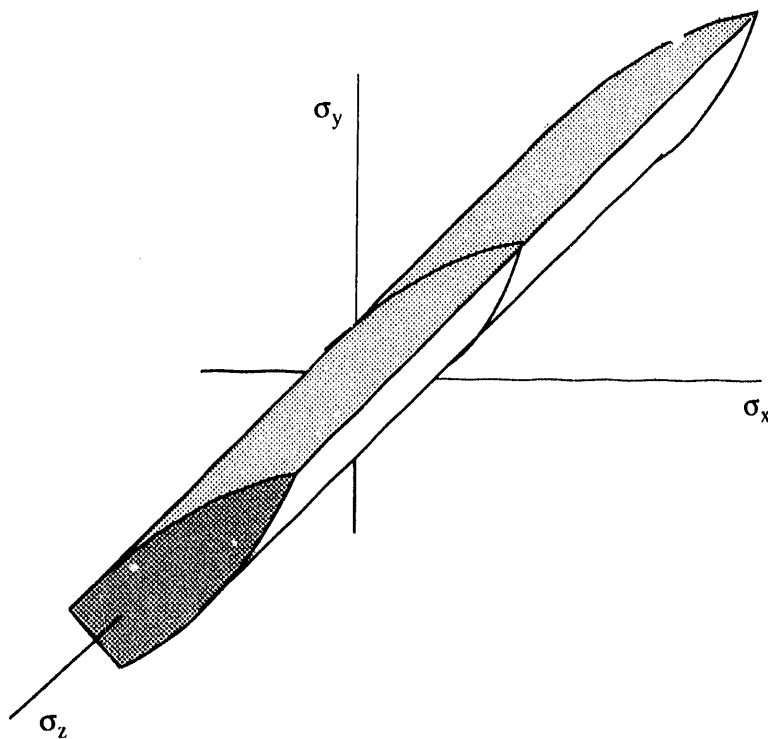
Figure 7.5. Yield Surface for Aluminum Honeycomb.

important behavior that must be captured is the crush of the material along the generator axis. A yield function which uses the principal projection operator, Equation 7.7, is able to predict the localization which occurs when the material is subjected to uniaxial compression along the generator axis. By using this yield function to describe planar caps for the yield surface described by Klintworth and Strong's (1988) in-plane yield functions, we obtain the yield surface shown in Figure 7.5.

8. FINITE ELEMENT ANALYSIS OF AN IMPACT EVENT

A typical impact problem was analyzed using the two-dimensional finite element model shown in Figure 8.1 and the code PRONTO-2D (Taylor and Flanagan, 1986). This plane strain model represents an infinitely long steel cylinder surrounded by a foam layer which is covered with a thin aluminum shell. Three analyses were performed using different constitutive theories for the foam material to investigate the effects of the foam constitutive theory on the predicted response of the impact limiter.
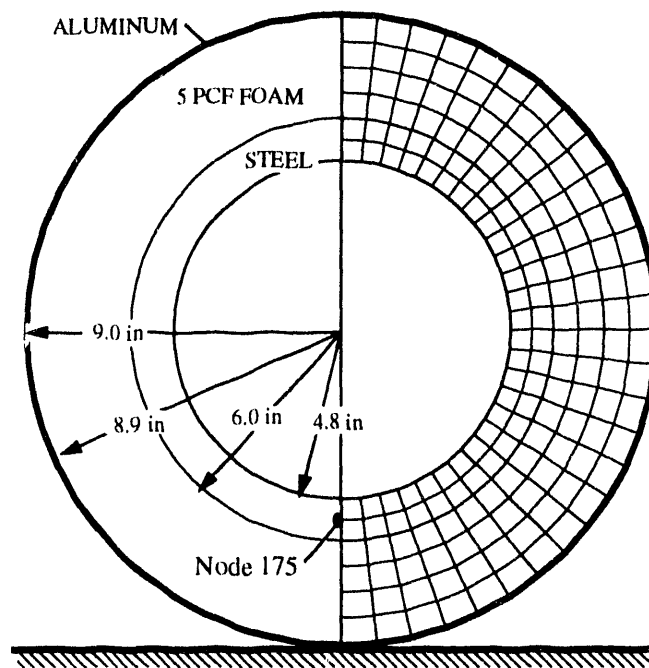
Figure 8.1. Finite Element Model Used in Dynamic Analyses.

The package was dropped onto a rigid surface at an initial velocity of 528 inches per second, and the resulting deformations and accelerations were computed. The impact velocity of 528 inches per second results from a regulatory drop of 30 feet onto an unyielding target for nuclear waste shipping containers.

Material properties used in these analyses are given in Table 8.1. Properties typical of a 5 pound-per-cubic-foot rigid polyurethane foam were used for the foam layer. In the

first analysis, the foam layer was modeled using a von Mises plasticity model for which properties were determined based on results from uniaxial compression tests on the foam. For this model, the material was assumed to be elastic-perfectly plastic and was given a yield strength equal to the plateau stress for the foam. In the second analysis, the foam was modeled using the original foam plasticity model developed by Neilsen, Morgan and Krieg (1987). In the final analysis, the foam was modeled using the new theory consisting of plasticity coupled with isotropic continuum damage. Results from both the uniaxial and the hydrostatic tests were used to determine material properties for the foam plasticity and new coupled models.

Results from these analyses are shown in Figures 8.2 to 8.6. Displaced shapes of the finite element model at maximum crush-up are shown in Figure 8.2. When the von Mises plasticity model (Figure 8.2a) is used for the foam material, the foam is not able to exhibit permanent volume changes and is forced to try to flow from beneath the impacting cylinder. On the other hand, when the original foam plasticity model or the new foam model are used, the permanent volume changes exhibited by foam are captured (Figures 8.2b and 8.2c).

The predicted vertical displacement, velocity and acceleration of Node 175 (see Figure 8.1) in the steel cylinder is plotted as a function of time from initial impact in Figures 8.3, 8.4 and 8.5. The new coupled theory predicts a slightly larger amount of foam crush and a higher rebound velocity than the original plasticity theory. The acceleration time histories generated using the original foam plasticity model and the coupled foam model are very similar. An accurate prediction of the acceleration time history is very important as it provides a measure of the amount of protection provided by the impact limiter. The displacement, velocity and acceleration predictions generated using the von Mises plasticity theory are significantly different than the predictions generated with either of the foam theories. When the foam is modeled with a von Mises plasticity theory, it is not allowed to exhibit any permanent volume changes and unrealistic foam behavior is predicted. Thus, the von Mises theory predicts a peak acceleration level and a rebound velocity that is much higher than that predicted by either foam theory.

Finally, a plot of damage in the foam material at maximum crush-up is shown in Figure 8.6. This plot shows that the largest amount of foam damage is generated in the foam material near the sides of the steel cylinder and not between the steel cylinder and the impact surface. Damage occurs here because the originally circular impact limiter is deformed into an oval shape during the impact event which leads to the generation of large tensile stresses and thus damage near the sides of the steel cylinder. In these analyses, we have assumed that the limiter is foamed in place and that the foam remains bonded to the steel cylinder. The analyses with the coupled theory suggests that debonding or foam failure will occur near the sides of the steel cylinder.

104

Table 8.1. Material Parameters Used in Finite Element Analyses.

Aluminum:	Young's Modulus = 10.0E+06 psi
	Poisson's Ratio = 0.30
	Density = 2.5E-04 lb s^2/in^4
Steel:	Young's Modulus = 29.0E+06 psi
	Poisson's Ratio = 0.30
	Density = 7.0E-04 lb s^2/in^4
Foam:	(von Mises Plasticity Model)
	Young's Modulus = 3000.0 psi
	Poisson's Ratio = 0.0
	Density = 7.5E-06 lb s^2/in^4
	Yield Strength = 110.0 psi
	Hardening Modulus = 0.0 psi
Foam:	(Original Plasticity Model)
	Young's Modulus = 3000.0 psi
	Poisson's Ratio = 0.0
	Density = 7.5E-06 lb s^2/in^4
	Volume Fraction, Φ = 0.09
	Initial Air Pressure, p_0^{air} = 14.7 psi
	Yield Func. Constant, A = 49.2 psi
	Yield Func. Constant, B = 60.8 psi
	Yield Func. Constant, C = -0.5
Foam:	(Coupled Model)
	Young's Modulus = 3000.0 psi
	Poisson's Ratio = 0.0
	Density = 7.5E-06 lb s^2/in^4
	Volume Fraction, Φ = 0.09
	Initial Air Pressure, p_0^{air} = 14.7 psi
	Compressive Yield Constant, A = 110.0 psi
	Compressive Yield Constant, B = 0.0 psi
	Compressive Damage Ratio, M = 0.1
	Tensile Yield Constant, A = 110.0 psi
	Tensile Yield Constant, B = -100.0 psi
	Tensile Damage Ratio, M = 1.0
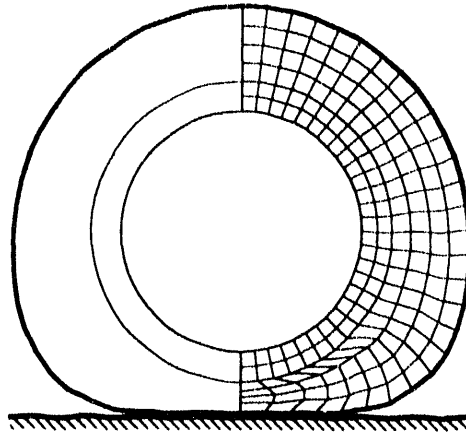
(a) conventional deviatoric plasticity
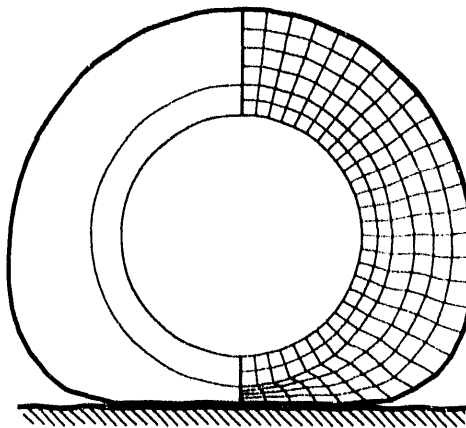
(b) original foam plastiticy
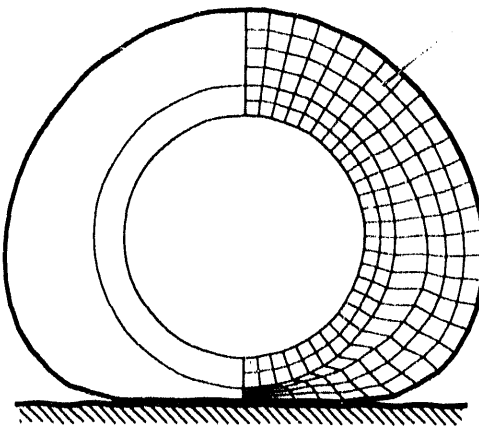
(c) continuum damage coupled with plasticity

Figure 8.2. Deformed Shape of Finite Element Model at Maximum Crush-Up.
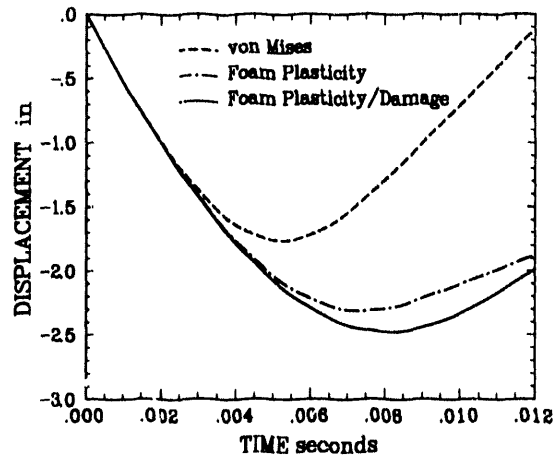
Figure 8.3. Displacement of Steel Cylinder Predicted by the Analyses.
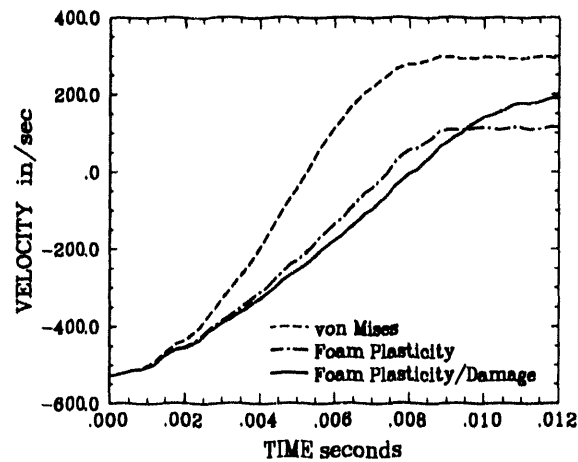
Figure 8.4. Velocity of Steel Cylinder Predicted by the Analyses.
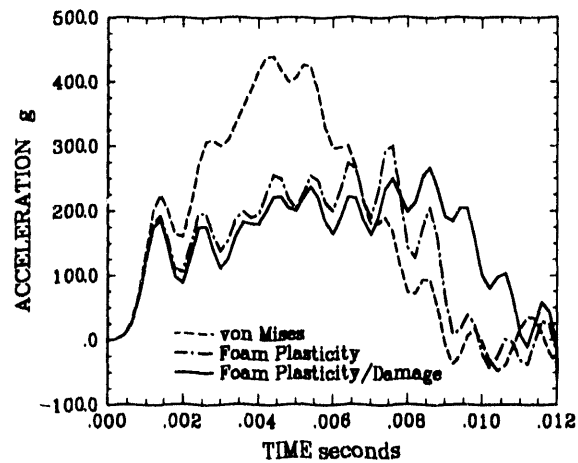
Figure 8.5. Acceleration of Steel Cylinder Predicted by the Analyses.

DAMAGE

	.000
	.167
	.333
	.500
	.667
	.833
	1.000

✳ = .9866
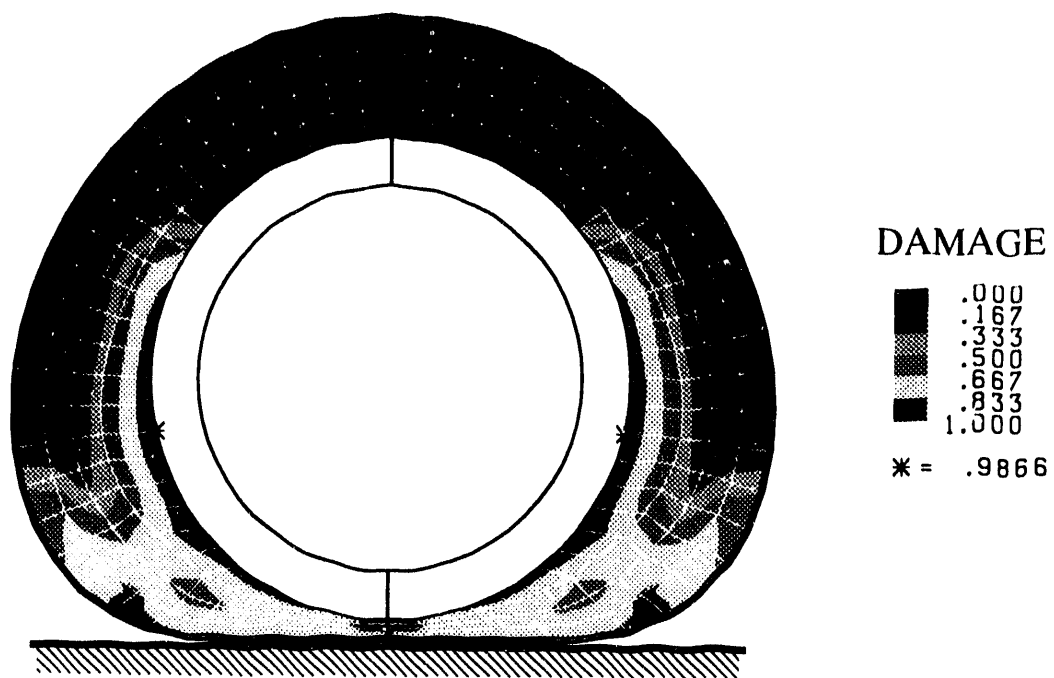
Figure 8.6. Damage in Foam Layer Predicted with Coupled Constitutive Theory.

9. CONCLUSIONS AND FUTURE WORK

The primary focus of this research was the development of constitutive theories for cellular materials that not only capture the elastic response of these materials but also the plastic deformation, damage and localized deformation that is generated when these materials are subjected to crushing loads. The constitutive relations developed for these materials use a combination of plasticity and continuum damage theories. Plasticity is a constitutive theory with a well-developed structure. Continuum damage theories, on the other hand, are just currently being developed (Krajcinovic, 1989). In this paper, a rather general continuum damage theory with a structure similar to existing plasticity theories is developed. Use of a similar structure simplifies the development of coupled plasticity-continuum damage theories which share common yield (damage) surfaces. In this report, a coupled theory was developed for rigid polyurethane foam.

When cellular solids are loaded into the inelastic regime, they often exhibit deformations that are localized into small regions at some point in the loading process. Localization is often associated with satisfaction of the classical discontinuous bifurcation criterion. Here we propose that the loss of strong ellipticity condition should be used in place of the classical discontinuous bifurcation criterion as a necessary condition for localization. The application of the strong ellipticity criterion implies that a bifurcation mode associated with loss of positive definiteness of the symmetric part of the acoustic tensor must be identified rather than a mode associated with the first zero eigenvalue of the acoustic tensor itself. The eigensystem for the symmetric part of the tangent stiffness tensor is obtained for several different plasticity and continuum damage models. This eigensystem provides information about both diffuse and discontinuous bifurcations. Material properties, boundary conditions, and body geometry are all shown to affect the diffuse and localized deformation modes that are generated. Numerous experimental observations of necking and localization in metal specimens subject to various boundary conditions are explained with a bifurcation analysis of a von Mises plasticity model. Bifurcation analyses were then performed on potential constitutive theories for cellular solids. A comparison of results from the bifurcation analyses with experimental observations of localized deformations helped in the identification of appropriate constitutive theories for cellular materials.

Constitutive relations for aluminum honeycombs and rigid polyurethane foams were developed and implemented in both static and dynamic finite element codes. A number of static tests on rigid polyurethane foam were analyzed and the results from the finite element analyses were compared with experimental observations. Finally a typical impact problem was analyzed using various constitutive models for the polyurethane foam to demonstrate the effects of using various constitutive descriptions for the foam.

Cellular solids exhibit some additional features that are not captured by the constitutive theories which were developed in this work. First, dynamic tests on cellular solids indicate that the strength of these materials is strain-rate dependent. The models developed in this paper could be modified to capture this rate dependence. For example, the yield function for the skeleton part of the models could be modified to include the strain-rate dependence. Next, the cyclic tests on this material indicated that a hysteresis loop is generated by unloading and reloading in the elastic regime. For the models developed in this paper, the elastic response is assumed to be linear. The hysteresis exhibited in the experiments may be due to the behavior of the polyurethane cell wall material or to the escape and reentry of the air from the sample during the cyclic loading. The motion of the fluid would have to be modeled and coupled with the skeleton model to capture the effect of fluid flow. The coupling between the fluid flow calculation and the structural calculation could be rather complex. For example, a large pressure gradient could cause damage and the amount of damage generated by crushing or fluid flow would have an effect on the rate of fluid flow. The solution of this coupled problem was beyond the scope of the current work. Finally, it is clear that a significant amount of work is still needed in the area of developing robust numerical procedures before it will be possible to routinely solve localization problems.

The response of cellular materials is complex with several modes of localized deformation exhibited when stress paths are allowed to span a large range. One aspect of the verification of a constitutive model is to show that the predicted orientation and nature of these localized deformation modes agree with experiments. Because of the lack of a routine procedure for theoretically obtaining such modes, this type of verification is practically never done for any material model, let alone those developed for cellular materials. The study of bifurcation phenomena presented here represents a significant enhancement to current technology, and provides an additional important mechanism for evaluating constitutive theories.

110

10. REFERENCES

Aronofsky, J. (1951), *The Formation of a Necked Region and Fracture Along an Oblique Line in Flat Tensile Bars*, Proc. 1st U.S. National Congress of Applied Mechanics, ASME Press, New York, 521-532.

Bazant, Z.P., and Lin, F. (1988), *Nonlocal Smeared Cracking Model for Concrete Fracture*, J. Struct. Engr. **114**, 2493-2510.

Beaver, P.W. (1983), *Localized Thinning, Fracture and Formability of Aluminium Sheet Alloys in Biaxial Tension*, J. Mech. Work. Technol. **7**, 215-231.

Belytschko, T., Fish, J. and Engelmann, B.E. (1988), *A Finite Element with Embedded Localization Zones*, Comp. Meth. Appl. Mech. Engr. **70**, 59-89.

Benallal, A., Billardon, R. and Geymonat, G. (1989), *Conditions de bifurcation a l'interieur et aux frontieres pour une classe de materiaux non-standards*, C.R. Acad. Sci. Paris **308**, 893-898.

Benallal, A., Billardon, R. and Geymonat, G. (1990), *Phenomenes de localisation a la frontiere d'un solide*, C.R. Acad. Sci. Paris **310**, 679-684.

Biffle, J. H. (1989), *JAC3D - A Three-Dimensional Finite Element Computer Program for the Nonlinear Quasi-Static Response of Solids with the Conjugate Gradient Method*, SAND87-1305, Sandia National Laboratories, Albuquerque, New Mexico.

Bigoni, D. and Hueckel, T. (1991), *Uniqueness and Localization - Associative and Non-Associative Elastoplasticity*, Int. J. Solids Struct. **28**, 197-213.

Chen, Z., Neilsen, M.K., and Schreyer, H.L. (1991), *A Secant Structural Solution Scheme for Incremental Damage and Plasticity*, Proceedings of the 3rd Intl. Conf. on Constitutive Laws for Engineering Materials, Edited by Desai, C.S., Krempl, E., Frantziskonis, G. and Saadatmanesh, H., ASME Press, New York, 677-682.

Coleman, B.D. and Gurtin, M. (1967), *Thermodynamics with Internal State Variables*, J. Chem. Phys. **47**, 597-613.

Crisfield, M.A. (1981), *A Fast Incremental/Iterative Solution Procedure that Handles Snap-Through*, Comput. Struct. **13**, 55-62.

de Borst, R. (1986), **Nonlinear Analysis of Frictional Materials**, Ph. D. Dissertation, Delft University of Technology, Delft, The Netherlands.

Donald, S. and Maji, A. (1992), *Static Testing of Aluminum Honeycomb and Polyurethane Foams*, contractors report to Sandia National Laboratories, Albuquerque, New Mexico, in press.

Doyle, E. N. (1971), **The Development and Use of Polyurethane Products**, McGraw-Hill Book Co., New York, 256-263.

Drucker, D.C. (1950), *Some Implications of Work Hardening and Ideal Plasticity*, Quart. Appl. Math. **7**, 411-418.

Drucker, D.C. (1959), *A Definition of a Stable Inelastic Material*, J. Appl. Mech. **26**, 101-106.

Gibson, L.J. and Ashby, M.F. (1988), **Cellular Solids - Structure and Properties**, Pergamon Press, New York.

Hadamard, J. (1903), **Lecons sur la Propagation des Ondes et les Equations de L'Hydrodynamique**, Hermann, Paris.

Hill, R. (1958), *A General Theory of Uniqueness and Stability in Elastic-Plastic Solids*, J. Mech. Phys. Solids **6**, 236-249.

Hill, R. (1962), *Acceleration Waves in Solids*, J. Mech. Phys. Solids **10**, 1-6.

Hill, R. (1991), *A Theoretical Perspective on In-plane Forming of Sheet Metal*, J. Mech. Phys. Solids **39**, 295-307.

Hutchinson, J.W., and Miles, J.P. (1974), *Bifurcation Analysis and the Onset of Necking in an Elastic/Plastic Cylinder Under Uniaxial Tension*, J. Mech. Phys. Solids **22**, 61-71.

Kachanov, L.M. (1986), **Introduction to Continuum Damage Mechanics**, Martinus Nijhoff, Dordrecht, The Netherlands.

Klintworth, J.W. and Stronge, W.J. (1988), *Elasto-Plastic Yield Limits and Deformation Laws for Transversely Crushed Honeycombs*, Int. J. Mech. Sci. **30**, 273-292.

Krajcinovic, D. (1989), *Damage Mechanics*, Mech. Mater. **8**, 117-197.

Larsson, R. and Runesson, K. (1991), *Finite Element Simulation of Localized Plastic Deformation*, Arch. Appl. Mech. **61**, 305-317.

Leroy, Y. and Ortiz, M. (1989), *Finite Element Analysis of Strain Localization in Frictional Materials*, Int. J. Numer. Anal. Meth. Geomech. **13**, 53-74.

Malvern, L.E. (1969), **Introduction to the Mechanics of a Continuous Medium**, Prentice-Hall, Englewood Cliffs, New Jersey.

Mandel, J. (1966), *Conditions de Stabilite' et Postulat de Drucker*, Published in **Rheologie et Mecanique des Sols**, Symposium Grenoble, Edited by Kravtchenko, J. and Sirieys, P.M., Springer-Verlag, New York.

Miles, J.P. (1975), *The Initiation of Necking in Rectangular Elastic/Plastic Specimens Under Uniaxial and Biaxial Tension*, J. Mech. Phys. Solids **23**, 197-213.

Nadai, A. (1950), **Theory of Flow and Fracture of Solids**, McGraw-Hill Book Co., New York.

Needleman, A. (1972), *A Numerical Study of Necking in Circular Cylindrical Bars*, J. Mech. Phys. Solids **20**, 111-127.

Needleman, A. and Tvergaard, V. (1984), *Finite Element Analysis of Localization in Plasticity*, Published in **Finite Elements - Special Problems in Solid Mechanics**, Edited by Oden, J.T. and Carey, G.F., Prentice-Hall, Englewood Cliffs, New Jersey.

Neilsen, M.K., Morgan, H.S., and Krieg, R.D. (1987), *A Phenomenological Constitutive Model for Low Density Polyurethane Foams*, SAND86-2927, Sandia National Laboratories, Albuquerque, New Mexico.

Neilsen, M.K., Chen, Z., and Schreyer, H.L. (1991), *A Structural Constitutive Algorithm Based on Continuum Damage Mechanics for Softening with Snap-Back*, Proceedings of the 3rd Intl. Conf. on Constitutive Laws for Engineering Materials, Edited by Desai, C.S., Krempl, E., Frantziskonis, G. and Saadatmanesh, H., ASME Press, New York, 751-754.

Ortiz, M., Leroy, Y., and Needleman, A. (1987), *A Finite Element Method for Localized Failure Analysis*, Comp. Meth. Appl. Mech. Engr. **61**, 189-214.

Ottosen, N.S., and Runesson, K. (1991), *Properties of Discontinuous Bifurcation Solutions in Elasto-Plasticity*, Int. J. Solids Struct. **27**, 401-421.

Patel, N.R. and Finnie, I. (1969), *The Deformation and Fracture of Rigid Cellular Plastics Under Multiaxial Stress*, Report UCRL-13420, Lawrence Livermore Laboratory, Livermore, California.

Pietruszczak, S.T. and Mroz, Z. (1981), *Finite Element Analysis of Deformation of Strain-Softening Materials*, Int. J. Numer. Meth. Engr. **17**, 327-334.

Raniecki, B. and Bruhns, O.T. (1981), *Bounds to Bifurcation Stresses in Solids with Non-Associated Plastic Flow Law at Finite Strain*, J. Mech. Phys. Solids **29**, 153-172.

Rice, J.R. (1976), *The Localization of Plastic Deformation*, Published in **Theoretical and Applied Mechanics**, 14th IUTAM Congress, Edited by Koiter, W.T., North-Holland Pub. Co., Amsterdam.

Rice, J.R. and Rudnicki, J.W. (1980), *A Note on Some Features of the Theory of Localization of Deformation*, Int. J. Solids Struct. **16**, 597-605.

Riks, E. (1979), *An Incremental Approach to the Solution of Snapping and Buckling Problems*, Intl. J. Solids Struct. **15**, 524-551.

Rudnicki, J.W. and Rice, J.R. (1975), *Conditions for the Localization of Deformation in Pressure-Sensitive Dilatant Materials*, J. Mech. Phys. Solids **23**, 371-394.

Runesson, K., Ottosen, N.S., and Peric, D. (1991), *Discontinuous Bifurcations of Elastic-Plastic Solutions at Plane Stress and Plane Strain*, Intl. J. Plast. **7**, 99-121.

Schreyer, H.L. and Chen, Z. (1986), *One-Dimensional Softening with Localization*, J. Appl. Mech. **53**, 791-797.

Schreyer, H.L. (1990a), *Inelastic Constitutive Theories*, Department of Mechanical Engineering Class Notes, University of New Mexico, Albuquerque, New Mexico.

Schreyer, H.L. (1990b), *Analytical Solutions for Nonlinear Strain-Gradient Softening and Localization*, J. Appl. Mech. **57**, 522-527.

Shaw, M.C. and Sata, T. (1966), *The Plastic Behavior of Cellular Materials*, Int. J. Mech. Sci. **8**, 469-478.

Simo, J.C. and Hughes, T.J.R. (1986), *Elastoplasticity and Viscoplasticity - Computational Aspects*, monograph.

Stone, C. M. (1992), *SANTOS - A Two-Dimensional Finite Element Program for the Quasistatic, Large Deformation, Inelastic Response of Solids*, SAND90-0543, Sandia National Laboratories, Albuquerque, New Mexico.

Storen, S. and Rice, J.R. (1975), *Localized Necking in Thin Sheets*, J. Mech. Phys. Solids **23**, 421-441.

Taylor, L. M. and Flanagan, D. P. (1986), *A Two-Dimensional Transient Solid Dynamics Program*, SAND86-0594, Sandia National Laboratories, Albuquerque, New Mexico.

Thomas, T.Y. (1961), **Plastic Flow and Fracture in Solids**, Academic Press, New York.

Triantafillou, T.C., and Gibson, L.J. (1990), *Constitutive Modelling of Elastic-Plastic Open-Cell Foams*, J. Engr. Mech. **116**, 2772-2778.

Valanis, K.C. (1989), *Banding and Stability in Plastic Materials*, Acta Mech. **79**, 113-141.

Vardoulakis, I., Goldscheider, M., and Gudehus, G. (1978), *Formation of Shear Bands in Sand Bodies as a Bifurcation Problem*, Int. J. Numer. Anal. Meth. Geomech. **2**, 99-128.

114

Warren, W.E., Kraynik, A.M. (1987), *Foam Mechanics: The Linear Elastic Response of Two-Dimensional Spatially Periodic Cellular Materials*, Mech. Mater. **6**, 27-37.

Warren, W.E., Kraynik, A.M., and Stone, C.M. (1989), *A Constitutive Model for Two-Dimensional Nonlinear Elastic Foams*, J. Mech. Phys. Solids **37**, 717-733.

Zaslawsky, M. (1973), *Multiaxial Stress Studies on Rigid Polyurethane Foam*, Exper. Mech. **13**, 70-76.

Unlimited Release

Prof. S. Karnawat
Turtle Mountain College
Box 340
Belcourt, ND 58316

Prof. R.D. Krieg
Engineering Science and Mechanics
301 Perkins Hall
University of Tennessee
Knoxville, TN 37923-6819

M.W. Lewis, MS J-576
Los Alamos National Lab
P.O. Box 1663
Los Alamos, NM 87545

Prof. A.K. Maji
Dept. of Civil Engineering
University of New Mexico
Albuquerque, NM 87131

Prof. H.L. Schreyer (3)
Dept. of Mechanical Engineering
University of New Mexico
Albuquerque, NM 87131

Prof. S. Steinberg
Dept. of Mathematics and Statistics
University of New Mexico
Albuquerque, NM 87131

Prof. D.Y. Tzou
Dept. of Mechanical Engineering
University of New Mexico
Albuquerque, NM 87131

Prof. W.E. Warren
Dept. of Civil Engineering
Texas A & M University
College Station, TX 77843-3136

Prof. F. Yazdani
Department of Civil Engineering
North Dakota State University
Fargo, ND 58105

Prof. H.M. Zbib
Dept. of Mechanical and Matls. Engineering
Washington State University
Pullman, WA 99164-2920

Internal Distribution:

1000 P.A. Fleury
1425 J.H. Biffle
1425 S.W. Attaway
1432 H.E. Fang
1500 D.J. McCloskey
1501 C.W. Peterson
     Route to: 1512, 1513, 1551, 1552
1502 P.J. Hommert
     Route to: 1503, 1511, 1553, 1554
1512 A.M. Kraynik
1561 H.S. Morgan
1561 M.K. Neilsen (25)
1561 M.W. Heinstein
1561 E.L. Hoffman
1561 C.M. Stone
1561 J.R. Weatherby
1561 G.W. Wellman
1562 R.K. Thomas
1562 F.J. Mello
1562 G.D. Sjaardema
1562 A.M. Slavin
5165 N.R. Hansen
5165 A.R. York
6642 J.D. Pierce
6642 D.C. Harding
8700 R.C. Wayne
8702 C.W. Robinson
8741 G.A. Benedetti
8741 M.L. Chiesa
8742 P.E. Nielan
8743 M.L. Callabresi
8743 D.J. Bammann
8746 W.A. Kawahara
7141 Technical Library (5)
7151 Technical Publications
7613-2 Document Processing for DOE/OSTI (15)
8523-2 Central Technical Files

END

DATE
FILMED

12 / 9 / 93